Dissertation zur Erlangung des Doktorgrades
der Fakultät für Chemie und Pharmazie
der Ludwig-Maximilians-Universität München

Structural characterization of the Swi2/Snf2 ATPase Mot1 in complex with protein and DNA substrate

Agata Anna Butryn
aus
Stalowa Wola, Polen

2015

Erklärung

Diese Dissertation wurde im Sinne von § 7 der Promotionsordnung vom 28. November 2011 von Herrn Prof. Dr. Roland Beckmann betreut.

Eidesstattliche Versicherung

Diese Dissertation wurde eigenständig und ohne unerlaubte Hilfe erarbeitet.

München, am 16.04.2015

....

Agata Anna Butryn

Dissertation eingereicht am	16.04.2015
1. Gutachter:	Prof. Dr. Roland Beckmann
2. Gutachter:	PD. Dr. Dietmar Martin
Mündliche Prüfung am	12.06.2015

This PhD thesis has been prepared from September 2010 to December 2014 in the laboratory of Prof. Dr. Karl-Peter Hopfner at the Gene Center of the Ludwig-Maximilians-Univeristy of Munich.

Parts of this thesis have been presented at international conferences:

Poster presentation at the Congress and General Assembly of the International Union of Crystallography, August 5th - 12th 2014, Montreal, Canada.

Parts of this thesis have been included in scientific publications:

A. Butryn, J.M. Schuller, G. Stoehr, P. Runge-Wollmann, F. Förster, D.T. Auble, K.-P. Hopfer, “Structural basis for recognition and remodeling of the TBP:DNA:NC2 complex by Mot1.”, *eLife*, vol. 4, e07432, 2015.

Other publications:

A. Butryn, G. Stoehr, C. Linke-Winnebeck, K.-P. Hopfner, “Serendipitous crystallization and structure determination of cyanase (CynS) from *Serratia proteamaculans*”, *Acta Crystallogr. Sect. F*, vol. 71, no. 4, pp. 471–476, 2015.

P. Wollmann, S. Cui, R. Viswanathan, O. Berninghausen, M. N. Wells, M. Moldt, G. Witte, **A. Butryn**, P. Wendler, R. Beckmann, D. T. Auble, and K.-P. Hopfner, “Structure and mechanism of the Swi2/Snf2 remodeller Mot1 in complex with its substrate TBP.” *Nature*, vol. 475, no. 9, pp. 403–407, 2011.

TABLE OF CONTENTS

1. SUMMARY 1

2. INTRODUCTION 3–25

2.1 MOT1 3
  2.1.1 Discovery 3
  2.1.2 Mot1 function in vivo 4
    Mot1 dissociates nonproductive TBP–DNA complexes 5
    Mot1 nucleates alternative PIC assemblies 5
    Mot1 redistributes TBP between the TATA and TATA-less promoter sites 6
    Mot1 and regulation of RNA pol I- and pol III-driven transcription 7
  2.1.3 Structural organization of the Mot1–TBP complex 8
  2.1.4 Underlying molecular mechanism of Mot1 action 10
    Mot1 is a Swi2/Snf2 family member 10
    Mot1 does not appear to remodel nucleosomes 11
    Swi2/Snf2 enzymes translocate along a DNA track 12
    Mot1 and DNA tracking 14
    Mot1 might utilize a DNA "handle" 15
    Mot1 might directly impact TBP or TATA-box DNA conformation 17
2.2 NC2 18
  2.2.1 Discovery and function in vivo 18
  2.2.2 Structure 19
  2.2.3 NC2 alters the TBP–promoter structure 21
  2.2.4 Mot1 and NC2 play similar roles in vivo 21
  2.2.5 NC2α and NC2β may function as separate subunits 23

3. AIMS OF THE RESEARCH PROJECT 27

4. RESULTS 29–67

4.1 ANALYSIS OF MOT1–NC2 COMPLEXES 29
  4.1.1 Gel filtration 29
    NC2 stabilizes formation of the Mot1–"substrate" complexes 29
    NC2β interacts with Mot1 in a TBP-dependent manner in the absence of DNA 30
  4.1.2 Electrophoretic mobility shift assay (EMSA) 33
    NC2β does not substitute for NC2 in DNA-containing complexes 33
4.2 X-RAY CRYSTALLOGRAPHIC ANALYSIS OF THE MOT1^{NTD}–TBP–DNA–NC2 COMPLEX 34
  4.2.1 Crystallization and structure determination 34
  4.2.2 Overview of the structure 40

Mot1$^{\text{NTD}}$ and NC2 directly interact on the promoter-bound TBP 40
Mot1$^{\text{NTD}}$ binding affects the conformation of TBP, NC2, and DNA 41

4.3 EM AND CX-MS ANALYSES OF THE MOT1–TBP–DNA–NC2 COMPLEX 44

4.3.1 Chemical site-specific protein–protein crosslinking 45

Conformation of Mot1$^{\text{CTD}}$ is dictated by its nucleotide state 48
Position of Mot1$^{\text{CTD}}$ within the complex can be determined via CX-MS analysis 50

4.3.2 Electron microscopy negative stain 53

Rigid-body fitting 54

4.3.3 Pseudo-atomic model of Mot1–TBP–DNA–NC2 complex 55

4.4 PRELIMINARY X-RAY CRYSTALLOGRAPHIC ANALYSIS OF THE MOT1$^{\text{NTD}}$–TBP–NC2B COMPLEX 57

4.4.1 Crystallization and structure determination 57

4.4.2 Overview of the structure 58

Mot1 has a tight grip on TBP 58
NC2β adopts an unusually extended conformation 60

4.5 ACTIVITY MEASUREMENTS 64

4.5.1. Electrophoretic mobility shift assays 64

Mot1 dissociates TBP–DNA–NC2 complexes in presence of ATP and the latch 64
Mot1 dissociates TBP–NC2 from DNA substrates with obstructed ends 66

5. DISCUSSION 69–81

5.1 TBP–DNA–NC2 COMPLEX IS A *BONA FIDE* SUBSTRATE FOR MOT1 69

5.2 THE LATCH PLAYS CRUCIAL ROLE IN DISSOCIATION MECHANISM 70

5.3 MOT1 INITIALLY ALTERS PROTEIN SUBSTRATE–DNA INTERACTION IN AN ATP-INDEPENDENT WAY 71

5.4 MOT1 AND OTHER SWI2/SNF2 ENZYMES 76

5.5 NOVEL ROLES FOR MOT1 AND NC2B? 80

6. EXPERIMENTAL PROCEDURES 83–105

6.1 MATERIALS 83

6.1.1 Media and antibiotics 83

6.1.2 Strains 84

6.2 MOLECULAR BIOLOGY METHODS 84

6.2.1 Polymerase chain reaction (PCR) 86

6.2.2 Site-directed mutagenesis 86

6.2.3 In-Fusion cloning reaction 86

6.2.4 Transformation into *E. coli* 87

6.2.5 Plasmid DNA isolation and sequencing 87

6.2.6 Transposition into bacmid and bacmid DNA isolation 87

6.3 PROTEIN EXPRESSION AND PURIFICATION 88

6.3.1 Insect cell expression system 88

Propagation of the virus in the Sf21 insect cells 88
Protein expression 89
Protein purification 89
Selenomethionine labeling 90

6.3.2 Escherichia coli expression system 90

Protein expression 90
Protein purification 91
Selenomethionine labeling 92

6.4 PROTEIN BIOCHEMISTRY 92

6.4.1 Protein quantification 92

6.4.2 SDS-PAGE 92

Coomassie staining 93
Silver staining 93

6.4.3 Electrophoretic mobility shift assays (EMSA) 94

6.4.4 Sample preparation for crystallization and analytical purposes 94

6.5 X-RAY CRYSTALLOGRAPHY 95

6.5.1 Crystallization 95

Mot1$^{\mathrm{NTD}\Delta\mathrm{latch}}$/Mot1$^{\mathrm{NTD}}$–TBP–DNA–NC2 complex crystals 96
Mot1$^{\mathrm{NTD}}$–TBP–NC2β complex crystals 98

6.5.2 Data collection and processing 98

Mot1$^{\mathrm{NTD}\Delta\mathrm{latch}}$/Mot1$^{\mathrm{NTD}}$–TBP–DNA–NC2 structure 98
Mot1$^{\mathrm{NTD}}$–TBP–NC2β structure 99

6.6 ELECTRON MICROSCOPY 100

6.6.1 Sample preparation 100

6.6.2 Modeling into EM density 100

6.7 CHEMICAL PROTEIN–PROTEIN CROSSLINKING AND MASS SPECTROMETRY ANALYSIS 101

6.7.1 Sample preparation 101

6.7.2 Titration of the crosslinker 101

6.7.3 Analysis of the theoretical crosslinks within the Mot1$^{\mathrm{NTD}}$–TBP–NC2 module 102

6.7.4 Analysis of the crosslinks between the Mot1$^{\mathrm{NTD}}$–TBP–NC2 module and Mot1$^{\mathrm{CTD}}$ 102

6.8 FIGURE PREPARATION 105

7. REFERENCES 106–119

8. ABBREVIATIONS 121–122

9. ACKNOWLEDGEMENTS 123

10. CURRICULUM VITAE 125

1. SUMMARY

Mot1 is an essential factor that in response to physiological signals regulates global redistribution of TATA box-binding protein (TBP), thereby ensuring rapid and tight control of the transcription process in eukaryotes. Mot1 belongs to Swi2/Snf2 family (Switching defective/Sucrose nonfermenting 2) of helicase-like translocases, which form a large and diverse class of proteins playing important roles in DNA replication, recombination, repair, and transcription. Despite all the efforts, it is not clear how Swi2/Snf2 ATPase motors couple nucleotide binding and hydrolysis to alteration of protein–DNA contacts in their substrates.

Crystal structure of the N-terminal HEAT repeat domain of the *Encephalitozoon cuniculi* Mot1 (Mot1^{NTD}) in complex with TBP showed how Mot1 binds to its substrate after the remodeling reaction has taken place ("product" complex). This work presents the 3.8 Å X-ray structure of the *E. cuniculi* Mot1^{NTD} in complex with TBP, DNA, and NC2, another transcriptional regulator, thereby providing the first atomic view at a Swi2/Snf2 remodeler bound to its protein and DNA substrate in a single complex. The analysis of the structural data suggests that ATP-dependent dissociation of protein substrates from DNA is preceded by Mot1-induced ATP-independent destabilization of the TBP–DNA and NC2–DNA interactions. Second crystal structure described in this thesis, the *E. cuniculi* Mot1^{NTD}–TBP–NC2β complex at 3.3 Å resolution, represents so far uncharacterized dimeric assembly in which the histone fold domain of the NC2β subunit adapts unexpectedly extended conformation. Protein–protein crosslinking coupled to mass spectrometry experiments (CX-MS) performed on the Mot1–TBP–DNA–NC2 complex in the presence of different nucleotides enabled to statistically determine the relationship between the conformation and the nucleotide state of the ATPase domain of Mot1 (Mot1^{CTD}). Combination of CX-MS and modeling methods, which was further independently confirmed by the negative stain electron microscopy (EM) studies, provided the means to define the localization of Mot1^{CTD} within the full complex. Finally, the structural analysis and biochemical methods enabled to propose the pseudoatomic model of the Mot1–TBP–DNA–NC2 complex.

These results reveal structural and functional similarities between Mot1 and other Swi2/Snf2 enzymes, which are in particular relevant to nucleosome-related activities applied by chromatin remodeling machineries. Additionally, the initial structural data provide novel insights into possible distinct roles for Mot1 and NC2 in transcriptional regulation.

2. INTRODUCTION

Regulation of transcription in eukaryotes is a highly dynamic process requiring the coordinated interaction of multiple regulatory proteins. Initiation of transcription by all RNA polymerases (RNA pol) requires TATA box-binding protein (TBP), which is a limiting factor for this process [1], [2]. Due to extremely long half-life time of the TBP–DNA complex—up to 50 minutes *in vitro* [3]—living organisms require rapid and tight regulation of TBP's redistribution in global response to physiological signals.

On class II promoters, driving the expression of protein-encoding genes, global response to physiological signals can be directly modulated by two conserved and essential TBP regulators, Mot1 (Modifier of transcription 1, also denoted as BTAF1 in human) and NC2 (Negative Cofactor 2), a heterodimer composed of α and β subunits.

2.1 Mot1

2.1.1 Discovery

In addition to the multisubunit RNA pol II enzyme itself, *in vitro* transcription by RNA polymerase II requires a set of at least five general transcription factors (GTFs): TBP, TFIIB, TFIIE, TFIIF, and TFIIH [4]. GTFs were first purified from human whole cell extracts (WCE) and classified according to their affinity to phosphocellulose column [5]. In human WCE, two of the distinct GTF fractions, called B-TFIID and D-TFIID, were shown to contain TBP and support basal transcription *in vitro* [6]. Subsequently, the B-TFIID fraction was shown to exhibit ATPase activity and, apart from TBP, to contain a 170 kDa polypeptide that was not present in the D-TFIID fraction [7]. Electrophoretic mobility shift assays (EMSAs) and DNase I footprinting experiments performed by the Hahn group on GTFs purified from *Saccharomyces cerevisiae* WCE demonstrated the presence of a factor responsible for the ATP-dependent inhibition of TBP–DNA interaction [8]. Finally, this ATP-dependent inhibitor (ADI) was shown to be encoded by *MOT1* gene and to function as an RNA pol II-specific repressor essential for the yeast cell grow [9]–[12]. Subsequently, other groups published analogous results, identifying yeast TBP-associated factor Taf170 as Mot1 and $\mathrm{TAF_{II}}$170/TAF-172 as its human ortholog [13]–[15]. Mot1 in *Drosophila,* Helicase 89B (Hel89B), was also partially characterized [16].

As much as 75% of the total TBP pool in human cells was shown to be tightly associated with BTAF1 in the B-TFIID form [6]. Consistently, Wade *et al.* reported that even more than 90% of TBP pool in yeast is Mot1-bound [17]. However, some studies in HeLa cells showed that Mot1–TBP association is not so abundant [14]. Correspondingly, Poon *et al.* showed that only up to 5% of the total TBP pool co-immunoprecipitates with Mot1 in yeast [13]. Most likely, these discrepancies are due to the differences in the purification protocols. In any case, no free TBP was found in HeLa WCE [6].

2.1.2 Mot1 function *in vivo*

Global analysis of the changes in mRNA expression levels in *mot1-1* mutant revealed that the conditional depletion of Mot1 upon the shift to nonpermissive temperature affects transcription of 11–15% of yeast genes [18], [19]. In the case of the temperature sensitive *mot1-14* mutant at permissive temperature, 3% of all of the yeast genes tested were affected [20]. Similarly, approximately 4% of all genes were deregulated in a mouse cell line defective in the integrity of the BTAF1–TBP complex [21].

Although Mot1 has been first shown to have a negative impact on transcription [8], [9], [11], [22], large body of data demonstrates an activating role for Mot1 on certain promoters not only *in vitro* [23], [24], but also *in vivo* in yeast [18], [19], [25]–[27] as well as *in vivo* in mouse [21]. Since both activation and repression functions of Mot1 require its functional ATPase activity [20], Mot1's localization to both activated and repressed promoters *in vivo* could suggest that these effects depend on the promoter context in which Mot1 is found [19]. How could the activity to dissociate TBP from promoter lead to activation of some sets of genes?

Mot1 dissociates nonproductive TBP–DNA complexes

Mot1 associates with multiple positions within the protein coding regions of the yeast genome [19], [28]. This is, however, unusual for a transcriptional regulator. Moreover, Mot1's conditional loss increases TBP occupancy not only on promoter, but also on coding sequences [19]. The presence of Mot1–TBP complexes at coding regions can be explained by the fact that TBP is known to bind to high-affinity nonpromoter sites [3]. Recently published experiments performed in Δ*SET2* and Δ*ASF1* strains (impaired for the maintenance of repressive chromatin) showed synthetic growth phenotypes caused by anchor-away depletion of Mot1, thereby confirming a role for Mot1 in suppression of intragenic transcription [30]. Mot1 conditional depletion was also found to result in high levels of aberrant antisense transcripts resulting from TBP being incorporated in functional PICs at cryptic sites [31], [32]. Moreover, TBP and Mot1–TBP complexes were shown to bind to the TATA promoter elements defined by the opposite strand, which do not support functional transcription [29]. Thus, it appears that the ability to release TBP trapped in nonproductive transcriptional complexes at the promoter and/or nonpromoter sites could at least partially account for Mot1's activation function.

Mot1 nucleates alternative PIC assemblies

Numerous chromatin immunoprecipitation (ChIP) studies and mRNA expression profiling arrays have shown that Mot1's and TBP's occupancy is particularly high not only on promoters that are characterized by lowered but also enhanced mRNA expression levels [18], [19]. Therefore, it has been proposed that on some promoters Mot1 could directly contribute to the transcription initiation process in a positive manner. This question was further addressed in the analysis of GTFs association to Mot1's target promoters under normal and stress conditions [33]. Sequential ChIP data showed that under normal conditions Mot1 does not occupy promoters with TFIIA, TFIIB or RNA pol II. However, significant co-occupancy of Mot1, TFIIB and elongation-competent RNA pol II was observed upon heat shock or under hyperosmotic conditions. Therefore, is has been proposed that under environmental stress conditions Mot1 could be involved in the formation of distinct forms of PICs [33].

Further support for this hypothesis was shown by the Auble's group, where Mot1-activated *BNA1* and *URA1* promoters in WT and *mot1-42* cells were investigated [34].

Conditional depletion of Mot1 caused increased TBP levels at these promoters, whereas TFIIB and RNA pol II occupancy as well as mRNA levels were greatly decreased. These findings indicated that, in order to activate these promoters, Mot1 is not necessarily required to load TBP, but rather directs the formation of functional PICs [34]. More detailed functional and structural characterization of the *URA1* promoter also performed by the Auble's group showed that Mot1's positive function at *URA1* is partially facilitated by the displacement of improperly oriented TBP [29]. However, the activation of the analyzed promoter was still Mot1-dependent, even if a consensus TATA box sequence in proper orientation was introduced instead of the endogenous one [29]. Thus, although fixing TBP's reverse orientation was critical for the activation of *URA1*, Mot1-catalyzed redistribution of TBP's orientation does not entirely account for the activator role, further supporting the hypothesis for a direct role of Mot1 in PIC assembly.

Taken together, according to some results, Mot1–TBP complex on some promoters appears as a form of transcriptionally active TBP that forms preinitiation complexes analogous to TFIID. At activated promoters Mot1 could use the energy from ATP hydrolysis to reorganize PICs by inducing a conformational change in the TBP-containing complexes [20]. Alternatively, Mot1 at activated promoters could use a novel enzymatic activity, which has not been yet characterized.

Mot1 redistributes TBP between the TATA and TATA-less promoter sites

The first hypothesis that Mot1-dependent effects on transcription are affected by the presence or quality of the promoter sequence was after Mot1 was shown to be required for efficient *in vitro* transcription from yeast *HIS3* TATA-less but not *HIS3* TATA-containing promoter [19], [24], [35]. A similar trend was observed in *Drosophila*, where by RNAi depletion it was shown that TATA-containing promoters are preferentially repressed and, conversely, DPE-dependent promoters are preferentially activated by Mot1 [36]. This led to the hypothesis that Mot1 represses transcription from TATA promoters and activates TATA-less transcription by redistribution of TBP.

Importantly, functional TATA elements are enriched among heat shock promoters; on the contrary, the TFIID-dominated promoters, which drive the expression of housekeeping genes, do not generally possess canonical TATA boxes [26], [37]. Indeed, most of the Mot1-

repressed genes (77%) are induced during the diauxic shift, as part of environmental stress response or during mating and sporulation [20]. For example, a very elegant study involving ChIP and time-dependent monitoring of mRNA levels of TATA box-regulated *HSP26* gene (coding for small heat shock protein) performed in WT and *mot1* mutant strains showed that Mot1—although originally identified as the repressor of this gene [20]—in fact antagonizes the heat shock-activated state of *HSP26* [34]. Analogous conclusions have been drawn after the analysis of the same promoter during its heat shock activation in Mot1-depleted cells using anchor-away approach [26]. Recent TBP ORGANIC profiling experiments (sequencing of occupied regions of genomes from affinity-purified naturally isolated chromatin) performed in *mot1-42* strain at restrictive temperature additionally demonstrated that over 80% of the sites characterized by increased TBP occupancy possess robust TATA boxes [28].

The differential sensitivity of Mot1-affected promoters seems to be related to their regulation by different co-activator complexes. For example, genome-wide studies reported high co-occupancy of Mot1 and SAGA (Spt–Ada–Gcn5 acetyltransferase) complex at the target genes during acute heat shock [38]. Moreover, the TBP-interacting Spt3–Spt8 SAGA module was shown to be essential for the Mot1 recruitment to some promoters [39]. Additionally, yeast Δ*SPT3* mutation causes synthetic lethality in *mot1-24* [25] and synthetic sickness in *mot1-1* background [39]. Analogously, anchoring Mot1 in Δ*SPT7 or* Δ*SPT3/SPT8* mutant yeast cells causes synthetic lethality, further suggesting a functional interaction between Mot1 and SAGA complex [26]. What factors are responsible for the Mot1's recruitment to TATA-less promoters still awaits further investigation.

Mot1 and regulation of RNA pol I- and pol III-driven transcription

Although RNA pol III promoters often have consensus TATA elements that affect transcription via the specific DNA-binding activity of TBP [40], [41], initial studies of selected RNA pol I and RNA pol III-transcibed promoters showed that they are not regulated by Mot1 [9], [24]. However, more recent studies including higher number of promoters point out at a possible direct role for Mot1 in rRNA transcription and processing [42]. Furthermore, pull-down experiments performed with the N-terminus of *Drosophila* Hel89B showed that this factor can not only bind to dTBP but also to TBP-related factor-1 (dTRF-1) [43]. Analogously, next to yeast and human TBP, the N-terminus of human BTAF1, although with slightly reduced efficiency than hTBP, binds to dTRF-1 [44]. Therefore, although Mot1's regulatory role has been mostly linked to its activity at promoters of protein-encoding genes, a possible functional link between Mot1 and transcription by other RNA polymerases is not entirely excluded and needs to be analyzed on a genome-wide scale in more detail.

2.1.3 Structural organization of the Mot1–TBP complex

Mot1–TBP interaction controls Mot1's nuclear localization [43], is required for the stimulation of the Mot1's central ATPase activity [14], [45]–[47], and delineates Mot1's essential function *in vivo* [22], [37], [43]. In yeast, overexpression of TBP can suppress the negative-dominant phenotype of the C-terminally truncated Mot1 mutants, which form dead-end Mot1–TBP–DNA complexes *in vitro* [45]. Correspondingly, the N-terminal part of human BTAF1 was shown to be important for TBP's recognition in yeast two-hybrid assay [44]. Interestingly, TBP mutations localized not only on the convex, but also on its concave, DNA-binding surface abolish Mot1–TBP interaction [48], [49].

The first structural information that supported mentioned above *in vitro* and *in vivo* results was obtained from the electron microscopy studies (EM) of the native as well as recombinant human BTAF1–TBP complexes published by Timmers and co-workers [50]. The 28 Å negative stain reconstructions supported by immunolabeling revealed that Mot1 adopts an elongated shape with N-terminal TBP-binding thumb followed by a large globular domain corresponding to the ATPase portion at the C-terminus (hereafter referred to as Mot1^{CTD}). A more detailed picture of the Mot1–TBP complex organization was revealed after the crystal structure of the N-terminal domain of *Encephalitozoon cuniculi* Mot1's ortholog (Mot1^{NTD}, residues 1–778) in the complex with full-length TBP solved at 3.1 Å resolution was published by the Hopfner group [47]. The crystal structure confirmed previous structural predictions [43] and showed that the N-terminal part of Mot1 consist of an elongated stretch of α-helices organized in an array of HEAT (Huntingtin, elongation factor-3, protein phosphatase 2A, lipid kinase TOR) repeats (**Figure 1**). Acidic loops of the HEAT repeats 4 to 6 were shown to bind to the convex surface of TBP, while a "latch" loop,

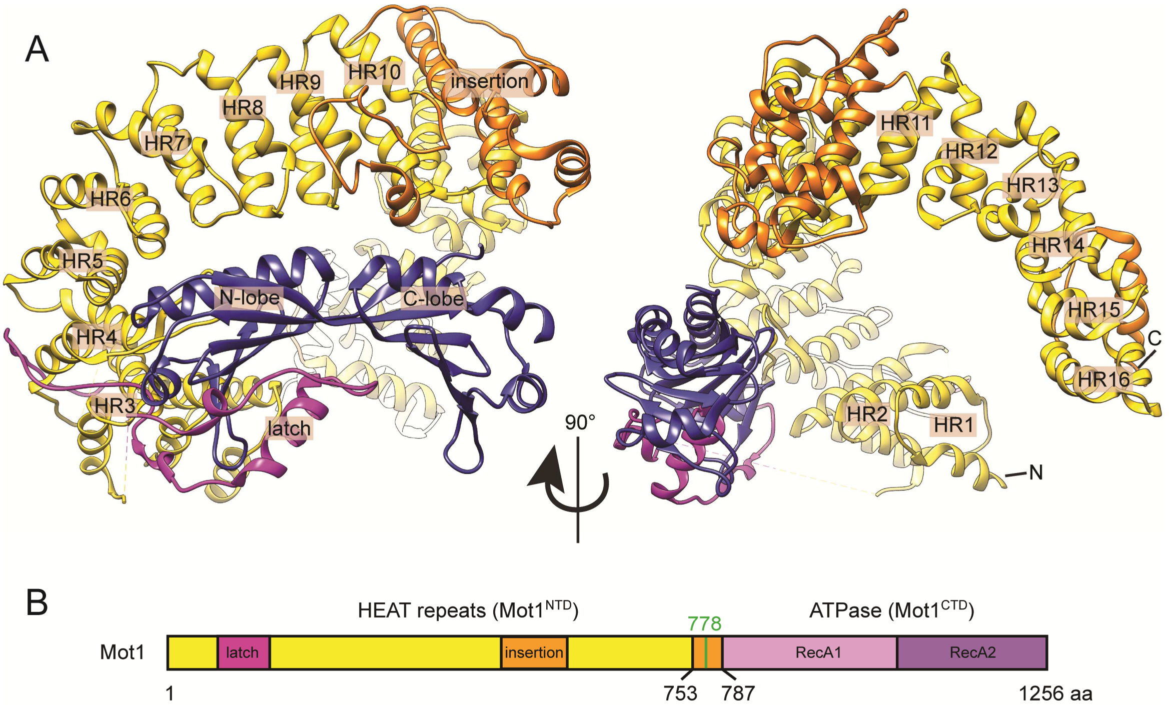

Figure 1. Crystal structure of the *Encephalitozoon cuniculi* Mot1^{NTD}–TBP complex.

(A) The crystal structure of the *E. cuniculi* Mot1^{NTD}–TBP "product" complex reported to 3.1 Å resolution [47]. TBP is shown in blue. The HEAT repeats of Mot1^{NTD} are shown in yellow, annotated as HR and numbered accordingly. Non-HEAT repeat parts, including the insertion domain and last C-terminal helix of the crystallized construct are shown in orange. The latch region is shown in magenta. N- and C-terminal ends of the Mot1^{NTD} construct are annotated as N and C, respectively. **(B)** Domain organization of the full-length *E. cuniculi* Mot1 visualizing the boundaries of the crystallization construct comprising the residues 1–778 (marked in green). RecA1 and RecA2 subdomains of Mot1^{CTD} are represented in pink and purple, respectively. The color code of the rest is as in (A).

protruding from between the HEAT repeats 2 and 3, was shown to shield the TBP's concave site. Additional biochemical characterization of Mot1$^{\Delta latch}$ and Mot1$^{NTD\Delta latch}$ mutants (Δ97–131) showed that the latch does not only shield TBP's concave site preventing from TBP's re-association with DNA. The latch, apart from being an important structural element, was found to be required for the TBP-stimulated Mot1's ATPase activity [47]. In addition, deletion of the latch region impaired Mot1's ability to dissociate TBP–DNA complexes in an ATP-dependent reaction, thereby proving a suggestion for its important role in the dissociation mechanism [47]. Moreover, Mot1 binding site to TBP clearly overlaps with the TFIIA binding site [47]. Thus, the structural data also explained the antagonistic effect of Mot1 and TFIIA [8], [44], and supported the hypothesis that Mot1 could form distinct PICs functionally replacing some GTFs [29], [34], [33].

2.1.4 Underlying molecular mechanism of Mot1 action

Mot1 is a Swi2/Snf2 family member

Based on the conserved motifs that are involved in coupling of nucleoside triphosphate (NTP) binding and hydrolysis to their DNA- and RNA-related functions, helicase-like proteins are classified into six superfamilies (SF1–SF6), which can be further divided into distinct families [51], [52]. As shown in **Figure 2**, Mot1 is a member of the Swi2/Snf2 family (Switching defective/Sucrose nonfermenting 2), forming a large and diverse class of proteins within the SF2 supefamily. A more detailed phylogenomic classification of the Swi2/Snf2 members, based on the similarities within the conserved motifs and the presence of family-specific insertions, additionally distinguishes 24 distinct subfamilies [52]. The differences among some groupings are apparent e.g. in requirements for the stimulation of the ATPase activity [53].

Swi2/Snf2 enzymes play important roles in various basic cellular processes like DNA replication, recombination, repair and transcription. Although Swi2/Snf2 enzymes very often act as multiprotein assemblies, some Swi2/Snf2 family members are fully active without any additional subunits, e.g. Chd1 [54], Rad54 [55] or Mot1 [8]. Many prokaryotic and archaeal relatives are also found among Swi2/Snf2 enzymes, e.g. *Escherichia coli* RapA [56] or *Sulpholobus solfataricus* Rad54-like protein [57]. Common feature of all SF2 members is the presence of a conserved catalytical core consisting of two subdomains that each resembles the fold of recombination protein RecA with characteristic helicase-related functional motifs mentioned above [58]. In addition, each member possesses auxiliary domains that confer the specificity of the RecA-like domains for particular function or substrate. Mot1 functional ATPase portion is required for efficient Mot1–TBP–DNA complex formation and its dissociation *in vitro* [9], [47], [59]. Moreover, Walker A or B mutants as well as deletion of Mot1^{CTD} show dominant-negative phenotype in yeast [9]. Interestingly, despite high sequence conservation within the ATPase region of Swi2/Snf2 members, swapping of this region between the family members has been shown to carry the properties of the remodeling complex with it [60]. For example, Mot1–Snf2 and Mot1–Iswi chimeric proteins do not support Mot1's function *in vivo,* although they bind to TBP both *in vitro* and *in vivo* [45]. This clearly shows that the Swi2/Snf2 motor domain is essential and contains

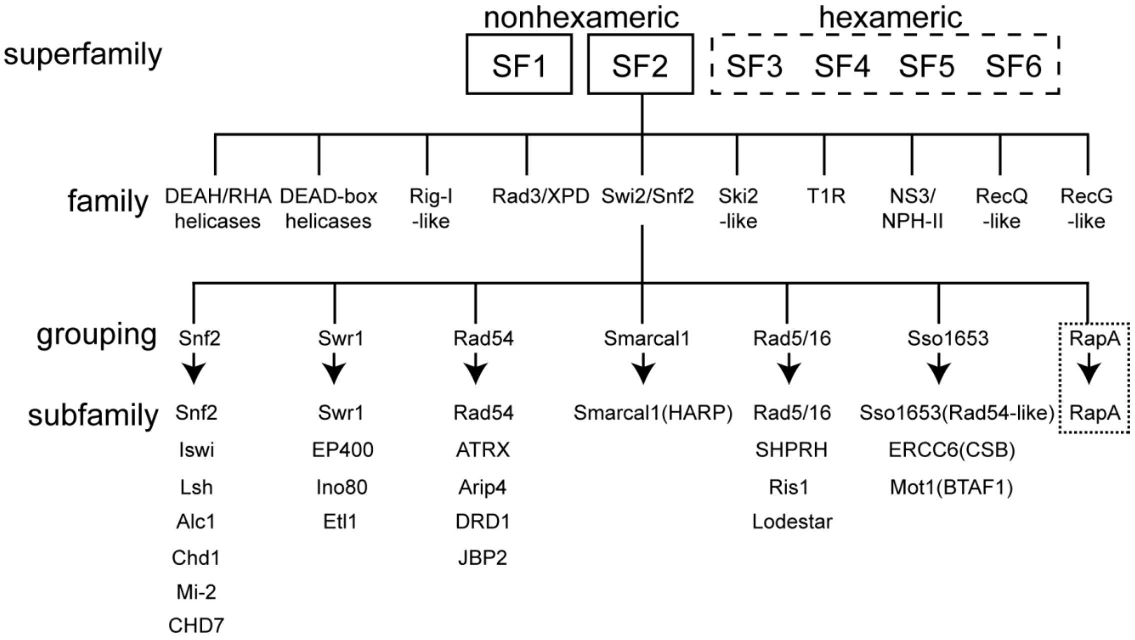
superfamily
nonhexameric
hexameric
SF1
SF2
SF3
SF4
SF5
SF6
family
DEAH/RHA helicases
DEAD-box helicases
Rig-I -like
Rad3/XPD
Swi2/Snf2
Ski2 -like
T1R
NS3/ NPH-II
RecQ -like
RecG -like
grouping
Snf2
Swr1
Rad54
Smarcal1
Rad5/16
Sso1653
RapA
subfamily
Snf2
Iswi
Lsh
Alc1
Chd1
Mi-2
CHD7
Swr1
EP400
Ino80
Etl1
Rad54
ATRX
Arip4
DRD1
JBP2
Smarcal1(HARP)
Rad5/16
SHPRH
Ris1
Lodestar
Sso1653(Rad54-like)
ERCC6(CSB)
Mot1(BTAF1)
RapA

Figure 2. Classification of helicase-like proteins.

Classification of putative helicases into superfamilies, families and subfamilies performed on the basis of primary structure analyses [51], [52]. Dotted box highlights the subfamily which members of are not found among eukaryotes. The figure is adopted from [52].

residues that are important for the specific action of each family member.

Mot1 does not appear to remodel nucleosomes

Chromatin remodelers are the largest and the best characterized group of Swi2/Snf2 ATPases to date, including SWI/SNF chromatin remodeling complex and its Swi2/Snf2 catalytic subunit, the prototype family member. Chromatin remodelers are multisubunit assemblies with combined molecular weights in the megadalton range, which are able to alter the chromatin structure, thereby enabling transcription factors and RNA polymerase to access the transcription start sites [61]–[63]. Chromatin remodelers act in response to DNA and histone modifications catalyzing nucleosome sliding in *cis*, transfer in *trans*, disassembly as well as histone variant exchange [64].

Consistent with the observation that many Mot1-related enzymes are involved in regulating chromatin structure in some way, Mot1—independently of its TBP recruitment—was suggested to play a direct role in nucleosome remodeling at *GAL1* promoter [69]. However, the chromatin structures at the *URA1* promoter in WT and Mot1-depleted cells tested by another group were indistinguishable [34]. Moreover, Mot1- and TBP-immunodepleted yeast chromatin samples were shown to be deprived of nucleosome-size fragments [28]. Therefore, the hypothesis that Mot1, apart from TBP-related functions, directly affects nucleosome positioning has not been well supported so far. Next to Mot1, there are other examples of Swi2/Snf2 enzymes which function is not directly related to chromatin, e.g. Cockayne syndrome protein B, CSB (transcription-coupled DNA repair [65]), Rad54 (DNA recombination [66]), Rad 16 (nucleotide excision repair [67]) or RapA (recycling of stalled RNA polymerase in *E. coli* [68]).

Swi2/Snf2 enzymes translocate along a DNA track

Considering the initial classification of Mot1 as a DNA helicase-like protein [10], ATP-driven helicase activity leading to the promoter DNA unwinding was among the first proposed mechanism by which Mot1 could catalyze the displacement of TBP from DNA. For example, ATP-dependent disruption of TBP–DNA complexes was tested on DNA substrates covalently crosslinked either in the TATA box or in the upstream DNA region [46], [70]. However, neither full-length Mot1 nor Mot1^{CTD} manifested strand displacement activity, with and without TBP [8], [46]. Importantly, although many enzymes among SF2 helicase-related proteins are indeed *bona fide* helicases, none of the Swi2/Snf2 family members has been demonstrated to possess a helicase activity so far.

Despite all the efforts to unravel the molecular basis of ATP-dependent remodeling, it is not entirely clear what mechanisms are employed by Swi2/Snf2 ATPase motors to couple NTP binding and hydrolysis to protein–DNA conformational changes. However, DNA length-dependent ATPase activity measurements and triplex displacement activity assays suggest that chromatin remodelers, similarly to some other SF2 enzymes, translocate along dsDNA [71]–[73]. Moreover, translocase activity of *bona fide* helicases can be physically uncoupled from their strand separation activity [74], further supporting the possibility that Swi2/Snf2 enzymes could exploit translocation as the principal mechanisms. In this process, the phosphate backbone is used as a track in a relatively unspecific manner. For the prototype dsDNA tracking SF2 enzyme, EcoR124I, modifications or discontinuities on the 3'–5' strand result in more severe inhibition of translocation than those on the 5'–3' strand [75]. Although contacts to the 5'–3' strand are not essential for motion, they do play a key role in stabilizing the motor on the DNA. Importantly, nucleosome remodeling assays using nicked and gapped DNA substrates showed that the translocation catalyzed by some Swi2/Snf2 members also predominantly occurs along the 3´–5´ DNA strand [71], [72]. Moreover, both chromatin remodeling complexes and their isolated catalytical subunits are active on ssDNA substrates [71], [73]. These findings fully support a model in which the SF2 motor contacts are maintained mainly by one strand of the duplex.

A detailed idea about how Swi2/Snf2 enzymes might function is mainly based on the high-resolution structural information available for SF1 and other SF2 helicases, which are much better characterized than the Swi2/Snf2 family. Unfortunately, only few structures of the Swi2/Snf2 ATPase domains are available (**Figure 3**A). These include: a) *S. solfataricus* Rad54-like Swi2/Snf2 ATPase portion in complex with dsDNA [76]; b) chromodomains and ATPase portion of S. *cerevisiae* Chromodomain helicase DNA-binding protein 1 (Chd1) crystallized in the presence of ATPγS (AGS) [54]; c) *Danio rerio* Rad54 Swi2/Snf2 ATPase domain [77]; and d) full-length *E. coli* RapA [78]. In the first two of the four mentioned, the Swi2/Snf2 motor domains were trapped in inactive conformations, which—according to the related SF2 enzymes—would not support proper formation of the ATP binding cleft [79]. In other two structures, the ATPase domains adopted fully closed conformation, but neither DNA nor ATP analog were co-crystallized. Thus, no novel insights into e.g. molecular mechanism of dsDNA tracking or the role of the family-specific protrusions were revealed.

Still, the limited structural information provides valuable information linking the molecular mechanism applied by Swi2/Snf2 family with these applied by other SF2 enzymes. Remarkably, when superimposed via their N-terminal RecA folds, the DNA duplex bound to the SsoRad54-like protein overlays very well with dsRNA bound to the innate immunity sensors Rig-I [80] and MDA5 [81]. These dsRNA-activated SF2 members, similarly to Swi2/Snf2 enzymes, do not robustly unwind nucleic acid substrates and have been shown to translocate along dsRNA [82]. Further analysis shows that the ssDNA 3’ overhang generated by NS3 and VASA, *bona fide* SF2 helicases, as well as PcrA [83], a SF1 *bona fide* helicase, overlays with the 3'–5' strand of the dsDNA bound to SsoRad54-like protein (**Figure 3**C). Thus, the comparative analysis of the available data implies that Swi2/Snf2 family members are likely to use similar mechanism as other SF2 helicases and translocases.

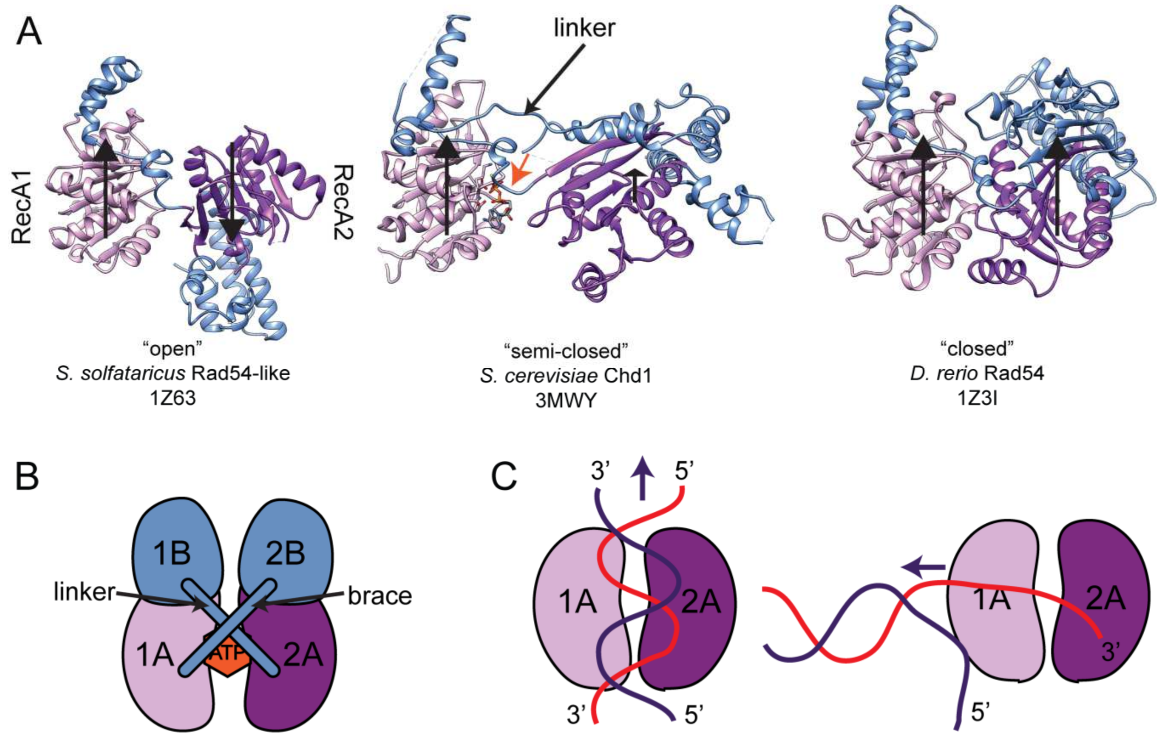

Figure 3. Crystal structures of nonbacterial Swi2/Snf2 ATPase domains.

(A) Crystal structures of Swi2/Snf2 domains. From left: *S. solfataricus* Rad54-like–DNA complex in an "open" conformation [76], *S. cerevisiae* Chd1 in an autoinhibited "semi-closed" conformation [54] and *D. rerio* Rad54 in a "closed" conformation [77]. PDB accession codes are listed. The structures are oriented with respect to the RecA1 subdomain. Relative orientations of the core RecA 1 (pink) and 2 (purple) subdomains joined by a short linker are represented by the black arrows. Family-specific insertion regions, i.e. protrusions 1B and 2B, linker region as well as C-terminal are indicated in blue. The location of AGS bound in the Chd1 structure is indicated by the red arrow. Auxiliary domains were omitted. **(B)** Schematic representation of the subdomain organization of a Swi2/Snf2 domain. Nucleotide molecule binds at the interface formed by core subdomains 1A and 2A [79]. Color code is as in (A). **(C)** In the *S. solfataricus* Rad54-like protein structure, the N-terminal RecA subdomain recognizes both DNA strands along the minor groove and the DNA retains essentially B-form conformation. The 3'–5' strand of the DNA duplex occupies a position that is virtually identical to the 3'–5' overhangs in the crystal structures of related SF2 helicases (see text). The black arrows show the direction (3'–5') in which ATPase domain is thought to translocate along DNA. Panel (C) was adapted from [84].

Mot1 and DNA tracking

Consistent with the data available for other SF2 enzymes, DNA tracking was proposed as a mechanism which could be also applied by Mot1 [85]. In this scenario, the presence of the HEAT repeat region would for example enable Mot1 to store the elastic tension generated during translocation process and to push or pull off TBP from the promoter DNA [47]. Consistent with the fact that Mot1^{CTD} forms primary contacts to the TATA-box containing strand [59] and a typical 3’–5’ translocation of SF2 enzymes [71], [72], [75], it seems that the “pulling off” would be a more imaginable possibility [86].

A very elegant study including EMSA and DNase I footprinting experiments clearly showed that Mot1-catalyzed disruption is not blocked by the presence of heterologous DNA-binding proteins preventing the Mot1–TBP–DNA complexes from falling off the ends of linear DNA substrates [85]. Therefore, the release of TBP from DNA by Mot1 does not appear to involve highly processive ATP-dependent DNA tracking over long distances. However, in the same study it was shown that Mot1 was able to transfer from TBP–DNA complex to another one localized in the upstream direction [85]. Interestingly enough, this occurred in the absence of ATP and was not observed when the second TATA box was localized downstream from the preloaded Mot1–TBP–DNA complexes. This process was dependent on an unobstructed path between the TBP–DNA complexes, suggesting that Mot1 could indeed slide along DNA. However, observed results might be explained by DNA looping. Therefore, although a direct clear proof for DNA translocation for Mot1 has not been shown experimentally, current data certainly do not exclude short-range, nonprocessive tracking.

Mot1 utilizes a DNA “handle”

Full-length *S. cerevisiae* and *E. cuniculi* Mot1 have no specific DNA binding affinity, regardless of the presence or absence of ATP [8], [46], [47], [70], [87], [88] and, consequently, their ATPase activity is not stimulated by DNA alone [9], [46], [47]. Similarly, human BTAF1 binds DNA very weakly in the absence of TBP [14]. In contrast, stimulation of yeast and *E. cuniculi* Mot1’s ATPase activity occurs in the presence of TBP [45], [46]. Unlike its fungal orthologs, human BTAF1 is not stimulated by TBP at all, but by a synergistic action of TBP and DNA [14]. These differences between Mot1 orthologs are not well understood, however. DNA alone can activate BTAF1 to some extent, but this activity comprises only 1% of the activity reported in the presence of both TBP and DNA [14]. *E. cuniculi* Mot1 exhibits somewhat mixed behavior, since it shows higher stimulation by TBP–DNA complexes than only by TBP [47].

Absence of the DNA-dependent stimulation of Mot1 ATPase activity is at odds with the data which has been accumulated for many Swi2/Snf2 ATPases showing robust DNA binding and DNA-dependent stimulation [53]. However, yeast Mot1^{CTD} does bind dsDNA on its own and this interaction is nucleotide-dependent [88]. In the presence of TBP–DNA complexes, Mot1^{CTD} was shown to protect the "upstream" (5' end according to the TATA box-containing strand) region of DNA in DNase I footprinting experiments [8], [59], [70] and to directly interact with it in DNA–protein photocrosslinking experimens [9] as well as in FeBABE-mediated hydroxyl radical cleavage assay experiments [47]. Additionally, biochemical experiments are fully supported by structural data suggesting that *E. cuniculi* Mot1^{CTD} localizes to the upstream DNA [47]. However, Mot1 does not have an upstream or downstream DNA fragment requirement for complex formation *per se* [70], [87]; however, the presence of the upstream DNA increases the stability of Mot1–TBP–DNA complexes *in vitro* [70], [87]. Moreover, although one study has shown no 5' DNA requirement for Mot1–TBP–DNA complex dissociation [87], other independent experiments including EMSA [8], [70], [88], DNase I footprinting [59] and fluorescence anisotropy [88] argue that the upstream region in critical for the Mot1-dependent catalysis. On the contrary, promoter-flanking regions in the 3' direction from the TATA box are dispensable for Mot1 action [8], [70]. No sequence specificity has been reported so far for the formation of stable Mot1–TBP–DNA complexes or for their disruption. Interestingly, however, not all TBP–promoter DNA substrates bind Mot1 with the same efficiency in direct comparison studies, pointing towards the possibility that base specificity may somehow contribute to the affinity [8], [59].

In a very elegant FRET (Förster resonance energy transfer)-based approach, it was shown that the upstream DNA provides a grip mediating conformational changes introduced by Mot1^{CTD}, probably propagating them towards TBP [88]. First, the alterations of the upstream DNA conformational changes being a direct result of Mot1^{CTD} action could be transferred towards TBP initiating the changes in the TBP–promoter DNA interaction. Next, ATP binding could alter the interaction between Mot1^{CTD} and the upstream DNA. Finally, ATP hydrolysis could trigger another conformational change, for example including short-range DNA translocation, which would result in the dissociation of the complex [88]. This model, however, cannot explain why Mot1 is able to unbend DNA independently of the upstream DNA [88], to dissociate TBP from DNA substrates which lack upstream DNA [87] or why Mot1^{NTD} dissociates TBP–DNA complexes in the absence of Mot1^{CTD} [47]. Finally, the introduction of single nucleotide gaps in either strands of the upstream DNA has no effect on the ATP-dependent dissociation [70] and Mot1 can efficiently dissociate TBP from highly constrained minicircle DNA substrates [70]. Thus, the upstream DNA “handle” and the TBP–DNA complex appear to be conformationally uncoupled.

Mot1 might directly impact TBP or TATA-box DNA conformation

EMSA experiments performed on I–C (inosine–cytosine)-substituted DNA substrates and unmodified TATA boxes revealed that although Mot1 bound all TBP–DNA substrates with the same affinity, modified nucleic acids did not efficiently support the Mot1-dependent catalysis upon ATP addition [45]. Interestingly, Mot1 binding affects TBP’s DNA protection pattern in DNase I footprinting experiments [8], [70]. This raised the possibility that Mot1 requires a direct contact with the TATA box in order to dissociate TBP–DNA complexes [45]. In fact, site-specific photocrosslinking of Mot1 to DNA performed in the presence of TBP as well as TBP’s mutagenetic studies suggested that Mot1 contacts not only upstream DNA but also the TATA box itself [49], [59]. However, since Mot1 is able to efficiently dissociate TBP–DNA–NC2 complexes, Mot1 is unlikely to require a direct contact with the TATA major groove [48].

Alternatively, Mot1 could act via affecting the TBP–promoter interaction by a direct influence of TBP’s conformation. The idea that Mot1 might directly influence TBP structure has been broadly discussed [45], [46], [48], [59], [87], [90], although there has not been yet any direct evidence for it. Mot1-induced alterations of TBP structure could force a state in which TBP would be incompetent to bind to the TATA box anymore. Mot1–TBP–DNA complex of altered TBP–promoter interaction could be then more easily dissociated. However, inducing a huge conformational change in the conserved TBP core domain seems to be rather unlikely. The analysis of available structural data presenting TBP in complex with various factors, including the Mot1^{NTD}–TBP crystal structure, revealed that TBP remains in a rather similar conformation [47]. Nevertheless, Mot1 could possibly perturb e.g. TBP stirrups or the β-strands connecting the two subdomains [59].

Another intriguing way to regulate DNA binding behavior of TBP and—at the same time—promoter DNA conformation could be regulated by a direct interaction between Mot1 and nonconserved N-terminal tail of TBP [92]. Full-length yeast TBP was shown to form complexes with promoter DNA in a two step manner, forming first unbent transient product of TBP sensing a TATA box-containing DNA, which then slowly formed stable, bent DNA complexes. The N-terminal tail of TBP was required for the formation of the unbent species. Additionally, mutations localized on the convex, solvent-exposed surface of the full-length TBP (inhibitory DNA binding surface, IDB) were shown to indirectly affect the promoter DNA conformation [92]. Interestingly enough, the IDB surface overlaps with the region recognized by Mot1 [49]. Therefore, DNA conformation could be potentially regulated through protein–protein contacts between Mot1 and DNA-bound TBP by promoting unbent DNA conformation via displacing TBP's N-terminal tail from the IDB surface. BTAF1 does not interact with hTBP's N-terminus [14], but Mot1 binds $\mathrm{TBP}^{\mathrm{core}}$–DNA complexes more strongly than DNA complexes formed on full-length TBP [8]. Moreover, the DNase I protection pattern of the TATA box in Mot1–TBP–DNA complexes was reported to differ for the full-length TBP and for $\mathrm{TBP}^{\mathrm{core}}$ construct [59]. However, more recent single-molecule studies did not report the presence of the unbent TBP–DNA complexes, thereby suggesting simultaneous TBP binding and DNA bending [93].

2.2 NC2

2.2.1 Discovery and function *in vivo*

NC2 (Negative cofactor 2) was initially described by Meisterernst and Roeder as a factor able to change the mobility of human TBP–DNA complex in EMSA [94]. NC2 was able to suppress the basal level of core promoter activity in an RNA pol II transcription assay by blocking the association of TFIIA and TFIIB with TBP–DNA complexes [94]. Independently, Reinberg and co-workers isolated and cloned a TBP-interacting protein, which they called Dr1, manifesting influence on the transcription similar to NC2 [95]. Despite many similarities, recombinant Dr1—in contrast to the endogenous one—failed to form a stable complex with TBP and promoter DNA and did not block the formation of TBP–DNA–TFIIA complexes in EMSA. The observed differences could be explained by *in vivo* Dr1 phosphorylation, which was shown to regulate the TBP–Dr1 interaction [95]. Further experiments performed by Meisterernts and colleagues revealed that NC2 is composed of two subunits, subsequently named α and β, and identified Dr1 to be identical to the latter one [96]. Therefore, previously reported differences between the recombinant and endogenous Dr1 observed by the Reinberg group [95] could be explained by the lack of the associated subunit, NC2α (also denoted as DRAP, standing for Dr1-associated protein). To date, a general co-association of both subunits of the NC2 heterodimer on chromatin has been well documented, e.g. by ChIP data [97].

Yeast genetic screen selecting for the suppressors of *SUC2* promoter upstream activating sequence (*SUC2*ΔUAS) identified the *bur6-1* mutation (for Bypass UAS Requirement) causing large defect in the gene encoding the NC2α subunit [11], [12]. Further investigations have shown that NC2 heterodimer negatively regulates transcription from class II promoters on a global scale *in vivo* [98] and that both subunits are essential for yeast cell viability [98]–[100]. Subsequently, NC2 was shown to play also a stimulating role on certain RNA pol II promoters *in vitro* and *in vivo* [26], [36], [97], [99], [101]–[105]. On a genome-wide scale, thermal inactivation of *bur6-1* conditional mutant affects approximately 17% of the yeast genes [101], [102].

2.2.2 Structure

N-termini of both NC2 subunits were predicted to contain a histone fold motif [106], which was shown to be absolutely essential for the yeast cells viability [100]. The crystal structure of the human NC2 heterodimer recognizing the complex of TBP bound to a 19 bp dsDNA containing a TATA element was published [107] (**Figure 4**). The structure reported to 2.6 Å resolution confirmed the presence of the histone fold dimerization domain and its resemblance to the molecular organization of the H2A/H2B heterodimer within the nucleosome [108] and, consequently, other histone fold-containing transcription factors, e.g. NF-Y complex [109], [110]. NC2 was demonstrated to "lock" TBP on the promoter between the histone fold domain ($NC2^{HF}$) bound to the underside of the DNA and the convex site

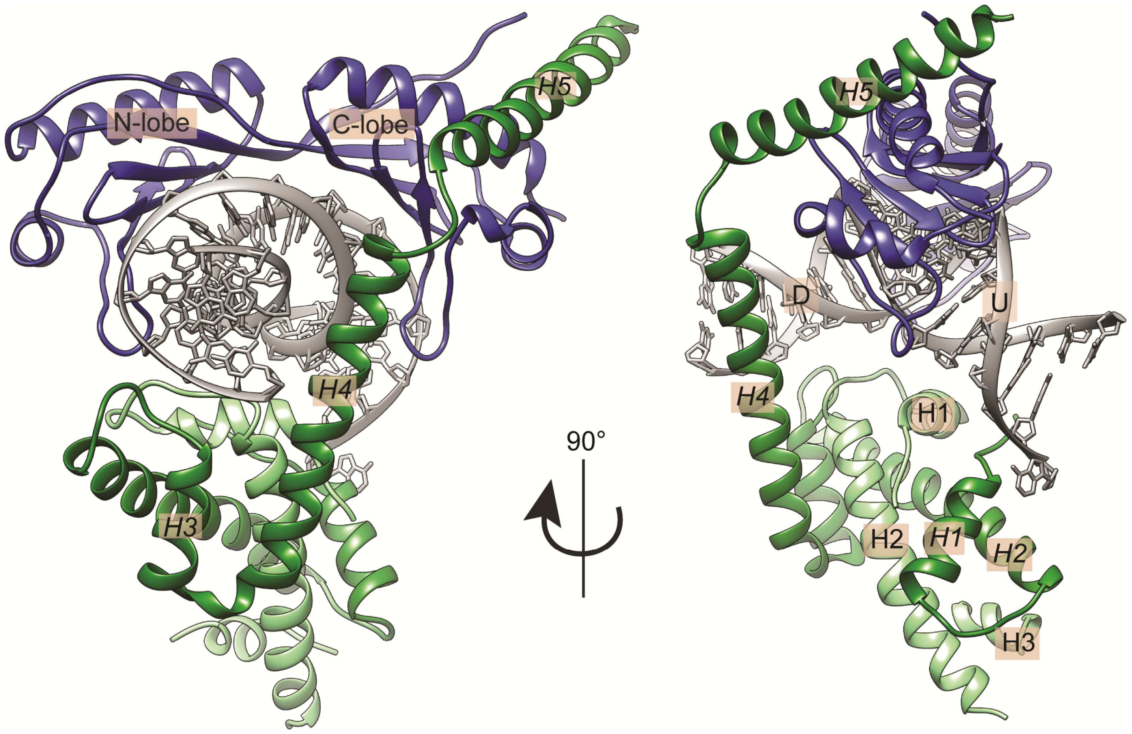

Figure 4. Cartoon representation of the *Homo sapiens* TBP–DNA–NC2 complex crystal structure solved at 2.7 Å resolution [107].

TBP is shown in dark blue. The TATA-containing DNA fragment is depicted in gray. The subunits of NC2 heterodimer: NC2α/DRAP and NC2β/Dr1 are shown in light and dark green, respectively. The key secondary structure elements as well as the upstream (U) and downstream (D) side of the promoter are annotated. Helices H1, H2 and H3 of NC2α as well as *H1*, *H2* and *H3* of NC2β assemble into histone fold domain and bind to the underside of the TATA box, opposite of the TBP's binding site. Helix *H5*, joined with the histone fold domain via helix *H4*, binds to the top surface of TBP, thereby locking it on the promoter DNA and blocking its association with GTFs.

bound C-terminal helix *H5* of NC2β. Thus, the localization of the NC2β's C-terminal helix provided the first structural explanation for blockage of TFIIB entry to PIC. Although the antagonistic effects of NC2 on TFIIA and TFIIB association with TBP–DNA complexes were shown in numerous biochemical experiments [94]–[96], [100], [102] and via complementation studies in yeast [100], [104], the sterical hindrance of NC2 and TFIIA binding was not obvious from the analyzed crystal structures [111], [112]. Eventually, Ebright and colleagues using a site-specific protein–protein photocrosslinking approach showed a sterical incompatibility between TFIIA and NC2α at TBP helix H2 in the regions which were omitted from the constructs used in the crystallization of TBP–DNA–NC2 and TBP–DNA–TFIIA complexes [113].

2.2.3 NC2 alters the TBP–promoter structure

DNase I footprinting experiments revealed that binding of NC2 to the TBP–DNA complexes influences DNA conformation [114]. Moreover, single-molecule FRET, restriction digest-coupled electrophoretic mobility shift (RCE) and crosslinking restriction digest-coupled immunoprecipitation (CRIP) experiments demonstrated that NC2 repositions TBP towards the DNA ends [114]. Observed NC2-induced lateral mobility of TBP on DNA was proposed to explained how NC2, sliding TBP off the promoter regions *in cis*, could negatively affect the very first stages of transcription initiation process [114]. The same mechanism was also proposed to account for NC2's activation role; NC2-induced sliding could theoretically enable TBP’s repositioning towards the promoter sites [114].

2.2.4 Mot1 and NC2 play similar roles *in vivo*

Several lines of evidence indicate that Mot1 and NC2 have related functions with respect to transcription *in vivo* (see below). For example, the *bur6* mutation was identified in the same genetic screen as *bur3*/*mot1* mutation and displayed the same phenotype [11], [12]. ChIP and mRNA level profiling of the temperature sensitive strains as well as comparison of individual microarray profiles have shown that Mot1 and NC2 not only interact genetically, but largely overlap in localization and function both *in vitro* and *in vivo* [18], [20]. For example, a study in which 90% of all class II genes in yeast were analyzed by ChIP-chip revealed that more than 97% of all Mot1-bound promoters overlap with NC2α or NC2β-bound promoters in exponentially growing cells [97]. Analogously, highly overlapping sets of Mot1- and NC2β-dependent genes, be it up- or downregulated, were shown in a direct study applying an anchor-away technique [26]. Consequently, NC2β-repressed genes are preferentially TATA-enriched and SAGA-dominated, in contrast to activated housekeeping genes, which are TATA-less and TFIID-dependent promoters [26], [35]. In *Drosophila,* NC2 heterodimer next to Mot1 serves as general activator of DPE-dependent transcription with a TATA-specific repression function [36], [115]. Furthermore, the anchor-away depletion of NC2β results in synthetic lethality in Δ*SPT7* background, thereby implicating a functional link to the SAGA complex and Mot1 [26]. Some single studies, however, do not report significant correlation between NC2α association and TATA box on human promoters [116]. Instead, negative correlation between NC2 occupancy and the presence of TFIIB responsive elements (BREs) was found [103], [117].

Interestingly, the promoter association of NC2 is dramatically increased in the absence of functional Mot1, which would imply that these two regulators compete for the association with TBP or that the decreased level of Mot1 results in inefficient dissociation of NC2 from promoter sites [19], [118]. The latter option was supported by the results presented in Schluesche *et al.,* where extremely low off-rate of the TBP–NC2 complexes from the promoter sites were shown *in vitro* [114] and by Timmers group who observed slowed dissociation of TBP and NC2 from *HXT2* promoter in *mot1-1* conditional mutant strain after the glucose shift [97]. Consistent with these results, Auble's group identified a TBP mutant bypassing the requirement of Mot1 *in vivo* with greatly decreased affinity to NC2 *in vitro* [59]. Moreover, fluorescence recovery after photobleaching (FRAP) live cell imaging in yeast [119] and in human cells [118] showed that Mot1 regulates the release of TBP from chromatin. Importantly, the same method revealed that NC2 has a totally opposite effect of Mot1 and that combined knock-down of NC2 and Mot1 restored the dynamics of TBP to the level of the untreated cells [118]. Thus, Mot1 appears to function as a factor, which regulates the accessibility of poised TBP–NC2 complexes in the cell.

Finally, yeast recombinant Mot1 and NC2 were able to simultaneously bind TBP–DNA complexes in EMSA [48]. Stable Mot1–TBP–DNA–NC2 complexes were subsequently isolated from yeast chromatin extracts [97]. In both cases, these complexes were shown to be disrupted upon ATP addition. A proteomic analysis of yeast Mot1-associated factors also confirmed robust association of Mot1, TBP and NC2 subunits [120]. Although the formation of BTAF1–TBP–DNA–NC2 complexes was not observed in the case of human proteins [121], simultaneous binding of Mot1 and NC2 to the same TBP–DNA complex is fully supported by the structural data [47], [107]. However, the exact character of Mot1–NC2 interplay is still barely understood.

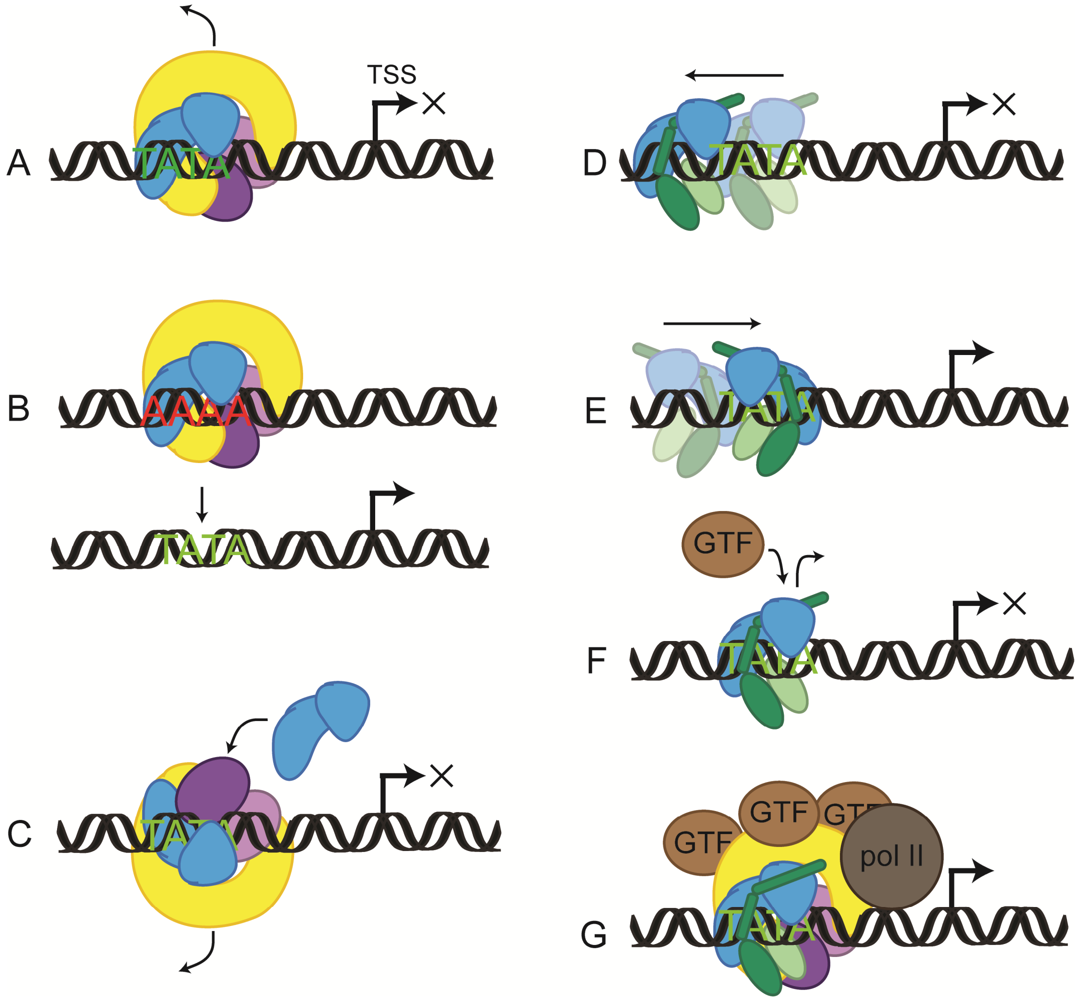

Figure 5. Impact of Mot1 and NC2 action on gene expression.

Transcription start site (TSS) is depicted by an arrow. The black cross (x) represents events, which lead to blocked transcription initiation. **(A)** Mot1 ejects TBP from core promoter. **(B)** Mot1 displaces TBP from inappropriate genomic locations (i.e. nonpromoter DNA) to increase free TBP pool. **(C)** Mot1 removes TBP bound in the "wrong" direction to free the promoter and allow productive TBP binding. **(D)** NC2 diffuses TBP away from the promoter. **(E)** NC2 diffuses TBP in the direction of the promoter. **(F)** NC2 sterically prevents the entry of GTFs like TFIIA and TFIIB. **(G)** Mot1 and NC2 direct the formation of alternative functional PIC assemblies.

2.2.5 NC2α and NC2β may function as separate subunits

Formation of TBP-containing complexes is well documented not only for the NC2 heterodimer, but also for the separate α and β subunits. Human NC2β was shown to interact with TBP in EMSA [94], [106], pull-down experiments [106], [121] and in yeast two-hybrid assay [106]. Moreover, formation of TBP–DNA–NC2β and TBP–DNA–NC2β–TFIIA complexes in EMSA was reported [94]. In contrast to the human NC2β, its yeast ortholog, however, did not bind TBP–DNA [22]. The TBP–NC2α interaction as well as the presence of TBP–DNA–NC2α–BTAF1 and TBP–NC2α–BTAF1 complexes was observed in pull-down and EMSA experiments [121]. Furthermore, human NC2α was reported to interact with BTAF1 in yeast two-hybrid assay and this interaction was dependent on the C-terminal acidic domain of NC2α [121]. Additional pull-down assays have shown that this interaction is not mediated via DNA. Interestingly, human NC2β in the absence of NC2α, although less efficiently that as the NC2 heterodimer, was also able to repress RNA pol II transcription *in vitro* [94], [106], [122]. Moreover, NC2α and NC2β were not found to be stably associated in exponentially growing yeast cells. Instead, their association followed glucose depletion after diauxic shift [123]. Western blot analysis of yeast WCE revealed a high molecular weight population of NC2β that was free of NC2α [99]. Furthermore, ChIP at selected promoters [123] as well as genome-wide study [97] showed differential distribution of NC2α and NC2β subunits upon shift to low glucose. Thus, NC2α–NC2β association seems to be regulated in response to environmental stress.

Both human NC2 subunits possess classical nuclear localization signal sequence and are imported to the nucleus as separate subunits or, preferentially, as a pre-assembled heterodimer [124]. Interestingly, only the NC2β subunit possesses a nuclear export signal sequence, which is masked upon the dimerization with NC2α, thereby ensuring that only complexed NC2β remains in the nucleus. This strongly points toward an independent role for NC2α in the nucleus. Importantly, phosphate-mimicking mutations of NC2β hamper its nuclear localization [124]. Thus, posttranslational modifications of NC2, with phosphorylation as one of many possibilities, could be a way of direct regulation of interaction between both subunits and their association with transcriptional machinery. Indeed, both NC2α and NC2β subunits are *in vitro* and *in vivo* substrates of casein kinase II [106], [121] and were found to be phosphorylated *in vivo* [95]. Interestingly, phosphorylation was shown to affect the association of NC2β with TBP [94] as well as either subunit with DNA [96]. Furthermore, NC2β was shown to be involved in repression of selected RNA pol III-transcribed genes not only *in vitro* [125] but also *in vivo*, both in yeast [99] and in human cells [126]. To date, there has been no evidence that NC2 affects RNA pol I-driven transcription [99], [125], [126] or that NC2α has an effect on RNA pol III transcription [126].

Finally, partial disruption of the recombinant human NC2 heterodimer in the presence of purified TBP and BTAF1-enriched lysate [121] as well as ATP-dependent dissociation of the NC2 heterodimer in the Mot1–TBP–DNA–NC2 complex isolated from chromatin extracts [97] were observed. However, how Mot1 would contribute to the regulation of NC2α–NC2β association remains unknown.

3. AIMS OF THE RESEARCH PROJECT

Swi2/Snf2 enzymes play many important roles in various basic cellular processes like DNA replication, recombination, repair and transcription. Despite extensive studies, the detailed mechanism of Swi2/Snf2 translocation remains largely unknown. Many studies have aimed at understanding the mode of action of Swi2/Snf2 translocases. Nevertheless, the existing hypotheses are still primarily based on the results obtained for related SF1 and SF2 *bona fide* helicases and other SF2 translocases, which are much better characterized on structural level. In order to answer the piling up questions regarding the detailed mechanisms employed by Swi2/Snf2 ATPases, an atomic view at a Swi2/Snf2 remodeler in the presence of its substrate, DNA and nucleotide is required.

One of the major obstacles in studying Swi2/Snf2 ATPases is the fact that most of the family members assemble into multisubunit complexes and act on complex protein–DNA substrates, e.g. nucleosomes, which make the structural analysis very challenging. Thus, it appears that the fundamental properties of all Swi2/Snf2 ATPases that allow these enzymes to accomplish their specific tasks via translocation along double-stranded DNA form at the same time critical barrier across the way to understand them better.

The ultimate goal of this study was to provide a mechanistic model of the ATP-dependent remodeling reaction employed by Swi2/Snf2 enzymes based on a hybrid structural characterization of Mot1, the first Swi2/Snf2 member for which biochemical activity has been demonstrated *in vitro*. Importantly for the structural analysis, the function of Mot1—ATP-dependent disruption of TATA box-binding protein (TBP)–DNA complexes—does not require the presence of any associated subunits. Therefore, Mot1 in complex with its relatively simple TBP–DNA substrate serves as a perfect model system for *in vitro* studies of Swi2/Snf2 translocases.

4. RESULTS

4.1 Analysis of Mot1–NC2 complexes

4.1.1 Gel filtration

NC2 stabilizes formation of the Mot1–“substrate” complexes

Intact Mot1–TBP–DNA–NC2 complexes can be isolated from *Saccharomyces cerevisiae* chromatin extracts [97]. Formation of the Mot1–TBP–DNA–NC2 complex and its ATP-dependent disruption was also shown in EMSA performed on the recombinant yeast, but not the human proteins [48], [121]. Thus, the ability of Mot1 and NC2 to form stable complexes on DNA-bound TBP was tested on the *Encephalitozoon cuniculi* proteins.

TBP–NC2 complexes were shown to have limited specificity for TATA DNA sequences [127]. Similarly, Mot1-associated TBP does not discriminate between TATA and non-TATA DNA [49], [87]. Therefore, in order to ensure homogeneous binding, DNA substrates used in this test always contained TATA box consensus sequence (5´–TATAAAAG–3´). As shown in **Figure 6** (black lines), stable *E. cuniculi* Mot1–TBP–DNA–NC2 and Mot1^{NTD}–TBP–DNA–NC2 complexes could be efficiently formed in the presence of TATA-containing dsDNA and could be separated from the subcomplexes (e.g. TBP–DNA–NC2 complexes) and single protein or DNA components by size exclusion chromatography. In contrast, Mot1–TBP–DNA and Mot1^{NTD}–TBP–DNA complexes were much less stable in gel filtration (**Figure 6**, gray lines). Of note is that the formation of the full-length Mot1-containing complex was not affected by the presence of nonhydrolyzable ATP analogs or ADP. Formation of the NC2-containing complexes was also not affected by the presence of the latch region; Mot1 and Mot1^{NTD} constructs supported complex formation as efficient as Mot1$^{\Delta latch}$ and Mot1$^{NTD\Delta latch}$ mutants (not shown). This was unexpected, since the latch region was shown to be responsible for ATP-independent disruption of TBP–DNA complexes [47]. Additionally, the formation of Mot1–TBP–DNA–NC2 and Mot1^{NTD}–TBP–DNA–NC2 complexes was found to be strictly DNA-dependent. Although Mot1^{NTD} co-eluted with TBP and NC2 in the absence of DNA, full-length Mot1 bound only TBP (**Figure 7**).

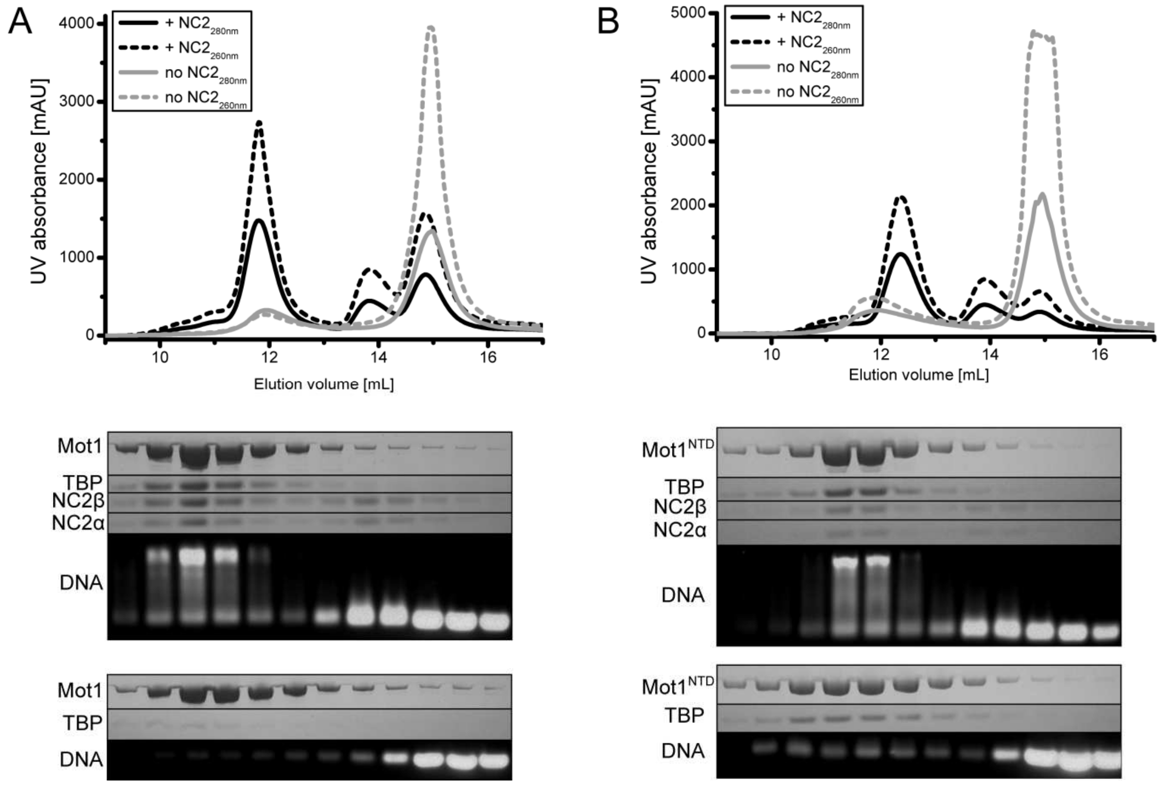

Figure 6. NC2 stabilizes the Mot1–TBP–DNA and Mot1^{NTD}–TBP–DNA complexes in size exclusion chromatography.

(A) Top: elution profiles of Mot1–TBP–DNA (gray) and Mot1–TBP–DNA–NC2 complexes (black) obtained in gel filtration experiments. Absorbance at 260 nm and at 280 is shown as dashed and solid lines, respectively. Bottom: analysis of the fractions by SDS-PAGE (Coomassie staining) and agarose gel electrophoresis (Gel-Red staining . **(B)** Same as (A) is shown for the Mot1^{NTD} construct.

Taken together, the addition of the NC2 subunits greatly increased the stability of DNA-containing complexes in the gel filtration. Therefore, NC2 was included in most of the crystal setups, which greatly contributed to the successful finalization of the crystallization experiments (see below).

NC2β interacts with Mot1 in a TBP-dependent manner in the absence of DNA

The ability of separate α and β subunits of NC2 heterodimer to form various TBP-containing complexes has been shown both for human and yeast orthologs [94], [106], [121]. Thus, the ability of NC2β to form alternative complexes in gel filtration chromatography was investigated. Experiments testing the ability of NC2α to form adequate complexes unfortunately could not be performed, since this subunit of the *E. cuniculi* heterodimer could

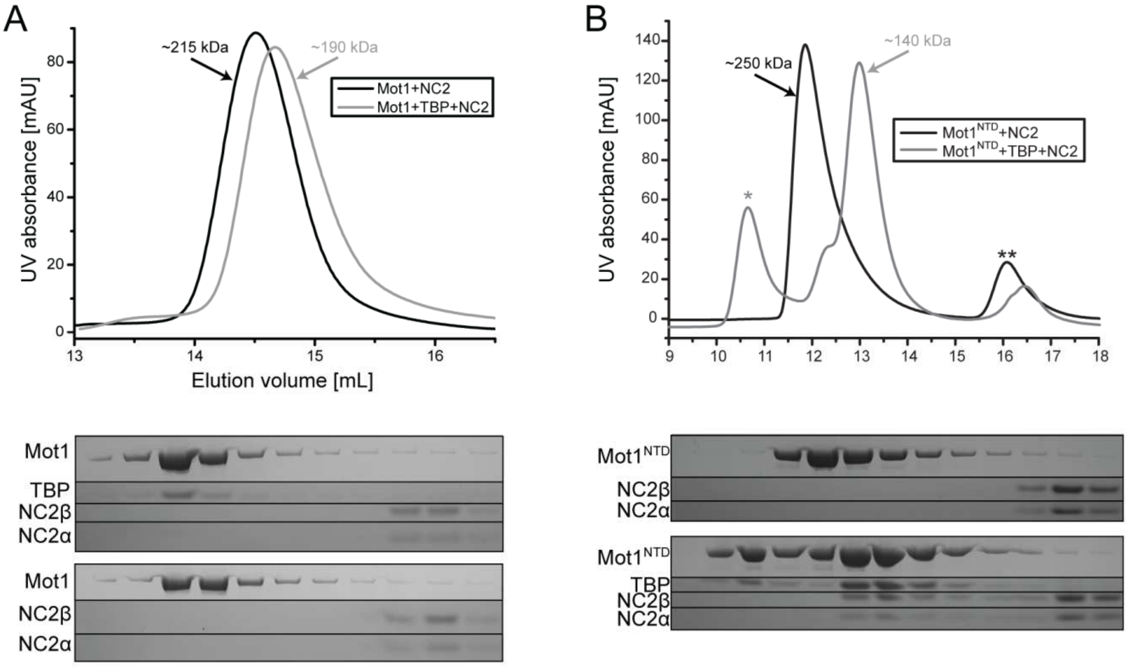

Figure 7. Gel filtration analysis of Mot1–TBP–NC2 and Mot1^{NTD}–TBP–NC2 complexes in the absence of DNA.

(A) Top: in gel filtration experiments, NC2 is not able to interact with Mot1 or Mot1–TBP complex in the absence of DNA. Absorbance at 280 nm is shown. Bottom: analysis of the fractions by SDS-PAGE (Coomassie staining). **(B)** Analogous analysis of the Mot1^{NTD} construct shows weak interaction between Mot1^{NTD}, TBP and NC2 in the absence of DNA. The approximate molecular weights of the complexes were estimated empirically by calibration of the columns with gel filtration protein standard. The peaks corresponding to higher-order Mot1^{NTD}–TBP complexes (*) and NC2β (**) are marked. Molecular weight of the *E. cuniculi* Mot1, Mot1^{NTD}, TBP, and NC2β is 144, 89, 22 and 17 kDa, respectively.

not be express solubly. As already discussed, the NC2 heterodimer was not able to form complexes with Mot1 and TBP in the absence of DNA (**Figure 7**). Interestingly however, the NC2β subunit readily formed complexes with Mot1^{NTD} or Mot1 and TBP (**Figure 8**). Moreover, the formation of the NC2α-deprived complexes in gel filtration was strictly dependent on the presence of TBP, since no Mot1–NC2β and Mot1^{NTD}–NC2β complexes could be detected. Interestingly, Mot1–TBP–NC2β complexes were present in two distinct "monomeric" and "dimeric" forms (**Figure 8**B), whereas Mot1^{NTD}–TBP–NC2β complexes formed only "dimers". The Mot1^{NTD} construct is known to form dimers in solution ([47] and **Figure 7**B), but multimeric species of the full-length Mot1 have not been detected. The transition between those states was not affected by the presence of magnesium and other divalent cations (zinc, calcium and manganese), ADP, AGS, different salt conditions,

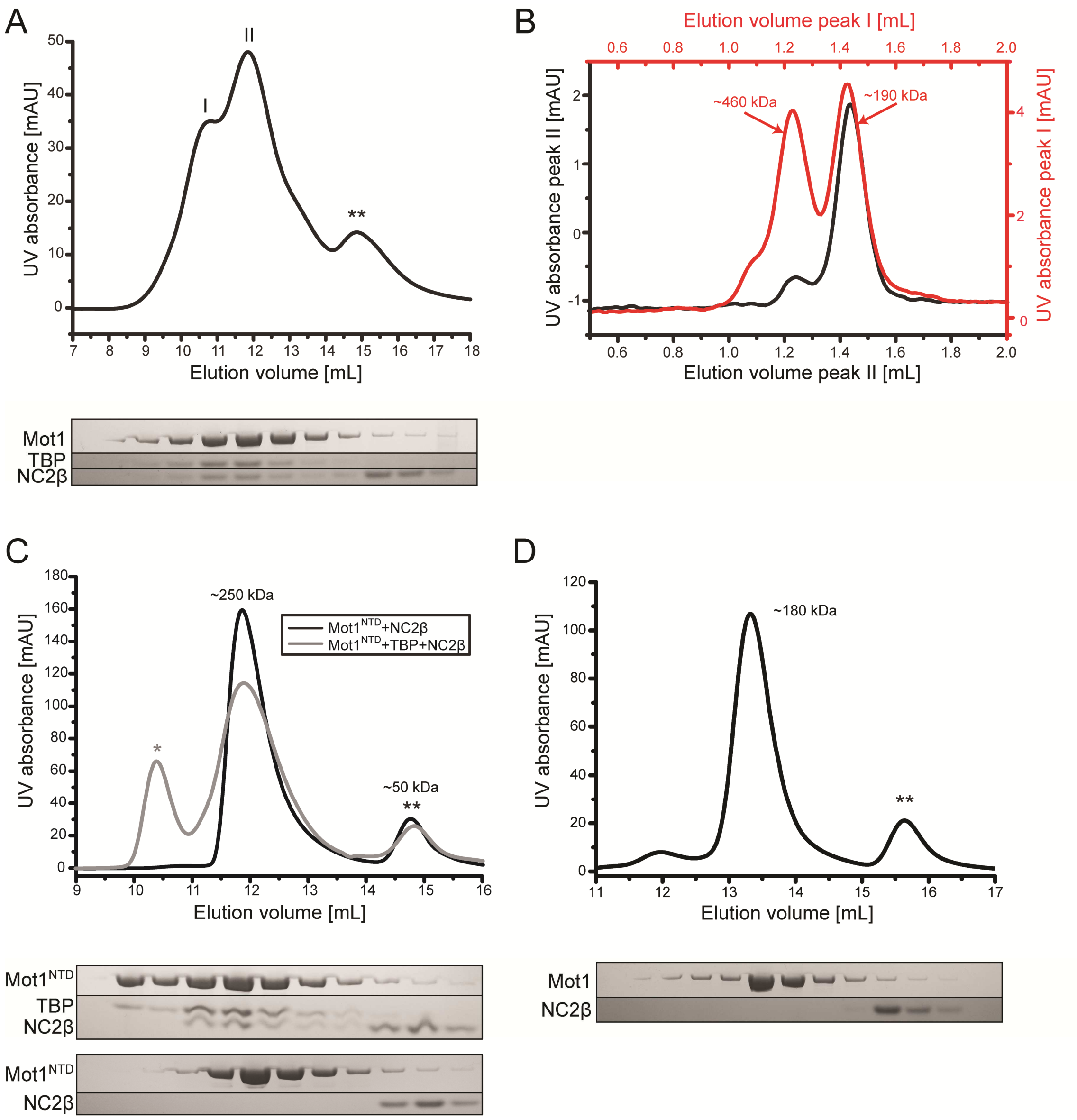

Figure 8. Gel filtration analysis of Mot1–TBP–NC2β and Mot1^{NTD}–TBP–NC2β complexes.

(A) In contrast to the results shown in Figure 7, Mot1 and NC2β form ternary complex in the presence of TBP (peak I and II). **(B)** Further analysis of peaks I and II, which were re-run on an analytical gel filtration column, suggests the presence of equilibrium between "monomeric" (peak II) and "dimeric" (peak I) Mot1–TBP–NC2β species. **(C)** Analogously to the full-length Mot1, the Mot1^{NTD} construct forms Mot1^{NTD}–TBP–NC2β but not Mot1^{NTD}–NC2β complexes. Panel **(D)** shows that Mot1 does not efficiently associate with NC2β in gel filtration in the absence of TBP. The approximate molecular weights of the complexes were estimated empirically by calibration of the columns with gel filtration protein standard. The peaks corresponding to higher-order Mot1^{NTD}–TBP complexes (*) and NC2β (**) are marked. The fractions were analyzed by SDS-PAGE (Coomassie staining). Molecular weight of the *E. cuniculi* Mot1, Mot1^{NTD}, TBP, and NC2β is 144, 89, 22 and 17 kDa, respectively.

presence/absence of a reducing agent or the order of mixing the components before gel filtration (not shown). Instead, these two forms appeared to persist in dynamic monomer/dimer equilibrium likely depending on the sample concentration.

Taken together, the initial experiments performed on the *E. cuniculi* proteins show strong interaction between the NC2β subunit and Mot1–TBP complex in the absence of the associated NC2α subunit. This is of potential interest, since separate role for NC2α and NC2β in transcription regulation has been proposed (see section **2.2.5**). However, adequate Mot1–TBP–NC2β complexes were not detected for human proteins [121] and not tested yet on yeast orthologs.

4.1.2 Electrophoretic mobility shift assay (EMSA)

NC2β does not substitute for NC2 in DNA-containing complexes

Given the fact that NC2β could efficiently incorporate into Mot1–TBP–NC2β complexes, the ability of NC2β to form DNA-containing complexes was tested. Human NC2β has been reported to form TBP–DNA–NC2β complexes in EMSA and to repress RNA pol II transcription *in vitro* [94], [106], [122]. In comparison to its human ortholog, the yeast NC2β could not form TBP–DNA–NC2β complexes [22].

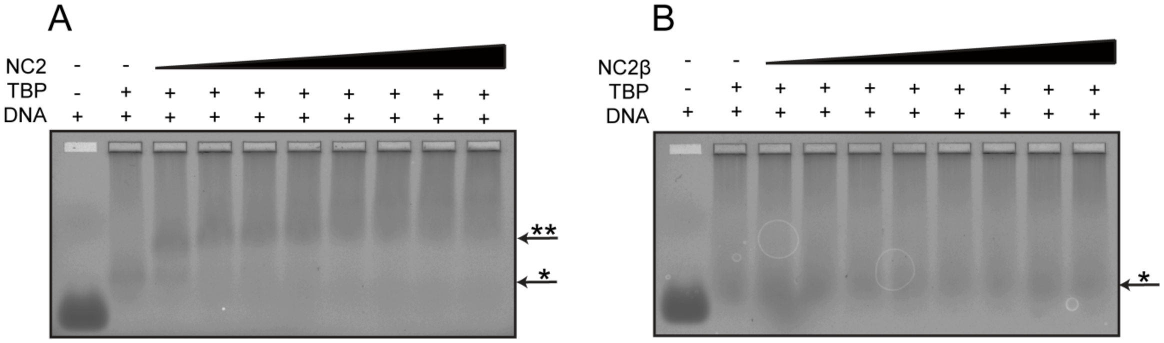

Figure 9. The NC2β subunit does not bind TBP–DNA complex in the absence of NC2α.

(A) NC2 readily forms ternary complexes with TBP and DNA in EMSA (**). **(B)** NC2β does not bind to TBP and DNA under the same conditions and in the same concentration range. Only TBP–DNA complexes are observed (*). To enable visualization of the DNA-bound complexes, 5'-FAM-labeled 42mer TATA dsDNA was used in both experiments.

As shown in **Figure 9**, *E. cuniculi* NC2β was unable to bind to TBP–DNA. In gel filtration, the addition of Mot1 did not rescue the disability of NC2β to form the complex (not shown). This demonstrates that the presence of NC2α subunit is required to form TBP–DNA–NC2 and Mot1–TBP–DNA–NC2 complexes in the *E. cuniculi* system, whereas NC2β associates with Mot1 in the absence of DNA. Thus, the *E. cuniculi* orthologs again behaved differently to the human and similarly to their yeast relatives. This might point towards functional differences between human and fungal proteins.

4.2 X-ray crystallographic analysis of the Mot1^{NTD}–TBP–DNA–NC2 complex

4.2.1 Crystallization and structure determination

The structural bases of the final product state of Mot1-catalyzed reaction, i.e. Mot1–TBP interaction have been described previously [47]. In order to gain structural information about how Mot1 engages TBP and DNA before the remodeling reaction takes place, various crystallization experiments were performed. Homogeneous samples of *E. cuniculi* Mot1–TBP–NC2 complexes in the presence of different TATA box-containing DNA substrates of various lengths and including all available Mot1 constructs (Mot1, Mot1$^{\Delta latch}$, Mot1^{NTD}, and Mot1$^{NTD\Delta latch}$) were screened for the ability to form crystals or crystalline precipitate. The Mot1^{NTD} portion (residues 1–778) and TBP (full-length) used in this study had exactly the same residue boundaries as the construct which has been used in previous studies [47] but lacked the N-terminal His$_6$-tag, which was cut off during the purification process thanks to the introduction of TEV protease recognition site. Full-length NC2β subunit also possessed a cleavable N-terminal His$_6$ tag, whereas NC2α subunit was untagged.

All the attempts to obtain crystals of the ensembles containing Mot1^{CTD}, also in the presence of different nucleotides, e.g. ADP, AGS, and ABF, were not successful. After extensive screening, the Mot1^{NTD}–TBP–DNA samples after long incubation times (up to several weeks) in some cases led to Mot1^{NTD}–TBP crystals, confirming the inherent instability of the ternary complex observed in the gel filtration experiments. In contrast, in the presence of NC2 and only for a specific subset of DNA substrates (see **Table 13** and **14**) Mot1^{NTD}–TBP–NC2–DNA and Mot1$^{NTD\Delta latch}$–TBP–DNA–NC2 complexes crystallized together (**Figure 10**). Both complexes exhibited almost identical preference for the crystal growth conditions. However, shorter DNA samples (14 bp) did not support the NC2-dependent complex stability and, again, the Mot1^{NTD}–TBP crystals were obtained. The presence of the DNA in the crystals could be effectively assessed based on the strength of light polarization properties (**Figure 10**B).

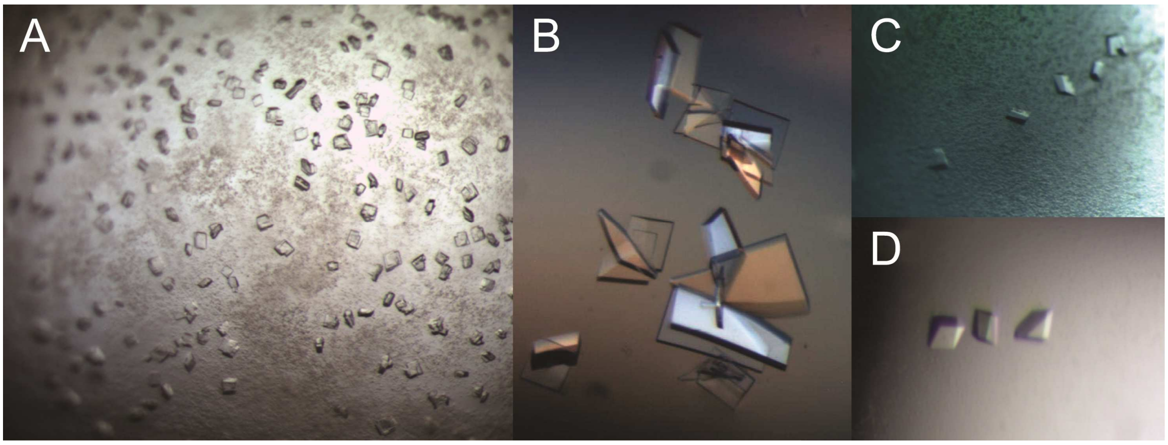

Figure 10. Results of the crystallization experiments.

(A) Initial crystals of *E. cuniculi* Mot1$^{NTD\Delta latch}$–TBP–DNA–NC2 complex forming numerous small plate clusters. **(B)** Crystal morphology in condition shown in (A) after optimization. The picture was taken using a polarization filter. **(C)** Crystals of the selenomethionine-derivatized *E. cuniculi* Mot1^{NTD}–TBP–DNA–NC2 complex obtained in the course of streak seeding experiments. **(D)** View of the streak-seeded crystals grown in the condition used for the actual data collection (0.2 M imidazole malate pH 5.1 and 11% PEG4000).

Several hundred of Mot1$^{NTD\Delta latch}$–TBP–DNA–NC2 and Mot1^{NTD}–TBP–DNA–NC2 complex crystals originating from different crystallization conditions were screened for X-ray diffraction. Majority of the crystals diffracted to a limited resolution of 5 to 8 Å and were often characterized by “streaky”, poorly-defined reflections. The length of the DNA used had a great impact on the ability to obtain crystals, pointing out at possible involvement of DNA in the formation of the crystal contacts. Therefore, different lengths and variations of the overhangs were incorporated into the screening in order to find a DNA substrate improving crystal morphology and diffraction quality (listed in detail in **Table 13** and **14**). Additionally, different pre- and post-crystallization treatments like crystal annealing, glutaraldehyde crosslinking, dehydration [128] or lysine methylation [129] were applied. However, none of these methods showed any improvement in diffraction quality and, therefore, they are not described here in detail. Moreover, in order to test whether the cryocooling conditions negatively affect crystal diffraction, data collection at room temperature was performed but again, no difference in diffraction at room temperature and at 100 K was observed as well.

Finally, three crystals of the selenomethionine-derivatized Mot1^{NTD}–TBP–DNA–NC2 complex diffracting below 4.5 Å were found. Selenomethionine incorporation is a standard method for introducing heavy atoms to protein crystals (for Se, Z=34) [130]. In principle, selenomethionine has similar properties to methionine (Z=16), like volume and shape. This method facilitates not only experimental phase determination in crystallography by single- (SAD) or multiwavelength anomalous dispersion (MAD). The presence of selenium atoms often changes protein hydrophobicity it is possible that selenomethionine-derivatized protein crystals can be obtained even if no native crystals are present. It is, therefore, possible that selenomethionine derivatization directly contributed to the improved diffraction of the crystals. However, most of selenomethionine-derivatized Mot1^{NTD}–TBP–DNA–NC2 complex crystals still diffracted poorly.

A data set extending to 3.8 Å resolution was collected from a crystal formed using the Mot1^{NTD}–TBP–DNA–NC2 complex sample containing a 24 bp dsDNA oligonucleotide (5'–AGTAGGGCTATAAAAGGGGGTGGC–3', top strand). Unfortunately, the absorption spectrum of selenium atoms was not recorded due to technical problems at the beamline. Therefore, the data set was collected at the theoretical wavelength of K absorption edge of selenium (λ=0.9794 Å). The complex crystallized in the space group C 1 2 1 (a=150.6 Å, b=140.3 Å, c=90.8 Å, α=90.0°, β=113.7°, γ=90.0°) with 60% solvent content and one complex per asymmetric unit.

The structure was successfully solved by the molecular replacement method using *E. cuniculi* Mot1^{NTD} and TBP molecules from the Mot1^{NTD}–TBP complex crystal structure as well as human TBP–DNA–NC2 complex crystal structure as initial models [47], [107]. Unambiguous density interpretation, particularly helpful in defining side chains positions, was achieved using real space-based electron density modification method like solvent flattening using *PARROT* [131], [132] as well as modified 2 *Fo* – *Fc* maps using *B*-factor sharpening and Feature Enhanced Map (both implemented in *PHENIX* [133]). Solvent flattening method exploits the fact that average electron density of protein and solvent regions are different [134]. After the solvent and protein region masks are defined, the electron density of solvent region is set to a constant value and new structure factors are computed. Finally, the newly obtained phases are combined with the original ones and improved map is obtained. *B*-factor sharpening is also a very useful tool for the enhancement of low resolution maps [135]. It is a resolution-dependent weighting function applied to a particular electron density map. Adjusting the *B*-factor results in up-weighting of higher resolution terms and, therefore, increases detail for higher resolution features such as side chain conformations. Feature enhanced map is a modified $2Fo - Fc$ map which i.a. exploits the advantages of composite residual OMIT maps, *B*-factor sharpening and histogram equalization [133]. FEM maps are characterized by reduced noise and bias and eliminate the need to choose and arbitrary map contouring cutoff.

Applied density modification methods enabled *de novo* chain tracing of the very N-terminal region of Mot1 HEAT repeat domain (i.e. first 40 amino acids comprising helix H1 and H2 of HR1 as well as helix H3 of HR2) which had different sequence register than reported for the *E. cuniculi* Mot1^{NTD}–TBP crystal structure (**Figure 11**). The difference in the electron density quality between the two structures was likely a result of the crystal packing. In the Mot1^{NTD}–TBP–DNA–NC2 crystal structure reported here, the very N-terminus of

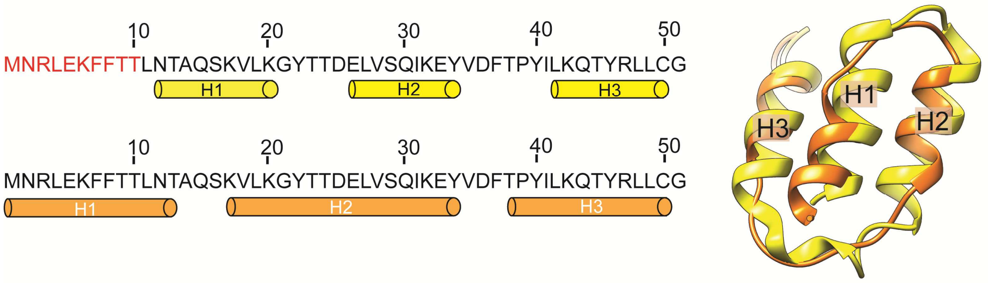
10
20
30
40
50
MNRLEKFFTTLNTAQSKVLKGYTTDELVSQIKEYVDFTPYILKQTYRLLCG
H1
H2
H3
10
20
30
40
50
MNRLEKFFTTLNTAQSKVLKGYTTDELVSQIKEYVDFTPYILKQTYRLLCG
H1
H2
H3
H3
H1
H2

Figure 11. Shift in the sequence register between Mot1^{NTD} in Mot1^{NTD}–TBP crystal structure [47] and Mot1^{NTD}–TBP–DNA–NC2 crystal structure.

Left: Assignment of the secondary structure for the first 50 amino acids of Mot1^{NTD} in Mot1^{NTD}–TBP crystal structure (top, yellow) and Mot1^{NTD} in Mot1^{NTD}–TBP–DNA–NC2 crystal structure (bottom, orange). Right: superimposition of the first 50 amino acids shows that in the Mot1^{NTD}–TBP–DNA–NC2 N-terminus of Mot1^{NTD} adopts more α-helical structure.

Mot1 is largely engaged in the crystal contact formation and the density of this region is well defined despite relatively low resolution. In contrast, the packing of the Mot1 N-terminus in the Mot1^{NTD}–TBP crystals was unfavorable. Additionally, the electron density of this region is very poor, even despite moderate resolution (3.1 Å).

Owing to poor diffraction, the anomalous signal of selenomethionine atoms did not allow the experimental phasing. Nevertheless, computing the anomalous difference map (using *FFT*, part of CCP4 suite [131]), which shows the positions of anomalous scatterers, was used for unambiguous assignment of the selenomethionine side chains. This was particularly important in the case of NC2α and NC2β polypeptide chains, since the side chains of the histone fold part of NC2 were omitted from the model owing to poor electron density map quality of this region. However, anomalous difference density peaks (up to 5σ) were present in some cases (**Figure 12**B). Final model of the Mot1^{NTD}–TBP–DNA–NC2 crystal structure is characterized by R_{work}/R_{free} of 23.5/25.8% (according to BUSTER) and good stereochemistry (**Table 1**).

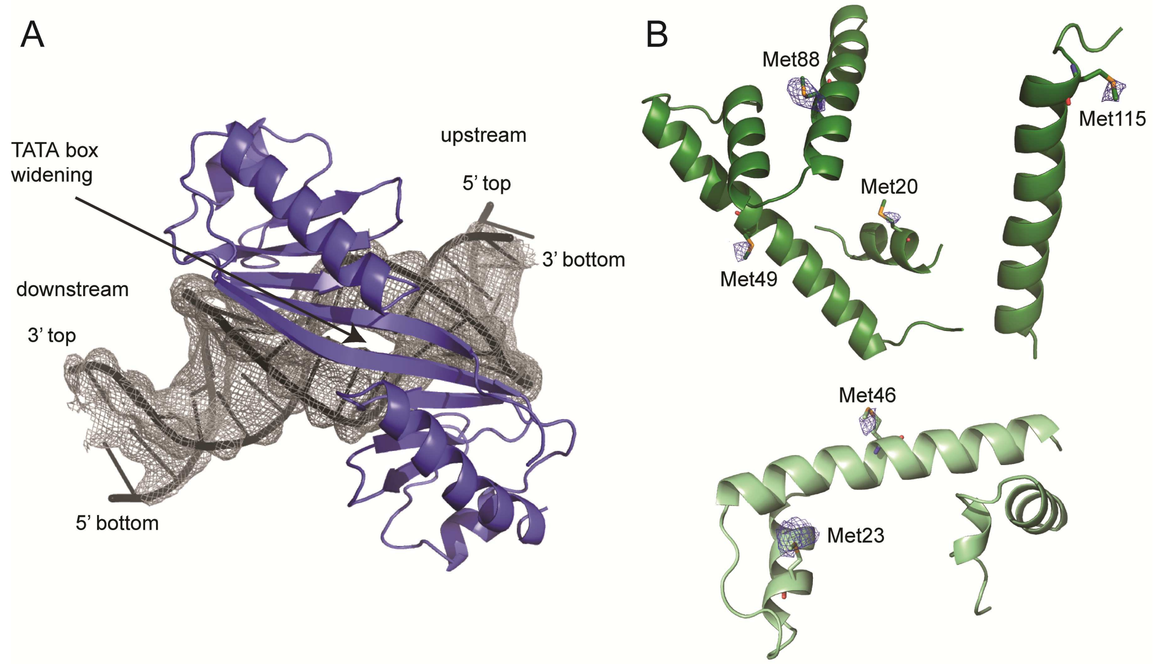

Figure 12. X-ray electron density maps.

(A) $2Fo - Fc$ electron density map of DNA bases displayed at 1σ contour level (gray mesh). TBP is additionally shown in blue. For clarity, electron density of the protein chain is not shown. The widening at the TATA box is nicely visible even at low resolution (marked with the arrow). **(B)** Weak anomalous signal of selenium atoms contoured at 4σ (gray mesh). Four out of seven (NC2β, top) and two out of five (NC2α, bottom) selenomethionine sites could be identified by this approach confirming the sequence register.

Table 1. Data collection and refinement statistics.

Equations defining R-values are standard and hence not defined.

Data collection		**Refinement**	
Space group	C 1 2 1	Resolution (Å)	49.17–3.8
Cell dimensions		$R_{\text{work}}/R_{\text{free}}$ (%)**	23.5/25.8(26.9/30.2)
a, b, c (Å)	150.6, 140.3, 90.8	No. atoms	
α, ß, γ (°)	90.0, 113.7, 90.0	Protein	8422
Resolution (Å)	49.17–3.8 (4.0–3.8)*	DNA	799
No. reflections		Ligand/ion	0
All	108074	Water	0
Unique	17163	Isotropic *B*-factors	
R_{merge} (%)	10.4 (78.9)	Protein	69
$CC_{(1/2)}$	99.8 (83.8)	DNA	135
$I/\sigma I$	7.5 (1.5)	R.m.s. deviations	
Completeness (%)	98.2 (93.5)	Bond lengths (Å)	0.009
Redundancy	3.4 (3.4)	Bond angles (°)	0.75
Wilson B factor (Å^2)**	139	Ramachandran (%)***	
		Favored	96
		Allowed	4
		Outliers	0

* Values in parentheses are for highest-resolution shell.
** Determined by BUSTER
*** Determined by MolProbity.

The model includes 39 out of 48 DNA bases present in the crystallization setup: bases 5–23 of the top TATA box strand and 2–21 of the bottom strand) as well as 89% of the protein residues; TBP 19–196, Mot1 1–97, 143–411, 415–484, 487–503, 510–778, NC2α 15–59 and 69–89, as well as NC2β 12–23, 29–101 and 110–137. The quality of the model can be additionally assessed by a fact, that a short 3_{10} helix located on the C-terminus of NC2α was observed, although it was not present in the initial model used during molecular replacement. This part of the NC2α polypeptide chain was omitted from the construct used for the crystallization of the human TBP–DNA–NC2 complex. This C-terminal helix is, however, an integral part of the fold present in crystal structures of other histone fold domain-containing proteins (e.g. NF-Y heterotrimeric transcription factor [109]). In the case of the *E. cuniculi*

NC2 ortholog, the presence of this region was responsible the NC2α–NC2β complex integrity, since NC2α$^{\Delta 79\text{-}95}$ could not have been co-purified with NC2β (data not shown).

4.2.2 Overview of the structure

In the crystal structure, show in **Figure 13**, one copy of each Mot1^{NTD}, TBP, NC2α, NC2β, and 24 bp DNA are found in the asymmetric unit and form an assembly of approximate dimensions of 100 Å x 100 Å x 95 Å. TBP slightly unwinds and sharply bends the TATA box DNA to form a unique saddle-shaped structure. Mot1 and NC2 seem to complement each other and form a "clamp" around promoter-bound TBP. The character of this interaction clearly explains NC2-dependent stabilization of the complex observed in EMSA and gel filtration and that Mot1 and NC2 do not interact in the absence of TBP and DNA. NC2 locks TBP on the promoter between its N-terminal histone fold domain (NC2^{HF}), which is bound to the underside of the promoter DNA, and the convex site-bound C-terminal helix *H5* of NC2β. The overall organization of the TBP–NC2–DNA complex in the Mot1^{NTD}–TBP–NC2–DNA crystal structure is highly similar to the human TBP–NC2–DNA complex [107]. Similarly, Mot1^{NTD} engages TBP mostly from the TBP's convex and "upstream" side, which is highly comparable for both Mot1^{NTD}–TBP and Mot1^{NTD}–TBP–NC2–DNA crystal structures.

Importantly, there is no interpretable electron density observed for the Mot1 latch region (residues 98–142), what indicates that this part of the polypeptide is disordered when Mot1 is bound to the TBP–DNA–NC2 substrate. This could occur because the Mot1^{NTD} does not possess a proper binding site for the latch or perhaps the latch is intrinsically disordered and undergoes a disorder-to-order transition only upon TBP binding. Alternatively, the association of the latch could be negatively affected by the crystal packing.

Mot1^{NTD} and NC2 directly interact on the promoter-bound TBP

Although the contacts of Mot1^{NTD} and NC2 within the complex are mainly TBP- and/or DNA-mediated, these two regulators interact directly on promoter-bound TBP molecule. Direct interaction of Mot1^{NTD} and NC2 leads to many small conformational alterations,

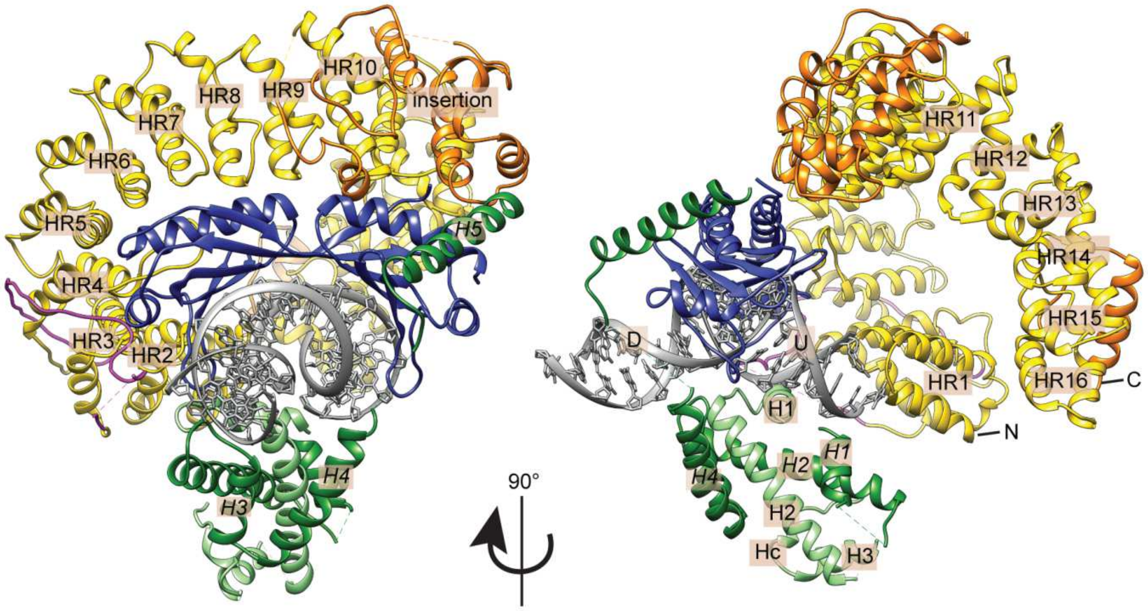

Figure 13. Crystal structure of the *E. cuniculi* Mot1^{NTD}–TBP–DNA–NC2 complex.

Front and side view of the structure and its secondary structure features. TBP is shown in blue. The HEAT repeats of Mot1^{NTD} are annotated as HR and shown in yellow. N- and C-terminal ends of Mot1^{NTD} are labeled N and C, respectively. The non-HEAT repeat regions and part of the latch region of Mot1^{NTD} are shown in orange and magenta, respectively. The subunits of NC2 heterodimer with their key secondary structure elements are shown in light green (NC2α) and dark green (NC2β). DNA is depicted in gray. The upstream (U) and downstream (D) side of the promoter are marked.

which will be discussed further in more detail.

First, the “anchor” helix *H5* of NC2β is bound to the upper side of the TBP’s convex side and forms direct contacts to the insertion domain of Mot1^{NTD}, the only non-HEAT repeat stretch in the N-terminal part of Mot1. As a consequence of this interaction, the interface between Mot1^{NTD} and TBP in the “substrate” state extends beyond HR 4 to 6 (as described for the “product” Mot1^{NTD}–TBP complex [47]) towards the C-terminus of Mot1^{NTD} and additionally engages HR7 to 10 and the insertion domain (**Figure 14**). Altogether, the interaction interface between Mot1^{NTD} and TBP’s convex site increases from ~900 Å^2 to over 1500 Å^2, as calculated using PISA server [136]. This interaction results in a substantial compaction of the α-helical HEAT repeat array.

Mot1^{NTD} binding affects the conformation of TBP, NC2, and DNA

The analysis of the root mean square deviation (r.m.s.d.) between different TBP crystal

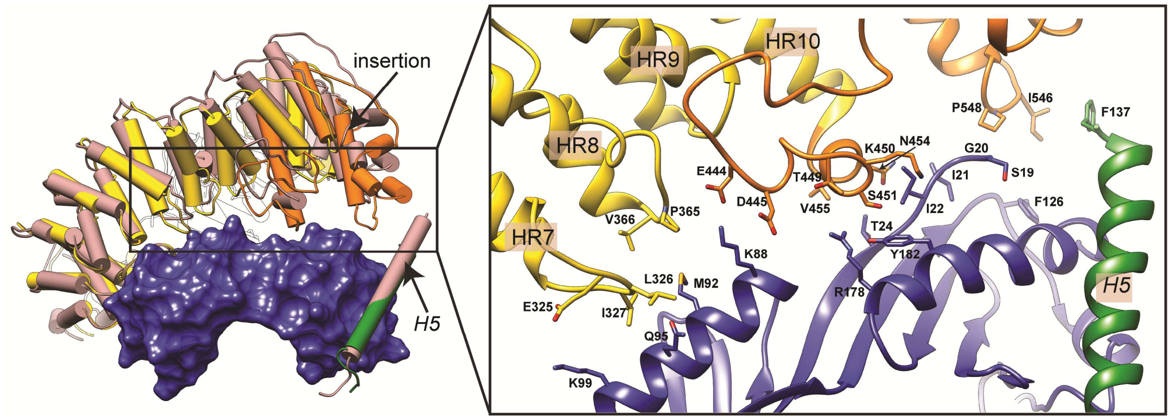

Figure 14. The interface between Mot1^{NTD} and TBP in the presence of NC2 and DNA.

Mot1^{NTD} and TBP from the Mot1^{NTD}-TBP structure, helix *H5* of NC2β and TBP from the TBP-DNA-NC2 structure as well as all three components from the Mot1^{NTD}–TBP–NC2–DNA crystal structure are here superimposed via TBP (represented by a blue surface). The elements from the Mot1^{NTD}–TBP–NC2–DNA crystal structure are color-coded as described in Figure 13, while the same elements from other structures are shown in light brown. This superimposition shows that Mot1 binding does not affect the position of *H5* on TBP. However, the HEAT repeat array of Mot1 undergoes reorganization in the presence of its substrate by shifting towards helix *H5*. The residues localized on the surface of the interaction sites are annotated.

structures shows that in the Mot1^{NTD}–TBP–DNA–NC2 complex structure TBP is mostly similar to its "product", Mot1-bound, state (r.m.s.d. of 0.69–0.87 Å) rather than to DNA-bound TBP (r.m.s.d. of 0.96) or free TBP (r.m.s.d. of 1.23 Å), superimposed in **Figure 15**A. This suggests that Mot1 binding might potentially have a destabilizing effect on the TBP–DNA interaction. Consequently, the ~90° kink in the TATA box region appears to be less distorted than reported for numerous TBP–DNA complex structures, including the TBP–DNA–NC2 complex (**Figure 15**B–C). This change results in the altered trajectory of the upstream DNA, bringing it closer to the N- and C-terminus of Mot1^{NTD} (**Figure 15**C). This is of potential interest since this DNA region has been shown to be directly occupied by Mot1^{CTD} [8], [9], [47], [59], [70]. Additionally, the first two HEAT repeats of Mot1 form a highly conserved and positively charged patch that is close to the upstream DNA and, in the context of full-length Mot1, could potentially contribute to a change in DNA trajectory induced by Mot1 binding.

Despite the changes in the DNA conformation, the interaction between the NC2^{HF} and upstream DNA closely resembles the interaction between the histones H2A/H2B and DNA within the nucleosome [108] and, consequently, in the TBP–DNA–NC2 crystal structure. A detailed analysis of the NC2^{HF}–DNA interaction site mediated by helix H1 of NC2α and

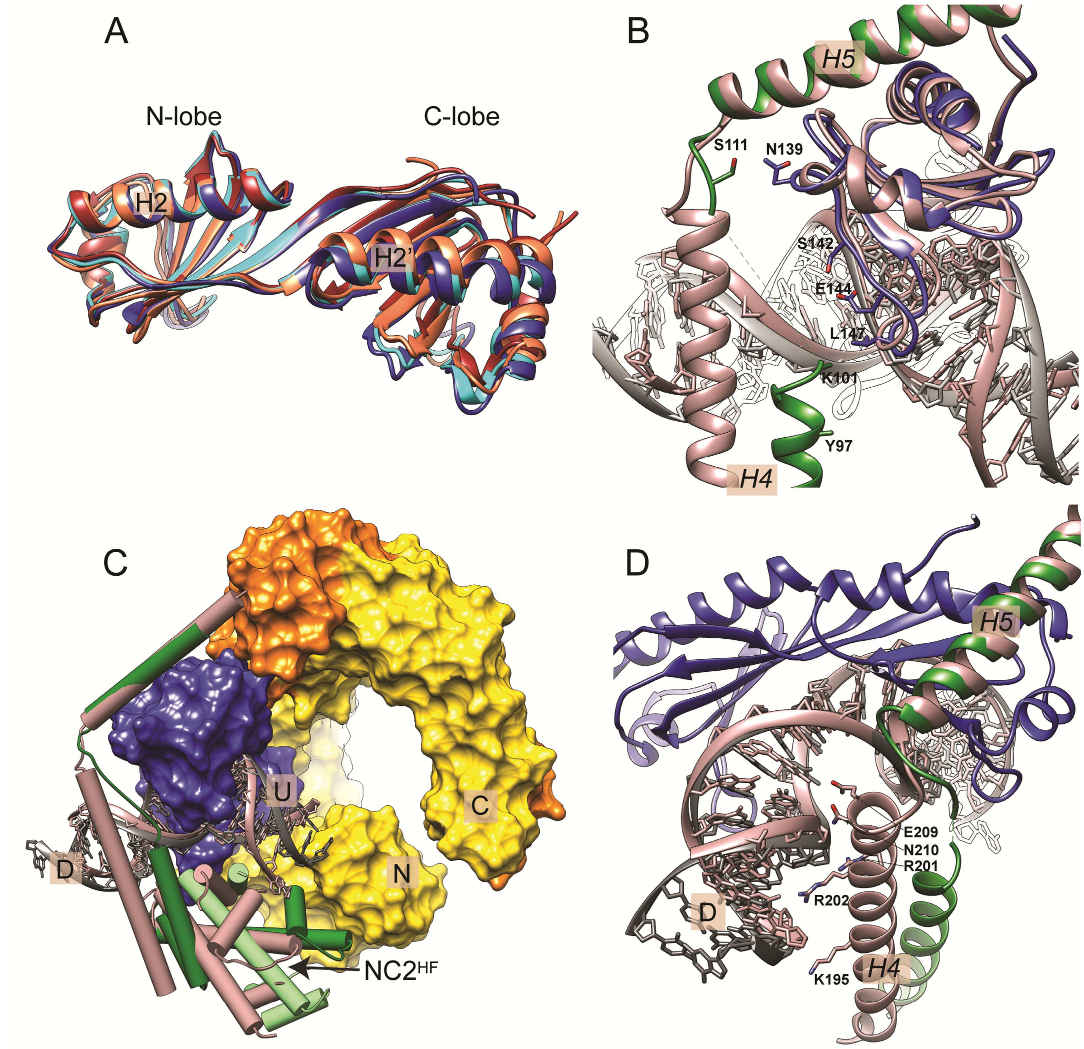

Figure 15. Changes in the TBP, NC2 and DNA conformation induced by Mot1^{NTD} binding.

(A) Comparison of the TBP conformation in *E. cuniculi* TBP dimer (coral [47]), *E. cuniculi* Mot1^{NTD}–TBP (cyan, [47]), *H. sapiens* TBP–DNA–NC2 (brown, [107]) and *E. cuniculi* Mot1^{NTD}–TBP–DNA–NC2 (dark blue) crystal structures superposed via TBP's helix H2. **(B)** and **(D)** Helix *H4* of NC2β, which joins the NC2^{HF} with helix *H5,* is partially unfolded and additionally loses its interaction with downstream DNA and may directly contact TBP's N-terminal stirrup. Unfortunately, no electron density is visible for the side chains in this region. **(C)** Mot1^{NTD} binding induces NC2^{HF} and the upstream DNA (U) to shift toward the N-terminus of Mot1^{NTD}. On panels **(B)**, **(C)** and **(D)** the Mot1^{NTD}–TBP–DNA–NC2 crystal structure is color-coded as in Figure 13 and superimposed with the TBP–DNA–NC2 structure (shown in light brown) via TBP.

helix *H1* of NC2β is not possible, since the side chains of this protein region are not visible in the electron density. However, general inspection supports the conclusion that the same interactions between positively charged side chains of H1 and *H1* with DNA are preserved.

The results of altered upstream DNA trajectory as well as the fact that NC2^{HF}–DNA interactions are maintained results in the situation, in which NC2^{HF} is rotated and shifted towards Mot1 with respect to TBP in comparison to the conformation observed in the "substrate" TBP–DNA–NC2 complex. This additionally result in significant straightening of *H4* of NC2β, which joins NC2^{HF} bound to the underside of TBP–DNA and helix *H5* bound to the TBP. Helix *H4* of NC2β is stretched and adopts a partially unfolded conformation (**Figure 15**B,D). Moreover, the interaction between *H4* and the major groove of the downstream DNA region is lost (**Figure 15**D). Instead, *H4* potentially has a direct contact to TBP's C-terminal stirrup, although this interaction is not well defined due to the poor side chain electron density.

Very importantly for the discussion of the potential biological relevance of the observed changes, the upstream end of DNA is partially disordered and involved in the formation of crystal lattice contacts (**Figure 25**). The downstream DNA side clashes against the HEAT repeats belonging to the other complex. It has to be noted that the upstream DNA is directly involved in the formation of DNA–DNA contacts with other upstream DNA region of the molecule in the same unit cell (twofold symmetry). Therefore, the changes in the DNA trajectory reported here could be less or more prominent in the solution.

4.3 EM and CX-MS analyses of the Mot1–TBP–DNA–NC2 complex

The crystal structure of the *E. cuniculi* Mot1^{NTD}–TBP–DNA–NC2 complex revealed that a direct interaction between the HEAT repeat domain of Mot1 and NC2 occur. Remarkably, the analysis also suggested that upon Mot1 binding the conformation of TBP and the upstream DNA in the TBP–DNA–NC2 substrate is affected. Therefore, additional analysis of the complex in the context of the full-length Mot1 was necessary to further investigate the protein and DNA rearrangements in the presence of Mot1^{CTD} and to probe potential nucleotide-dependent differences. In order to allow this, electron microscopy (EM) and protein–protein crosslinking coupled to mass spectrometry (CX-MS) techniques were applied.

The 5´ end flanking the TATA box promoter sequence was shown to be directly occupied by the Mot1^{CTD} and to have a positive impact on the Mot1–TBP–DNA complex stability [8], [9], [47], [59], [70], [87]. Moreover, the upstream DNA region is required for the ATP-mediated dissociation of the Mot1–TBP–DNA complex *in vitro* [8], [70], [88]. Therefore, to stabilize Mot1^{CTD} for the EM and CX-MS analyses, the Mot1–TBP–DNA–NC2 complex samples were formed on long TATA box-containing DNA substrates with at least 26 bp upstream from the TATA box. Additionally, FRET experiments showed that the conformation of Swi2/Snf2 domain depends on its nucleotide state [138]. Although the affinity of yeast Mot1^{CTD} to DNA seems to be the highest in its nucleotide-free state [88], under these conditions *Sso*Rad54-like Swi2/Snf2 protein was shown to freely switch between open and closed conformation in solution [138]. Such conformational heterogeneity would be highly undesirable for structural analysis. However, in agreement with structural analysis of other SF2 helicases, *S. sulpholobus* Rad54-like in the presence of ATP-mimicking analogues, was shown to adopt closed conformation in solution [138]. Importantly for this study, the addition of nonhydrolyzable ATP analogs does not lead to Mot1–TBP–DNA complex disruption [8], [45], [87], [88] and in some cases was even reported to stabilize the ternary complexes when compared to the ones formed in the absence of any nucleotide [45]. Thus, in order to ensure a uniform and rigid conformation of Mot1^{CTD}, different nucleotides or derivatives were added to the complex samples after assembling and purifying the complexes in gel filtration: ABF, AGS, and ADP to lock Mot1^{CTD} in ATP- or ADP-bound states, respectively [139].

4.3.1 Chemical site-specific protein–protein crosslinking

The principle of CX-MS technique is based on the ability of so-called crosslinking compounds to specifically link two targets via their two distal functional groups. The maximal theoretical distance between the potential targets is restricted by the length of the carbon linker joining the adjacent reactive ends of the crosslinker. The molecule used in this study, di-sulfo-succinimidyl-glutarate (DSSG), is a noncleavable crosslinker of a total length of 11.4 Å that contains an amine-reactive N-hydroxysuccinimide ester at both ends of an eight-carbon spacer arm. The ester groups react exclusively with primary amines at a certain pH (7–9), namely ε-amino groups of lysines and N-termini of polypeptide chains. Light and heavy forms of this reagent contain six deuterium or six hydrogen atoms, respectively. Such isotopic coding enables the detection of the crosslinked peptides in the mass spectra.

In the first step, different crosslinking agent amounts were added to the gel filtered complex samples, according to the molar excess of the reagent over lysine residues (here, from 0.1 to 2.0). The calculations were based on an estimation that 1 µg of protein contains 0.5 nmol of lysine residues, which reflects average occurrence of this amino acid in proteins. The crosslinked species were subsequently analyzed by SDS-PAGE and silver staining (**Figure 16**A). Initial testing enabled identification of the most optimal crosslinking ratio under tested conditions (30°C, 35 min). Excessive crosslinking may be too aggressive for the protein surface and lead to unspecific crosslinks or even aggregation. On the contrary, too low amounts of the crosslinking agent result in low crosslinking efficiency and only few crosslinks are detected.

In the scaled-up experiments (~55 µg each), 133, 129 and 97 crosslinks within the ABF-, AGS- and ADP-supplied Mot1–TBP–DNA–NC2 complexes originating from 116, 109

Table 2. Localization of the crosslinks identified in Mot1–TBP–DNA–NC2 complex.

The first numbers refer to the total number of crosslinks, including crosslinked sites which were detected more than once (i.e. from miss-cleaved peptides). Numbers in brackets refer to nonredundant linkages only.

	Crystal structure	**Within Mot1^{CTD}**		**Latch-crystal structure**	**Latch-Mot1^{CTD}**	**Crystal structure-Mot1^{CTD}**	**Tot.**	**Decoy[4]**
		Intralobe[1]	Interlobe[2]					
ABF	46 (42)	21 (17)	15 (12)	8 (8)	5 (5)	37 (31) + 1 (1)[3]	133 (116)	2
AGS	51 (44)	17 (14)	10 (9)	11 (11)	3 (3)	37 (28)	129 (109)	1
ADP	40 (36)	14 (11)	7 (7)	11 (10)	4 (3)	21 (15)	97 (82)	2

[1] Within RecA1 or RecA2 subdomain

[2] Between RecA1 and RecA2 lobe

[3] Between Mot1^{CTD} and the linker joining N- and C-terminal domains (could not be mapped)

[4] Detected from reverse database, estimating false-discovery rate

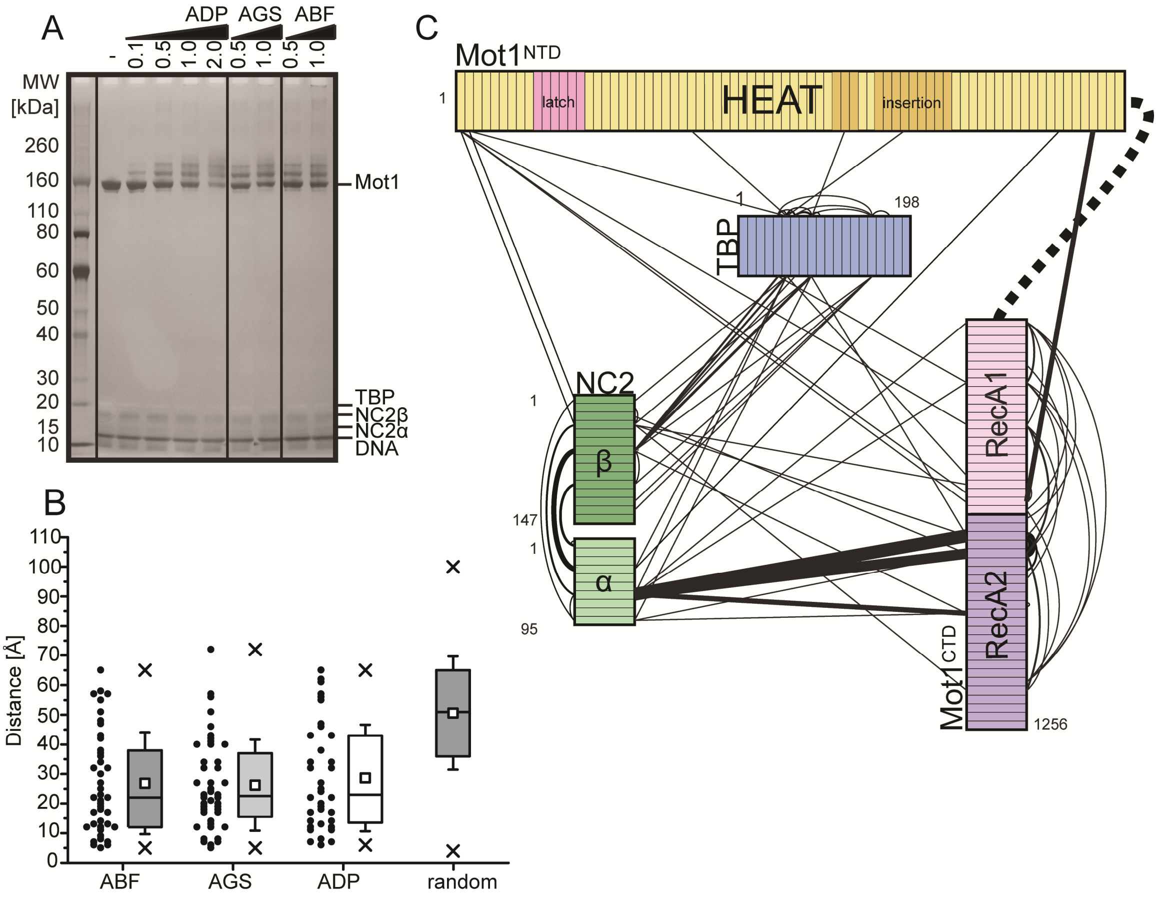

Figure 16. Chemical protein-protein crosslinking.

(A) Titration of the crosslinker (DSSG) to the Mot1–TBP–DNA–NC2 complex samples supplied with ADP, AGS or ABF visualized by SDS-PAGE and silver staining. Numbers correspond to the molar excess of the crosslinker over lysines. The samples analyzed in this study were crosslinked at 1:1 lysine:DSSG molar ratio and prepared for the further mass spectrometry analysis (described in [89]). **(B)** Distribution of theoretical linkages within the Mot1^{NTD}–TBP–NC2 module (right, n=5568) compared with the crosslinks detected in crosslinking experiments performed on Mot1–TBP–DNA–NC2 complex in the presence of ABF, AGS and ADP (n= 42, 44, 36, respectively). Only the nonredundant crosslinks were analyzed. The colored rectangles include distances within the first to the third quartile with the median value indicated as line. The whiskers represent one standard deviation above and below the mean (open square). Extreme values are represented by crosses. Raw data points were included for the experimentally determined crosslinks and were omitted for theoretical crosslinks due to the high n number. **(C)** General topology of the Mot1–TBP–DNA–NC2 complex in the presence of AGS derived from the CX-MS data. TBP (blue), Mot1^{NTD} (yellow, pink and orange), Mot1^{CTD} (purple), NC2α (light green), NC2β (dark green) are represented by blocks. Each polypeptide is divided into ten amino acid segments. The black solid lines represent the identified nonredundant crosslinks. For simplicity, crosslinks of the latch region were omitted. Line thickness is proportional to the number of crosslinks detected between the segments (redundant events). The dashed line between Mot1^{NTD} and Mot1^{CTD} segment represents the eight-amino acid linker joining these domains.

and 82 nonredundant linkage sites were detected. **Table 2** summarizes the number and the localization of all of the detected crosslinks. The false discovery rate (for all data sets below 2%) was calculated based on the total number of the detected crosslinks and the number of “decoy” crosslinks. Decoy crosslinks originate from the peptides included in a so-called “reverse” database, which consists of sequences of protein of interest but with amino acid sequences reordered from C- to the N-terminal direction. Most of the crosslinks from each data set could be placed within the Mot1^{NTD}–TBP–DNA–NC2 crystal structure or within the Mot1^{CTD} segment. The crosslinks that were detected between the latch residues Lys115 or Lys138 and other components of the complex could not be mapped, since the latch in the crystal structure is disordered. The rest of the crosslinks linked Mot1^{CTD} and other parts of the complex. For example, in all data sets numerous crosslinks between Mot1^{CTD} and NC2^{HF} were found, mainly between the helix Hc and loop L2 of NC2α (joning Hc with H3) and the RecA2 subdomain of Mot1^{CTD}. The crosslinks that could be mapped on the Mot1^{NTD}–TBP–DNA–NC2 crystal structure were compared with distribution of theoretical crosslinks originating from the linkages between all lysines within the complex. **Figure 16**B depicts the differences between the distribution of experimental and theoretical crosslinks. This analysis shows that the detected linkages have shorter distances (with median and mean values below 30 Å) that it would be expected for false positives or if the crosslinks were resulting from random unspecific events (median and mean values ~50 Å). Schematic representation of the crosslinks obtained in the experiment performed on the Mot1–TBP–DNA–NC2 complex in the presence of AGS is shown in **Figure 16**C.

Conformation of Mot1^{CTD} is dictated by its nucleotide state

The Swi2/Snf2 ATPase fold comprises two RecA-like subdomains which were shown to adopt a variety of different relative orientations in solution, even in the presence of DNA [138]. As has been shown for Mot1, the conversion between different states is necessary for the ATPase activity [59]. ATP binding site is located at the interface of the two subdomains and—according both to structural [79] and biochemical [138] characterization of other SF2 enzymes—has been shown to stabilize the catalytically active, “closed” state. Importantly, as indicated by FRET analysis, the Swi2/Snf2 ATPase domain persists in the closed state not

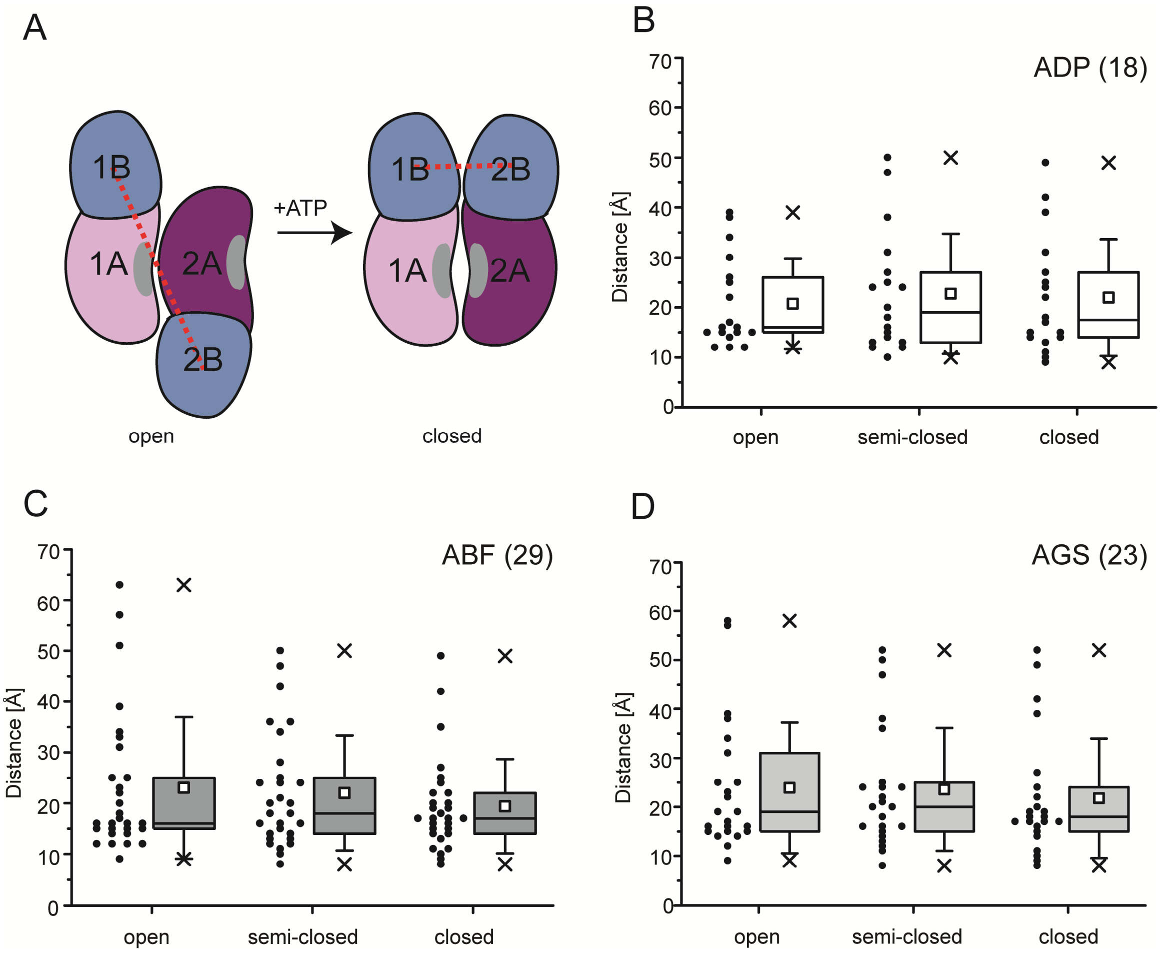

Figure 17. Statistical analysis of the crosslinks between the RecA-like subdomains of Mot1^{CTD}.

(A) Cartoon representation of the changes in the relative orientation of the RecA-like subdomains occurring during the ATP hydrolysis cycle. RecA1A and RecA2A folds of the ATPase core are represented by pink and purple shapes, respectively. Swi2/Snf2 family-specific insertions (1B and 2B) are depicted by blue shapes. The ATP binding pocket formed on the interaction surface between subdomains 1A and 2A is shown in gray. Only the closed conformation supports the ATP hydrolysis [79]. The linker and brace regions were omitted. The dotted red lines, which represent a theoretical crosslink between two sites, show that the relative orientation of RecA-like lobes will have a drastic effect on the crosslinking efficiency between particular sites. **(B)–(D)** Distance distribution of the nonredundant crosslinks detected within Mot1^{CTD} domain in the presence of different nucleotides. Numbers in the brackets refer to the number of crosslinks used in this analysis. The means were significantly heterogeneous in one-way repeated-measures ANOVA test for all three data sets ($p<0.05$) with the conformation as the factor. Box plot description is same as described in Figure 16.

only when bound to ATP, but also in the presence of ATP-mimicking analogs [138]. On the contrary, in the ADP-bound either a semi-open conformation or dynamic equilibrium between open and closed state occur [138].

In order to assess the Mot1^{CTD} conformation in the presence of different nucleotides, all crosslinks detected in the ATPase region (both inter- and intra-subdomain) were mapped on the three Mot1^{CTD} homology models. Of note is that only nonredundant crosslinks were used in this analysis. All redundant crosslinks—additional 7, 4 and 3 for ABF, AGS and ADP data sets, respectively (see **Table 2**) —were omitted, since including redundant events would be relevant only if the probability to detect each single crosslink would be the same. The models used in this analysis were generated using ESyPred3D Web Server [140] and based on the crystal structures of *D. rerio* Rad54 [77], *S. cerevisiae* Chd1 [54] and *S. solfataricus* Rad54-like protein [76]. Importantly for the analysis, each of the listed Swi2/Snf2 domains was trapped in a different conformation: “closed”, “semi-closed” and “open”, respectively (see **Figure 3**). As expected, the analysis of the crosslinks detected in different nucleotide state suggested that Mot1^{CTD} in the presence of ABF and AGS (ATP-mimicking analogs) adopts predominantly “closed” conformation, supporting properly formed nucleotide binding cleft (**Figure 17**B–C). In contrast, the distance distribution of the crosslinks in the presence of ADP suggests that Mot1^{CTD} has mixed conformations when bound to this nucleotide (**Figure 17**D).

Position of Mot1^{CTD} within the complex can be determined via CX-MS analysis

The analysis of Mot1^{CTD} conformation in the presence of ADP or ATP-mimicking analogs fully supported previous hypotheses and observations described for other Swi2/Snf2 ATPases [138]. Given that crosslinking data appeared as a potent source of valuable information, another test was carried out in order to assess the localization of Mot1^{CTD} within the *E. cuniculi* Mot1–TBP–DNA–NC2 complex, based exclusively on CX-MS data. The schematic cartoon presenting the workflow of this approach is depicted in **Figure 18**A). First step required high-throughput generation of a large number of potential relative orientations of Mot1^{CTD} and the Mot1^{NTD}–TBP–NC2 submodule. For this purpose, *EOM* (ensemble optimization method) package, which is used in one of the initial stages of small angle X-ray scattering data processing (SAXS) was used [141]. For flexible biological systems, interpretation of the scattering data is often not feasible because of significant conformational heterogeneity. *EOM* package allows quantitative analysis, which allows for a co-existence of multiple conformers in solution. First step of data analysis exploited *RANCH*, which according to given restrictions like symmetry operators or linker length, generates a pool of

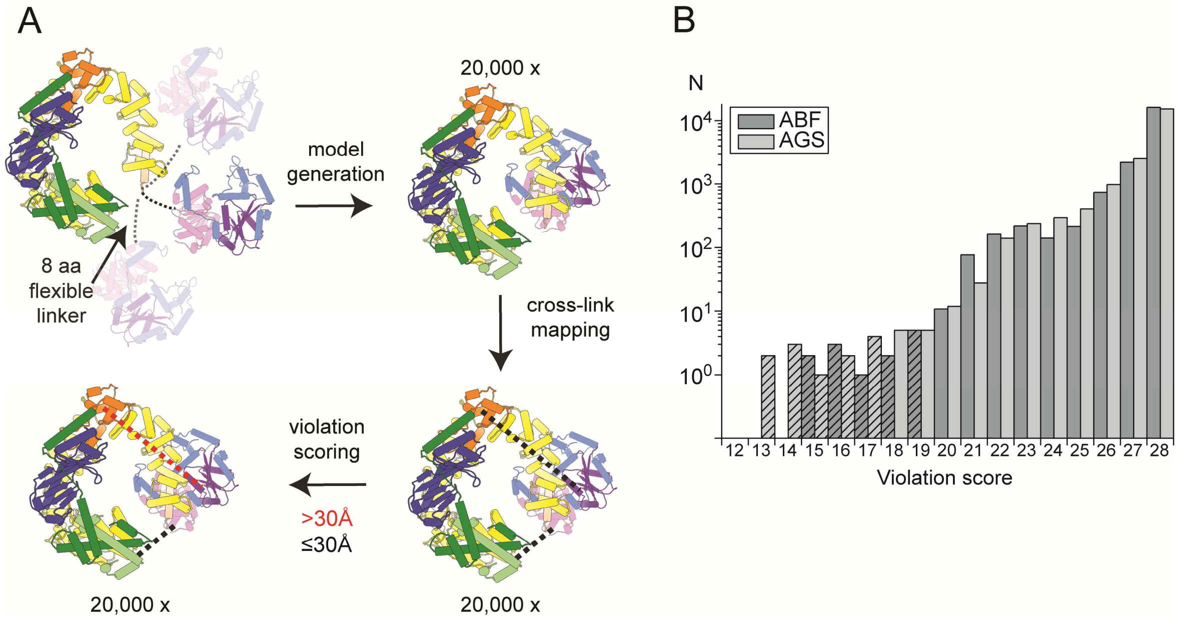

Figure 18. Analysis of the Mot1^{CTD} position and orientation via analysis of the crosslinking data.

Workflow of the high-throughput CX-MS-based approach. The Mot1^{NTD}–TBP–DNA–NC2 crystal structure and the Mot1^{CTD} homology model served as templates for the generation and scoring of 20,000 of different nonredundant Mot1^{CTD} placements (see text). **(B)** Distribution of the violation scores among all of the models for both of the analyzed data sets. Top 12 models with lowest violation scores (19 and below for ABF and 17 and below for AGS, additionally shaded) are shown in Figure 19.

random conformations of the given domains to construct the whole macromolecule. Models yielding sterical clashes are rejected such that the pool contains only physically relevant conformations. *RANCH* software allows generating the models in three different modes, depending on the C_α angle distribution used for modeling of the missing regions: random (C_α angle distribution consistent with chemically denatured proteins, therefore producing more extended models), native (consistent with disordered proteins) and compact (consistent with disordered proteins but forcing the reconstructed linkers to be rather compact). In accordance with the initial analysis of CX-MS data, the homology model of Mot1^{CTD} domain used in this test was based on the eukaryotic Rad54 structure in closed conformation. According to the *RANCH* protocol, the position of Mot1^{CTD} was restrained consistent with the presence of eight amino-acid linker between Mot1^{NTD} and the Mot1^{CTD} model (Mot1 residues 779–786). This short linker was not included in the construct used for the determination of the Mot1^{NTD} crystal structures. The models presented here were generated in compact mode, however no significant impact of the used mode of the model generation and further data interpretation was observed.

Next, all the nonredundant crosslinked pairs from the ADP, ABF, and AGS data sets detected between Mot1^{CTD} and the Mot1^{NTD}–TBP–NC2 submodule were mapped on the computed models. Further, the distances of each detected crosslink for all of the generated theoretical models were written out and scored according to a recently published protocol ([142] for the detailes, please see section **6.7.4**). The scoring protocol was based on the violation of an arbitrarily set cutoff distance, accounting for the length of the used crosslinker and linked side chains (here, lysines). For a particular model, to each crosslink a value was assigned: 0 if the distance between the C_α of the crosslinked residues was equal or below the given cutoff, or 1 in case the distance was longer. In this analysis, different cutoff values were tested: 30, 35 and 40 Å. The analysis performed applying a 40 Å cutoff did not allow to select a sharp solution, suggesting that the cutoff value was too high. However, applying 30 or 35 Å cutoff for the AGS and ABF data sets (with 28 and 31 crosslinks, respectively) sharp top solutions were obtained (**Figure 18**B). There was no substantial difference between the solutions obtained for 30 and 35 Å cutoffs. Remarkably, exactly the same models appeared as the global minimum (lowest number of violating crosslinks) for both of the analyzed data sets (shown in **Figure 19**B).

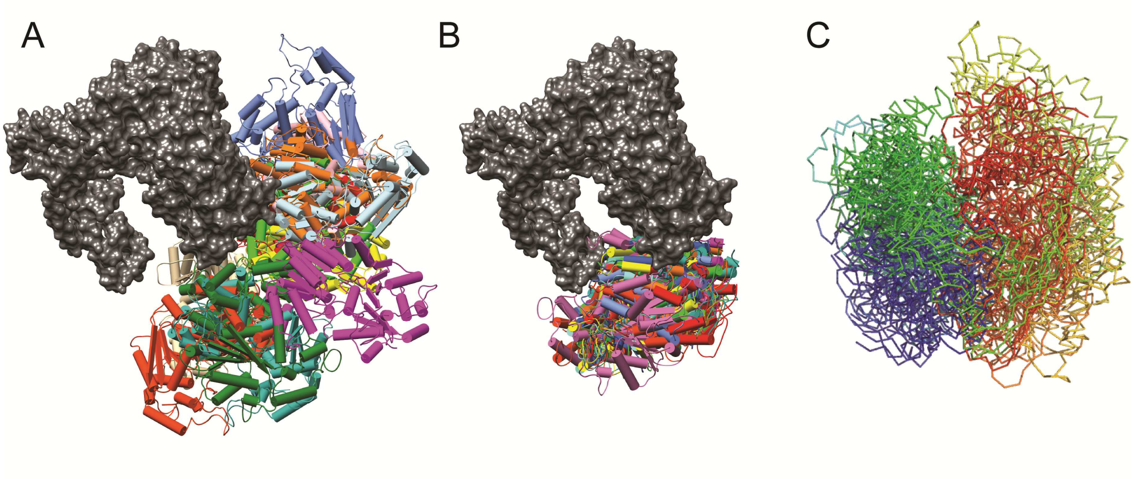

Figure 19. Mot1^{CTD} placement derived from the CX-MS data.

Superimposition of 12 randomly chosen **(A)** and 12 best-scoring models **(B)**, shown in different colors and superimposed via the Mot1^{NTD}–TBP–NC2 module (gray surface). **(C)** Comparison of the relative orientations of best-scoring Mot1^{CTDs} represented via rainbow-coloring from the N- (blue) to the C-terminus (red) of the Mot1^{CTD} model. This interpretation of the crosslinking data shows not only that this method allowed to narrow down the probed space suggesting an approximate position of Mot1^{CTD} within the Mot1–TBP–DNA–NC2 complex, but also that it consequently points at a defined orientation.

The number of the nonredundant crosslinks detected between Mot1^{CTD} and the rest of the complex in the ADP data set (15) was too small to select a subset of models representing the global minimum of the scoring function, regardless of the cutoff value used. For example, for the 30 Å cutoff there was 74 best-scoring solutions for the ADP data set (not shown) and only one best solutions for each ABF and AGS data sets (**Figure 18**B). Moreover, the solutions for the ADP data set were not related, further suggesting that the number of the crosslinks detected in this particular sample was not high enough.

4.3.2 Electron microscopy negative stain

In parallel to the CX-MS experiments, the Mot1–TBP–DNA–NC2 complex in the presence of different nucleotides was visualized by negative stain electron microscopy technique. In negative staining, the particles are fixed in a layer of heavy metal solution—in this case, uranyl acetate—which fixes protein structure on the millisecond timescale [143]. Using

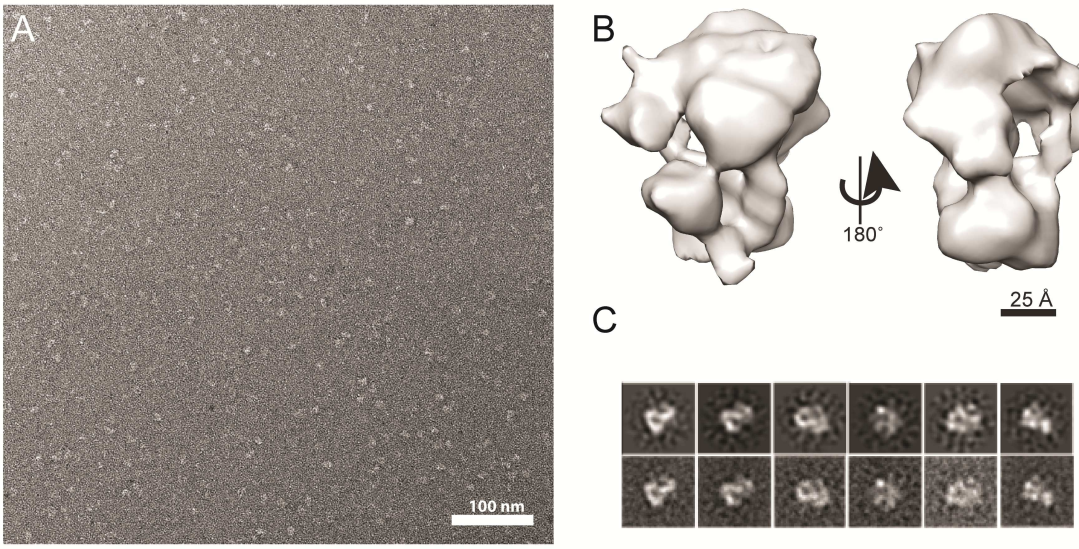

Figure 20. EM data.

(**A**) Negative stain micrograph of the *E. cuniculi* Mot1–TBP–DNA–NC2–ABF complex. (**B**) Electron density map of reconstruction. The map was contoured at a volume of ~300,000 Å^3 which corresponds to the theoretical volume of the atomic models. (**C**) 2D class averages (bottom) and the back-projections of the 3D model in the Euler angle directions assigned to the class averages (top).

computational tools, images of negatively stained specimens at different views are combined and used to produce three-dimensional reconstructions of the molecule. This, due to the size of the microcrystals formed by the staining solution, can be achieved to about 20 Å. The attempts to calculate EM reconstructions of the Mot1–TBP–DNA–NC2 complex in the presence of ADP or AGS were challenging and ineffective. However, the 22 Å negative stain reconstruction of the complex in the presence of ABF was successfully calculated from 8,192 selected particles (**Figure 20**). The reconstruction, of overall approximate dimensions of 115 Å x 115 Å x 100 Å, is in good agreement with the size of the partial complex observed in the crystals structure. Moreover, the characteristic C-like shape of Mot1^{NTD} is pronounced (**Figure 21**).

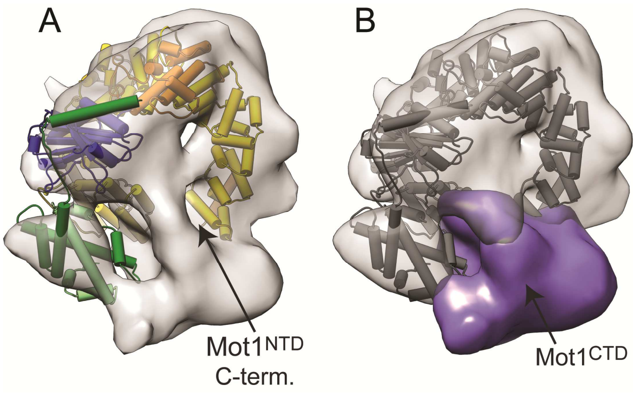

Figure 21. Results of the rigid-body fitting into the EM density.

(A) The crystal structure of the Mot1^{NTD}–TBP–DNA–NC2 complex (color-coded as in Figure 13) rigid-body docked into the negative stain density map of the Mot1–TBP–DNA–NC2–ABF complex (transparent, gray). **(B)** The map divided with the *Segger* tool (included in Chimera package [146]) into two segments: Mot1^{NTD}–TBP–NC2 module (transparent, gray) and Mot1^{CTD} part (opaque, purple).

Rigid-body fitting

To combine the structural information from the crystal structure and the EM reconstruction, an unbiased rigid body fitting approach was used in order to unambiguously localize the Mot1^{NTD}–TBP–NC2 submodule, with the DNA molecule omitted, in the EM density. The fitting was performed using *colores* tool [144], part of the *Situs* software package [145] (available at http://situs.biomachina.org). The program performs an extensive 6-dimensional contour matching of a down-filtered probe structure relative to the target EM density map. The fitting protocol resulted in a very convincing solution in which a centered additional density is visible. This additional density is situated upstream from the HEAT repeats of Mot1, directly next to the N- and, most importantly, the C-terminal end of the Mot1^{NTD} construct (**Figure 21**). Thus, this prominent segment likely harbors the Swi2/Snf2 domain.

4.3.3 Pseudo-atomic model of Mot1–TBP–DNA–NC2 complex

The in-depth CX-MS and EM analyses resulted in an equivalent outcome and suggested the same localization of Mot1^{CTD} relatively to the Mot1^{NTD}–TBP–NC2 module, placing it on the upstream side of TBP, in a direct proximity to the C-terminus of Mot1^{NTD} and NC2^{HF}. Very convincingly, in such configuration the DNA fragment from the Mot1^{CTD} component, which can be modeled based on the SsoRad54-DNA crystal structure superposed via RecA1 lobe, is a direct continuation of the upstream DNA from the Mot1^{NTD}–TBP–DNA–NC2 crystal structure (**Figure 22**A). The anticipated trajectory of the "handle" DNA engaged by Mot1^{CTD} with respect to Mot1^{NTD}–TBP does not seem to be altered and primarily follows the usual path of upstream DNA flanking the TBP-bound TATA promoter DNA. Thus, this localization agrees with the placement established in previous structural and biochemical studies [8], [9], [47], [59], [70]. The discrepancies between the exact placement (**Figure 22**B) result from the fact that the complex shape is likely more compact than it is suggested by the models generated for the CX-MS analysis. However, rigid-body fit of the Mot1^{CTD} model into its segment shows that the Mot1^{CTD} segment could theoretically hold the ATPase domain (**Figure 22**C) if small adjustments of the polypeptide chains, especially in the HEAT repeat region were allowed.

Although slight rearrangements within Mot1–TBP–DNA–NC2 complex at the TATA box cannot be excluded, the analysis also implies that Mot1^{CTD} would contact not more than 20 bp upstream from the TATA sequence (**Figure 22**D), which would be in agreement with the length requirement reported for the yeast Mot1, which ATPase domain was reported to contact around 17 bp upstream from the TATA box [47]. Furthermore, it seems plausible to reason that the non-TATA box-containing strand would be the one which Mot1^{CTD} uses

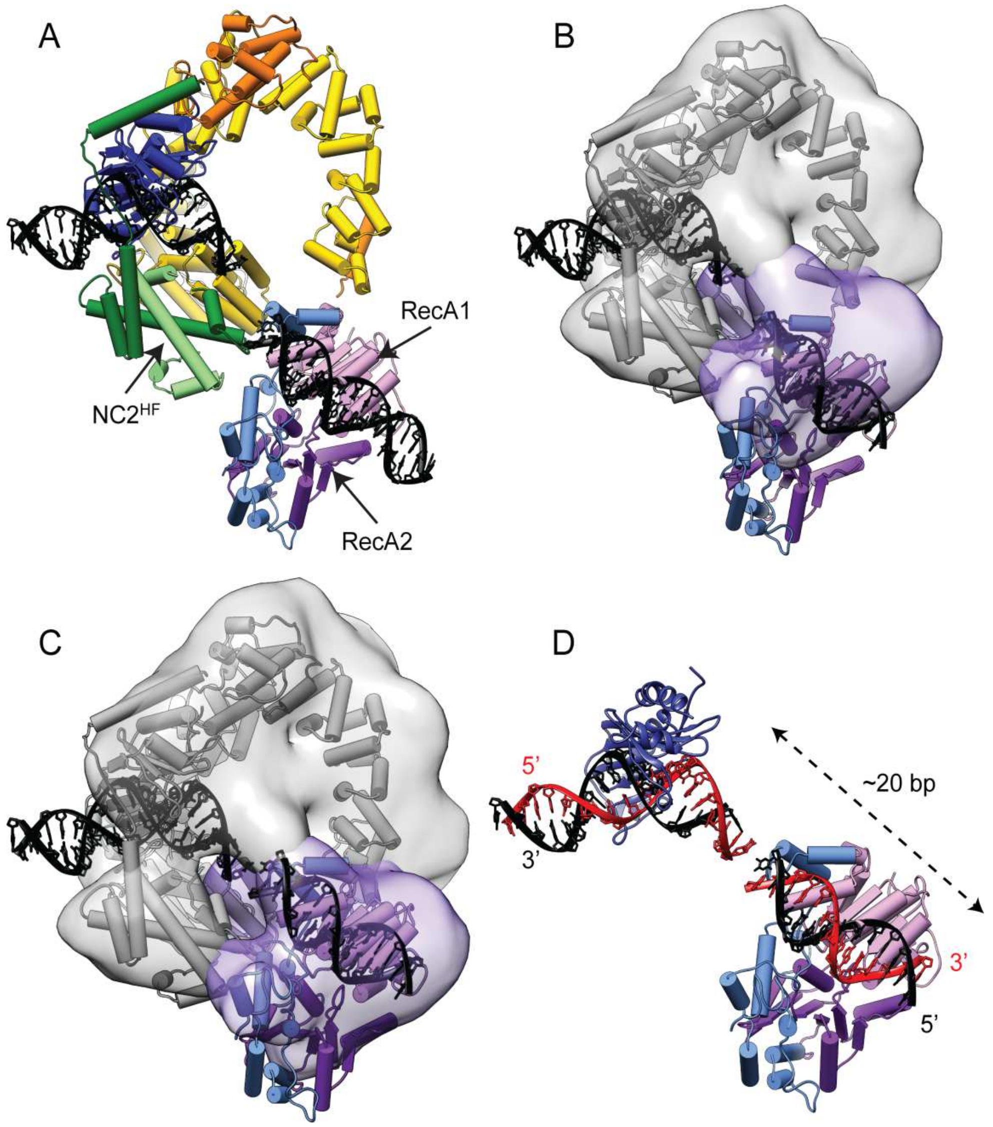

Figure 22. Comparison of the Mot1–TBP–DNA–NC2 complex model obtained from the CX-MS data with the EM electron density map.

(A) The model of the full Mot1–TBP–DNA–NC2 complex based on the CX-MS analysis. For clarity, one representative model was chosen. **(B)** Superimposition of the EM map segments, Mot1^{NTD}–TBP–DNA–NC2 crystal structure and one of the best-scoring CX-MS-based Mot1^{CTD} model fits. The transparent purple segment corresponds to the Mot1^{CTD} segment and the transparent gray one to the Mot1^{NTD}–TBP–NC2 module (same as in Figure 21). RecA1-like and RecA2-like subdomains of the Swi2/Snf2 domain are pink and purple, respectively. B1 and B2 insertions are in blue. The position of the DNA fragment bound to Mot1^{CTD} was modeled based on the *Sso*Rad54-like–DNA crystal structure by superimposing them via RecA1 subdomain **(C)** Mot1^{CTD} homology model from (A) and (B) rigid-body fitted into the Mot1^{CTD} segment using Chimera "Fit to segments" tool [146]. **(D)** Relative positions of TATA box-bound TBP and the Mot1^{CTD} bound to the upstream DNA. The top TATA box strand from the Mot1^{NTD}–TBP–DNA–NC2 crystal structure is in red. The TATA box sequence was additionally highlighted in orange. The DNA strand, which forms main contacts within the SsoRad54-like protein-DNA structure (the 3'–5' tracking strand, see Figure 3C) is also marked in red. Color coding of the Mot1^{NTD}–TBP–DNA–NC2 structure shown in (B) and (D) is same as described in Figure 13.

primary for tracking (3’–5’ strand, compare **Figure 22**D and **Figure 3**).

Interestingly, the analysis of the negative stain reconstruction suggests that the DNA substrate is partially visible, since clear density is present at the predicted DNA binding site (**Figure 22**B and C as well as **Figure 20**B, front view). Although local protein–DNA environment might distort stain adsorption, cases in which DNA could be well visualized by the negative stain method are reported, e.g. p53–DNA complex [147].

4.4 Preliminary X-ray crystallographic analysis of the Mot1^{NTD}–TBP–NC2β complex

4.4.1 Crystallization and structure determination

Mot1 catalyzes the ATP-dependent displacement of protein substrates from DNA [8]. However, the experiments performed on the *E. cuniculi* proteins revealed that Mot1 can not only bind to TBP–DNA and TBP–DNA–NC2 complexes, but also can simultaneously form complexes with TBP and NC2β in the absence of DNA. Thus, in order to gain some structural insights into potential physiological function of such Mot1–TBP–NC2β assemblies, Mot1–TBP–NC2β and Mot1^{NTD}–TBP–NC2β complex samples purified by gel filtration were subjected to crystallization experiments. In few of the tested conditions crystals of various morphologies were obtained. Initial poorly shaped crystals of the Mot1^{NTD}–TBP–NC2β complex diffracted only maximally to 5 Å (**Figure 23**A,B) and were subsequently used as a source of nucleation seeds in streak seeding experiments. After 3–14 days of incubation this approach led to well-shaped crystals diffracting maximally to 3.3 Å (**Figure 23**C). In some of the crystallization conditions the complex sample was not stable enough and only Mot1^{NTD}–TBP crystals were obtained (**Figure 23**D).

The data set from a crystal of the Mot1^{NTD}–TBP–NC2β complex, which was used for the refinement, was collected at λ=0.9797 Å and 100 K. The complex crystallized in the space group $P\ 1\ 2_1\ 1$ (a=116.8 Å, b=150.1 Å, c=172.8 Å, α=90.0°, β=107.1°, γ=90.0°) with 55% solvent content and four of each Mot1^{NTD}, TBP, and NC2β chains in the asymmetric

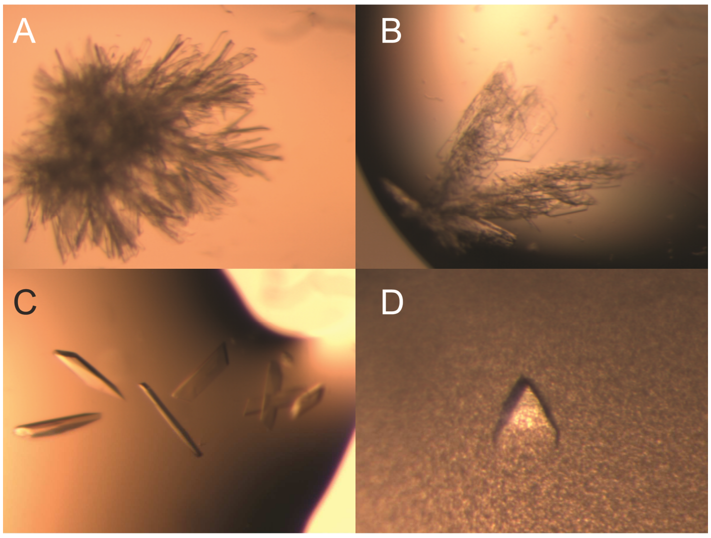

Figure 23. Results of the crystallization of *E. cuniculi* Mot1^{NTD}–TBP–NC2β complex.

(A) Initial hits of the *E. cuniculi* Mot1^{NTD}–TBP–NC2β complex crystals. Typical hedgehoge-like clusters of crystals were grown in 0.1 M sodium citrate pH 5–6, 0.2 M ammonium sulphate and PEG4000. **(B)** First hits of thin plate-like crystals grown in 0.1 M sodium citrate pH 5–6, 0.2 M sodium malonate and PEG4000. The crystals shown in **(C)** were obtained by streak seeding of the crystals presented in **(B)** and diffracted to 3.3 Å. **(D)** Crystal of Mot1^{NTD}–TBP complex covered in crystalline precipitate growing in 0.1 M magnesium acetate, 0.1 M sodium citrate 5.5 and 6% PEG4000. The crystal diffracted to 3.2 Å.

unit (~4500 residues in total). The structure was solved by molecular replacement using the *E. cuniculi* Mot1^{NTD} and TBP from the Mot1^{NTD}–TBP complex crystal structure [47] as separate search models. Subsequently, parts of the NC2β chains were modeled. Subsequently, the model was refined at 3.3 Å resolution to initial R_{work}/R_{free} of 23.5%/26.9%. Data collection, processing and refinement statistics can be found in **Table 3**.

4.4.2 Overview of the structure

Mot1 has a tight grip on TBP

In the Mot1^{NTD}–TBP–DNA–NC2 crystal structure the interface between Mot1^{NTD} and TBP extended from HR4 to HR10 and included the insertion domain (**Figure 14**). As shown in **Figure 24**, in the Mot1^{NTD}–TBP–NC2β crystal structure this interaction interface is preserved and further increases to reach ~1800 Å^2 (calculated by PISA server [136]). Thus, in the Mot1^{NTD}–TBP–NC2β crystal structure the contact surface between Mot1^{NTD} and the convex site of TBP is two times larger than in the Mot1^{NTD}–TBP complex.

Table 3. Data collection and refinement statistics.

Equations defining R-values are standard and hence not defined.

Data collection

Space group	$P\ 1\ 2_1\ 1$
Cell dimensions	
a, *b*, *c* (Å)	116.8, 150.1, 172.8
α, ß, γ (°)	90.0, 107.1, 90.0
Resolution (Å)	44.5–3.3 (3.5–3.3)*
No. reflections	
All	273046 (35071)
Unique	83621 (12355)
R_{merge} (%)	9.0 (78.1)
$CC_{(1/2)}$	99.8 (58.5)
$I/\sigma I$	11.15 (1.43)
Completeness (%)	96.8 (89.2)
Redundancy	3.3 (2.8)
Wilson B factor (Å^2)**	102

Refinement

Resolution (Å)	44.47–3.29 (3.33–3.39)
R_{work}/R_{free} (%)	23.5/26.9(38.5/43.6)
No. atoms	
Protein	32525
B-factors (Å^2)	
Protein	110
R.m.s. deviations	
Bond lengths (Å)	0.004
Bond angles (°)	1.020
Ramachandran (%)**	
Favored	96.0
Allowed	3.2
Outliers	0.8

* Values in parentheses are for highest-resolution shell.
** Determined by MolProbity.

In both of the crystal structures described in this thesis, Mot1^{NTD} molecule via its C-terminal ends packs against another Mot1^{NTD} molecule in the same asymmetric unit (Mot1^{NTD}–TBP–NC2β) or against a symmetry-related one (Mot1^{NTD}–TBP–DNA–NC2). Remarkably, similar interaction is found also in the crystal structure of the Mot1^{NTD}–TBP complex (all presented in **Figure 25**). Thus, it appears that Mot1^{NTD} has a preference for particular crystal packing in which the C-terminal HEAT repeats self assemble to form a pseudocontinuous domain. Although driven by an analogous interaction, in order to accommodate the crystal lattice packing, the HEAT repeat domains adapt slightly different conformations undergoing "accordion-like" adjustments (**Figure 25**, right panels). The capability to rearrange was shown to be an important property of long α-helical solenoids [137]. Therefore, it is possible that the shape adaptation and conformational changes play a crucial role in the function of Mot1's HEAT domain. For example, the position of helix *H5* of

NC2β—which remains bound in the same manner in all of the analyzed structures (shown in **Figure 14**, **Figure 24**, and **Figure 26**)—would be well suited for the recognition of NC2-bound TBP or TBP–DNA complexes via Mot1$^{\mathrm{NTD}}$. Remarkably, the very C-terminal unstructured regulatory region of NC2β extending beyond the ordered parts of the polypeptide chain was shown to be responsible for the repressive role of NC2 *in vitro* and *in vivo* [106], [122]. It is, however, important to stress that loosening or strengthening of the interface area between Mot1$^{\mathrm{NTD}}$ and TBP cannot be easily interpreted in the context of associated subunits, but is highly dependent on the organization of the crystal lattice contacts in particular crystal form.

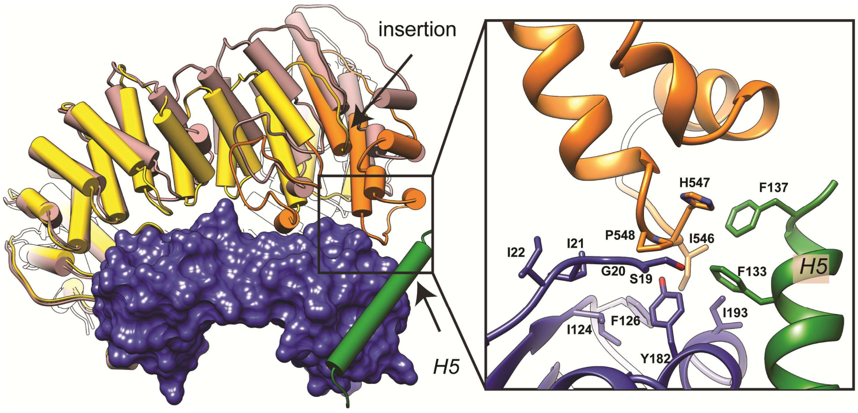

Figure 24. The interface between Mot1$^{\mathrm{NTD}}$ and TBP in the presence of NC2β.

Mot1$^{\mathrm{NTD}}$ (light brown) and TBP (not shown) from the Mot1$^{\mathrm{NTD}}$–TBP structure as well as Mot1$^{\mathrm{NTD}}$, TBP, and *H5* of NC2β from the Mot1$^{\mathrm{NTD}}$–TBP–NC2β crystal structure (color-coded as in Figure 13) were superimposed via TBP (blue surface). The residues forming a hydrophobic cluster—localized at the interface of NC2β’s *H5*, TBP’s convex side and Mot1$^{\mathrm{NTD}}$’ insertion domain—are displayed on the right side.

NC2β adopts an unusually extended conformation

Although the interaction site between Mot1$^{\mathrm{NTD}}$ and TBP’s convex surface remains largely unchanged, the latch region is 180° rotated about TBP’s twofold pseudosymmetric axis (**Figure 26**A). This unexpected feature can be explained by the fact that the latch does not form many specific contacts to TBP [47] and mimics DNA’s phosphate moiety, which also has internal pseudosymmetry. Of note is that the 180°-rotated binding mode is only possible because the latch binds TBP molecule from another complex as a result of “domain

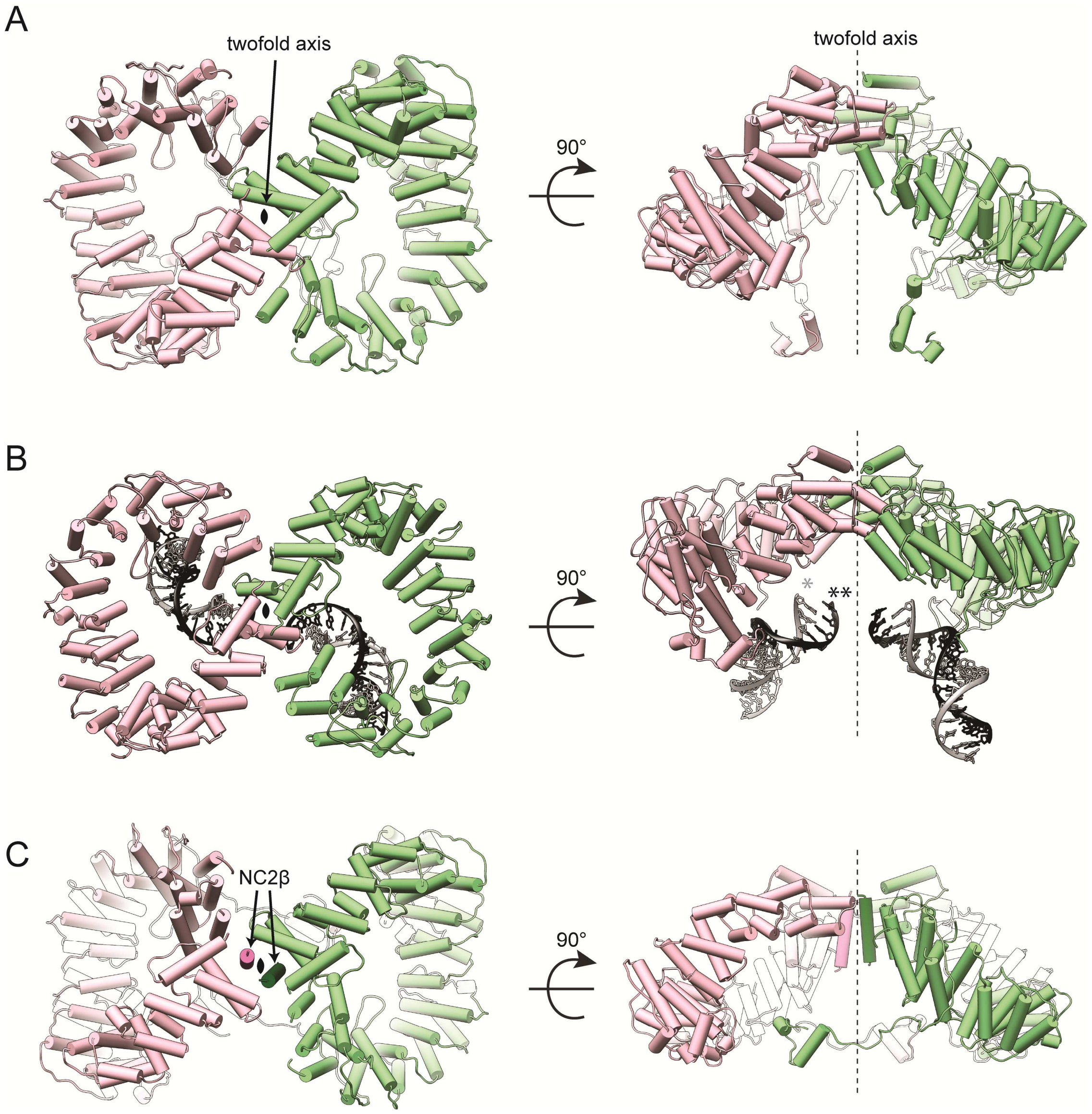

Figure 25. Crystal contacts between two Mot1^{NTD} molecules within the unit cell.

Packing of two Mot1^{NTD} molecules within the asymmetric unit of the Mot1^{NTD}–TBP crystal structure **(A)** and within the asymmetric unit of the Mot1^{NTD}–TBP–DNA–NC2 crystal structure **(B).** Panel (B) additionally shows that the upstream DNA ends probably form contacts in the crystal lattice. The 5' end of the TATA strand (*) shown here in gray has four nucleotides missing and the 3' end of the bottom strand (**) shown in black has three nucleotides missing. **(C)** Packing within the unit cell of the Mot1^{NTD}–TBP–NC2β crystal structure. Dimerization of Mot1^{NTD} molecules is mediated by two helices of NC2β inserted between the C-terminal HEAT repeats (darker pink and green). The black symbol in the middle of the left panel represents the twofold axis perpendicular to the plane of the screen. The axis on the right panel is represented by the dashed line. On panels (A) and (B) the twofold axis corresponds to the non-crystallographic axis, whereas on panel (C) it is the crystallographic axis. TBP and NC2α chains were omitted in all panels. Part of the NC2β chain is shown only in (C).

swapping" (**Figure 25**C, right side). Thus, the latch is unlikely to bind to TBP chain from the same complex in such manner, unless large conformational changes of the HEAT repeats would occur. Indeed, dimerization of Mot1^{NTD} in the crystal lattice is supported by the detection of dimeric Mot1^{NTD}–TBP–NC2β and Mot1–TBP–NC2β species in gel filtration. This implies that similar "dimeric" complexes could be also found in solution. However, it is not clear whether the dimerized form of the Mot1^{NTD}–TBP–NC2β complex observed in the crystals structurally represents the multimeric species of Mot1–TBP–NC2β complex detected in gel filtration (see discussion).

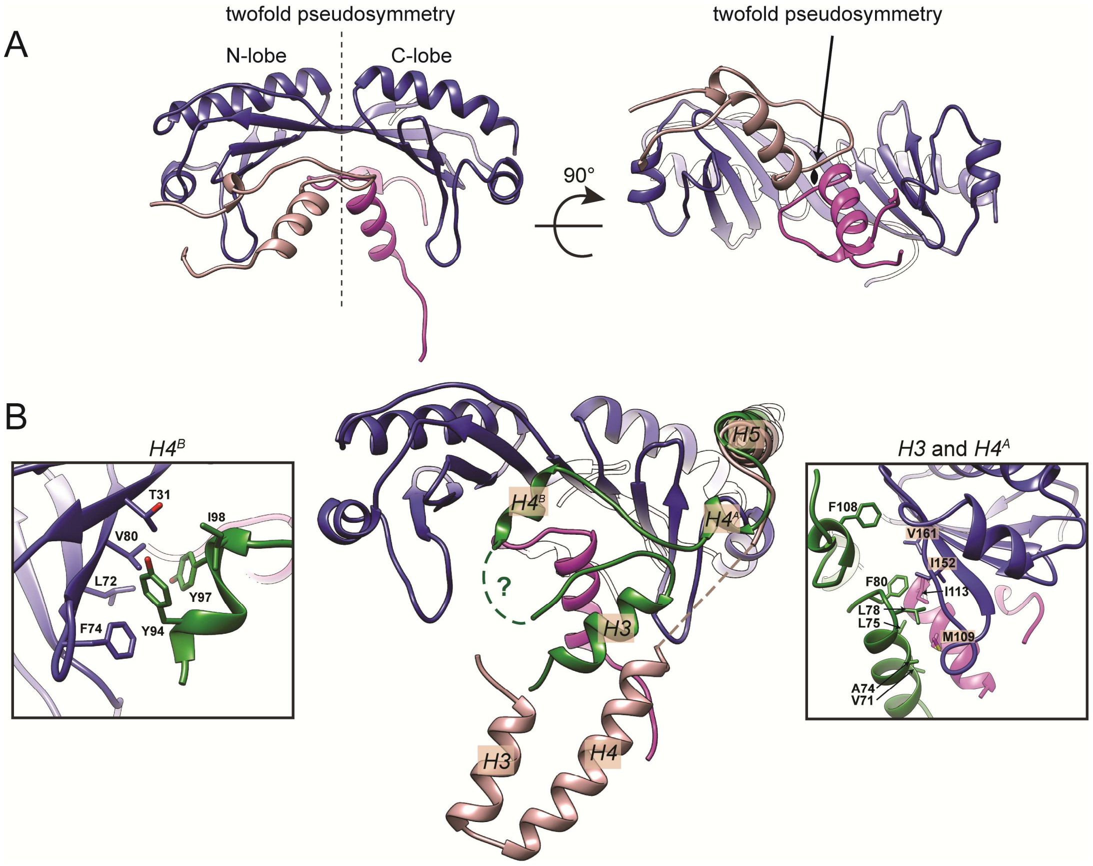
A
twofold pseudosymmetry
N-lobe
C-lobe
twofold pseudosymmetry
90°
B
H4B
T31
I98
V80
L72
Y97
F74
Y94
H5
H4B
H4A
?
H3
H3
H4
H3 and H4A
F108
V161
I152
F80
I113
L78
L75
M109
A74
V71

Figure 26. Unusual conformations of Mot1^{NTD} latch and NC2β observed in the Mot1^{NTD}–TBP–NC2β complex structure.

(A) The latch (magenta) bound to TBP (blue) in the Mot1^{NTD}–TBP–NC2β complex structure is 180° rotated about TBP's twofold pseudosymmetric axis. The binding mode of the latch region observed in the Mot1^{NTD}–TBP crystal structure (approaching from the N-lobe's side) is shown in light brown. Panel **(B)** shown unusually extended conformation of the NC2β chain (green) compared to the arrangement reported for the Mot1^{NTD}–TBP–DNA–NC2 crystal structure (light brown). Only helix *H5* remains in the same position. Helix *H4* is mostly unstructured or disordered and contacts TBP and the latch via shor helical regions (here referred to as $H4^{A}$ and $H4^{B}$). Helix H3 belongs to the same or to the symmetry-related NC2β chain (symbolized by a question mark).

Apart from the change in latch binding, the NC2β chain, when compared to its conformation observed in the Mot1$^{\text{NTD}}$–TBP–DNA–NC2 or TBP–DNA–NC2 crystal structures, adapts unusually extended conformation (**Figure 26**B). Helix *H5* remains bound to TBP's convex site, whereas mostly disordered helix *H4* binds both to the latch and TBP via two short helical structures (here referred to as *H4*^{A} *and H4*^{B}). Moreover, helix *H3*—typically participating in the formation of the histone fold—undergoes rotation and together with *H4*^{A} binds to TBP's C-terminal lobe (**Figure 26**B). Importantly, due to the relatively low resolution of the structure (3.3 Å) and the fact that NC2β residues 80–90 are unstructured, it is not clear to which complex each of the helices *H3* belongs to (**Figure 27**A). The tracing of the N-terminal part of the NC2β chain (residues 1–65) is even more challenging. This part of the polypeptide chain is not visible apart from a two short symmetry-related α-helical regions inserted between the N- and C-terminal ends of Mot1$^{\text{NTD}}$ (**Figure 25**C, left panel and **Figure 27**). Although these helices are up to 15 amino acids long, it is not possible to unambiguously determine the sequence register based on the electron density. However, these helices most probably correspond to *H2* (and related *H2´*) of NC2β, core helices of the histone fold

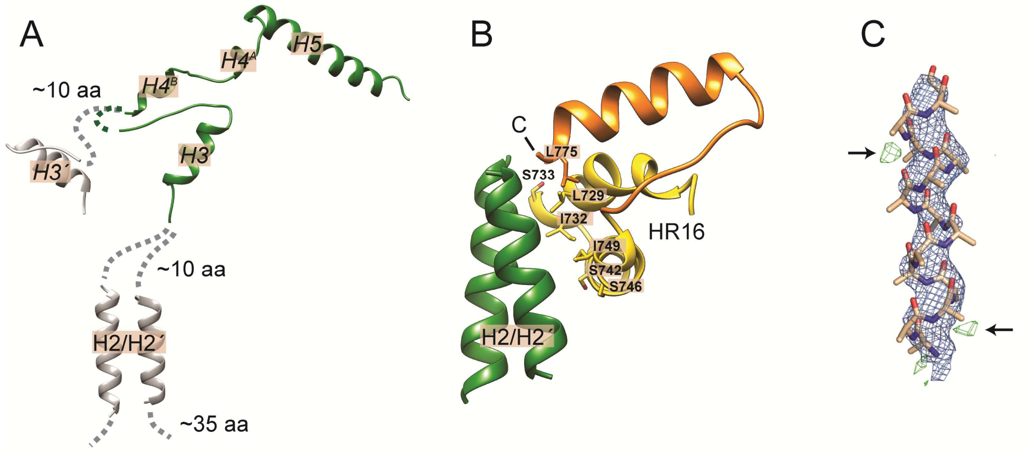

Figure 27. Tracing of the N-terminal residues of NC2β.

(A) The NC2β chain cannot be entirely traced and the sequence register cannot be assigned for the residues 1–65. **(B)** Only short ~15 amino acids long α-helical region (green) inserted between the C-terminal ends of Mot1$^{\text{NTD}}$ is visible. HR16 and C-terminal helix of Mot1$^{\text{NTD}}$ are shown in yellow and orange, respectively. The symmetry-related region of Mot1$^{\text{NTD}}$ was omitted, while both miscellaneous helices are shown. Panel **(C)** shows the $2Fo - Fc$ (blue mesh) and $Fo - Fc$ (green mesh) electron density maps contoured at 1.5 and 3σ, respectively. Positive difference density is visible for some of the side chains.

domain (see e.g. **Figure 4** or **Figure 13**). Like for its C-terminal part, the miscellaneous helices interact with neighboring molecules via very hydrophobic interaction, which likely compensate elongated conformation in the absence of the associated NC2α subunit of the NC2 heterodimer. However, the interaction between *H2* and *H2´* does not resemble the interaction within the histone fold.

Of note is that in this configuration the cysteine residues of NC2β (C43 and C58) would be in close proximity to each other. In particular, the distance of symmetry-related C43 residues, which are localized on helices *H2* and *H2´*, would theoretically allow the formation of disulfide bonds. The formation of disulfide bonds cannot be excluded, since reactive thiol groups are exposed and subjected to nonreducing conditions during crystallization process.

4.5 Activity measurements

4.5.1. Electrophoretic mobility shift assays

Mot1 dissociates TBP–DNA–NC2 complexes in presence of ATP and the latch

Mot1-catalyzed ATP-dependent disruption of TBP–DNA–NC2 complexes was already demonstrated for the recombinantly expressed yeast proteins in EMSA experiments [48] as well as for Mot1–TBP–DNA–NC2 complexes isolated from chromatin extracts [97]. Thus, EMSA experiments in the presence of ATP were performed for the *E. cuniculi* proteins in order to test if Mot1 is able to disrupt both TBP–DNA and more stable TBP–DNA–NC2 complexes in the presence or the absence of the latch.

As expected, Mot1 was able to efficiently dissociate TBP–DNA complexes when ATP was added (**Figure 28**A, lanes 3 and 4). The same effect was observed in the presence of NC2 (lanes 8 and 9). Interestingly, the presence of the latch was required to dissociate the Mot1–TBP–DNA–NC2 complexes, while Mot1 was able to disrupt the TBP–DNA complexes to some extent in the absence of the latch after ATP was added (**Figure 28**A, lanes 5 and 6 vs 10 and 11 and [47]). Additionally, the addition of NC2 prevented ATP-independent premature dissociation of TBP–DNA complexes observed in the presence of Mot1$^{\mathrm{NTD}}$

(**Figure 28**B).

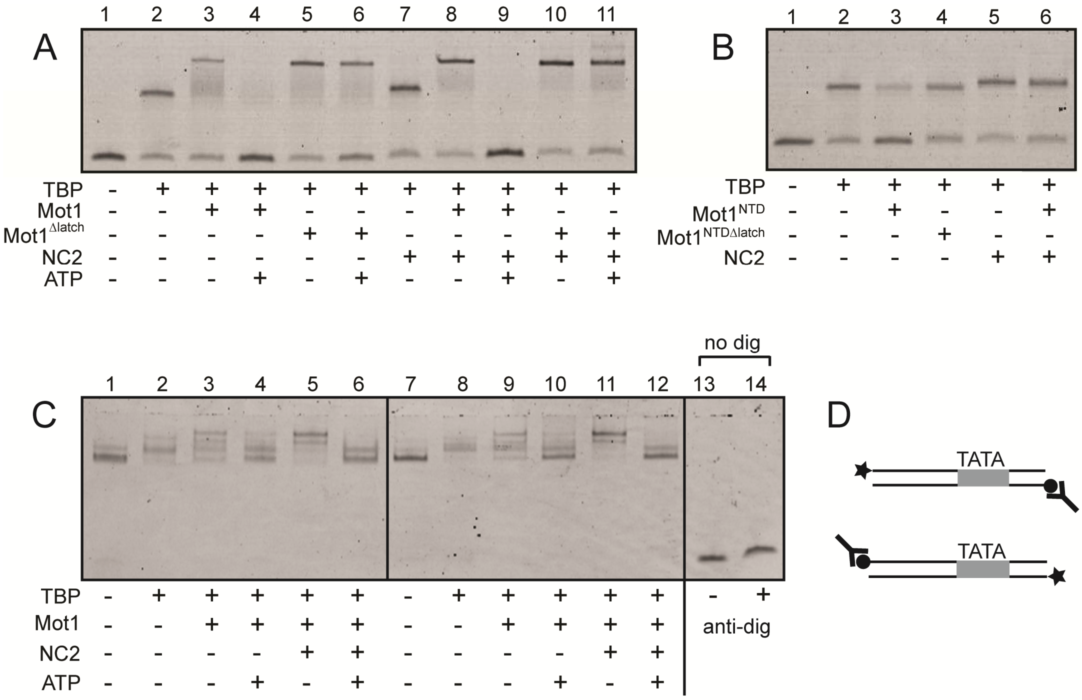
A
1 2 3 4 5 6 7 8 9 10 11
TBP - + + + + + + + + + +
Mot1 - - + + - - - + + - -
Mot1Δlatch - - - - + + - - - + +
NC2 - - - - - - + + + + +
ATP - - - + - + - - + - +
B
1 2 3 4 5 6
TBP - + + + + +
Mot1NTD - - + - - +
Mot1NTDΔlatch - - - + - -
NC2 - - - - + +
C
no dig
1 2 3 4 5 6 7 8 9 10 11 12 13 14
TBP - + + + + + - + + + + + - +
Mot1 - - + + + + - - + + + + anti-dig
NC2 - - - - + + - - - - + +
ATP - - - + - + - - - + - +
D
TATA
TATA

Figure 28. Electrophoretic mobility shift assays.

(A) Upon ATP addition, Mot1 dissociates TBP from DNA (lanes 3 and 4) as well as the TBP–DNA–NC2 complex (lanes 8, 9). Mot1$^{\Delta latch}$ is less efficient in TBP removal (lanes 5, 6) and is not able to dissociate the TBP–DNA–NC2 complex (lanes 10, 11). **(B)** Addition of NC2 prevents the Mot1^{NTD} from displacing TBP from DNA (lane 3 vs 6). **(C)** EMSA performed using DNA substrates, which had one of the 5' ends labeled with fluorescein. Second 5' end was labeled with digoxygenin and blocked by the addition of anti-digoxygenin antibody. **(D)** Cartoon representing the label placement of the substrates used in lanes 1-6 (top) and 7-12 (bottom). Fluorescein, digoxygenin, and anti-digoxygenin antibody are represented by star, filled circle and a Y-like shape, respectively.

Interestingly, the quantification of EMSA experiments showed no clear differences between the affinities of Mot1 to TBP–DNA–NC2, NC2 to Mot1–TBP–DNA or NC2 to TBP–DNA (not shown). Each of the affinities was in low nM range and was thus similar to the affinity of yeast Mot1 to TBP–DNA complex [43, 46], which could not be reliably measured for the *E. cuniculi* proteins. Moreover, the presence of NC2 did not significantly affect the ATPase activity of Mot1, which required only TBP or TBP–DNA for the full stimulation [47].

Taken together, both TBP–DNA and TBP–DNA–NC2 complexes are *bona fide* substrates for Mot1-catalyzed ATP-dependent activity *in vitro.* NC2 blocks the premature action of the latch but neither increases Mot1's affinity for the substrate nor affects its

ATPase activity. Moreover, the analysis of selected NC2 mutants was not possible, since they all showed WT behavior (data not shown).

Mot1 dissociates TBP–NC2 from DNA substrates with obstructed ends

Although Swi2/Snf2 ATPase motors couple ATP hydrolysis to dsDNA translocation [71]–[73], the release of TBP from DNA by Mot1 does not appear to involve highly processive ATP-dependent DNA tracking [85]. However, Mot1 was shown to induce changes in the upstream DNA conformation within the TBP–DNA complexes, which suggested that Mot1 straightens DNA [88]. Similarly to Mot1, lateral mobility of TBP–NC2 complexes on different DNA substrates was observed in single particle FRET experiments [114]. In addition, the same study showed that these mobile TBP–NC2 complexes were "trapped" on the DNA substrates and were not able to dissociate on their own, showing remarkable stability over long incubation times. Nevertheless, *E. cuniculi* Mot1 readily dissociated TBP from promoter DNA in the presence of NC2. Remarkably, in the Mot1^{NTD}–TBP–DNA–NC2 crystal structure, Mot1 and NC2 form a "clamp" on the promoter DNA-bound TBP. This kind of configuration would be well suited for ATP-dependent translocation along DNA track, since the structural analysis indeed indicates changes in the DNA trajectory that are consistent with increased lateral mobility of the Mot1–TBP–DNA–NC2 complex.

Thus, in the light of the data presented in this study, two possible models of the ATP-dependent Mot1's action could be proposed, both of them are represented schematically in **Figure 29**. First of the possibilities applies ATP-dependent translocation along DNA phosphate backbone (**A**). In an alternative scenario (**B**), the TBP–DNA–NC2 complex would be disrupted by locally occurring Mot1-induced conformational changes that do not require substantial translocation. To distinguish between these two possibilities, electrophoretic mobility shift assays, using digoxygenin labeled DNA and anti-digoxygenin antibodies. As shown in **Figure 28**C, although TBP–DNA complexes were not disrupted with 100% efficiency, the presence of the antibody in principle did not have any significant impact on the action catalyzed by Mot1, either in the presence or absence of NC2. Thus, these activity assays suggest that Mot1 does not motor the protein substrate along DNA over long distances, supporting similar results obtained with yeast proteins in an analogous set up [85]. Instead, Mot1 is more likely to locally disrupt the protein–DNA interaction. It is, however, possible that the Mot1-catalyzed reaction includes very short-range tracking of TBP–NC2 “clamps” (few base pairs), which cannot be distinguished from a local disruption on DNA substrates used in this study.

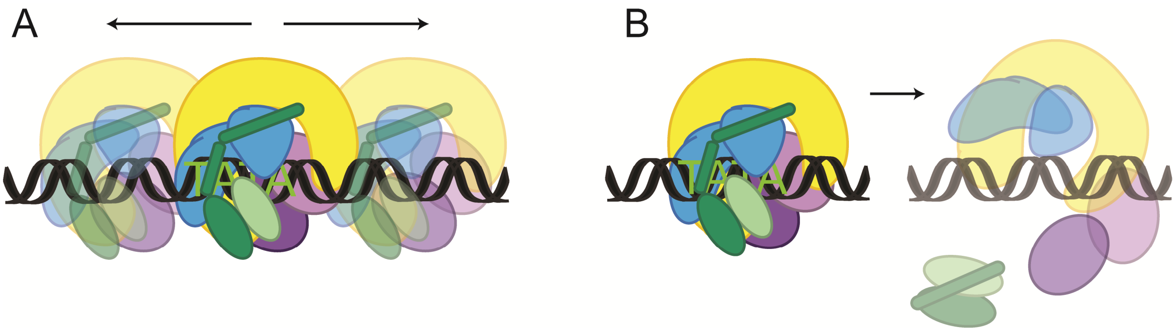

Figure 29. Possible models of Mot1’s action on TBP–DNA–NC2 substrates.

(**A**) Mot1 slides TBP–NC2 complexes along DNA away from the promoter or (**B**) Mot1 locally disrupts TBP–NC2 complexes in a reaction, which does not require DNA tracking.

5. DISCUSSION

5.1 TBP–DNA–NC2 complex is a *bona fide* substrate for Mot1

Mot1 is an essential gene regulator that, as has been shown in numerous *in vitro* as well as genome-wide *in vivo* studies, together with NC2 regulates TBP's genomic distribution [18], [20], [26], [97]. The question whether Mot1 and NC2 function through different but partially redundant mechanisms or whether they cooperate utilizing an unknown mechanistic relationship was not entirely clear. NC2 acts via preventing the interaction of TFIIA and TFIIB with TBP–DNA complexes, thereby blocking the PIC formation [94]–[96], [100], [102], [104], [113]. Interestingly, *in vitro* FRET experiments showed the extremely low off-rate of TBP–NC2 complexes from promoters suggesting a requirement for a factor that modulates promoter accessibility [114]. Subsequently, NC2 was shown to be retained on DNA *in vivo* in the absence of functional Mot1 [19], [97], [118]. Moreover, intact Mot1–TBP–DNA–NC2 complexes were isolated from yeast chromatin extracts and could be formed *in vitro* using recombinantly purified components [97], [48]. Finally, both endogenous and recombinant complexes were efficiently disrupted in the presence of ATP [97], [48]. In agreement with these results, the gel filtration and EMSA analyses performed on the *E. cuniculi* proteins showed that, next to TBP–DNA, also TBP–DNA–NC2 complex is a *bona fide* substrate for Mot1's ATP-dependent activity. Additionally, in the absence of NC2α, TBP–DNA–NC2β and Mot1–TBP–DNA–NC2β complexes could not be formed, showing that both NC2 subunits are required for the formation of the DNA-containing complexes. Thus, current body of data suggests that the co-association of Mot1 and NC2 observed in *in vivo* experiments results from the fact that Mot1 catalyzes the dissociation not only of TBP but also of TBP–NC2 complexes from the promoter sites. The exact role of NC2 in this setting is not entirely clear, but this additional factor appears to function as a marker of nonproductive TBP complexes poising them for Mot1 action, e.g. on intragenic regions [30], [32].

5.2 The latch plays crucial role in dissociation mechanism

The latch region has been initially characterized as a nonconserved structural element with the length largely varying between the species, which directly binds TBP's concave surface [47]. In this manner, the latch resembles the TAND1 region of the biggest subunit of TFIID complex, TAF1 [148]. Both elements prevent TBP–DNA association in a relatively unspecific manner structurally mimicking DNA moiety. Deletion of the latch impairs the dissociation process of the Mot1–TBP–DNA complex. However, in contrast to TBP–DNA substrates, TBP–DNA–NC2 complexes are disrupted by Mot1 only in the presence of the latch region and show resistance to premature ATP-independent latch-dependent dissociation of the complex. Therefore, in the presence of NC2, the latch seems to play an important functional role in the dissociation mechanism catalyzed by Mot1.

In the Mot1^{NTD}–TBP–DNA–NC2 crystal structure the latch region is disordered. Similarly, the CX-MS analysis implies that this region does not exclusively bind to a particular region of the complex. If the latch was ordered, due to its small size (~50 residues) it would not have been possible to localize it in the negative stain EM map. Interestingly however, many crosslinks between Mot1's latch and Mot1^{CTD} were detected for all CX-MS data sets, constituting surprisingly high subset of detected linkages. The N-terminal part of yeast Mot1 has been already proposed to inhibit Mot1^{CTD} action via electrostatic interactions under physiological conditions [46]. Similar mechanisms have been described for other Swi2/Snf2 members; for example the chromodomains of Chd1 and "leucine latch motif" of CSB localized upstream from the Swi2/Snf2 domains were shown to sterically modulate the ATPase activity as an autoinhibitory element and act in response to substrate recognition [54], [149]. Intriguingly, the ATPase activity of the Mot1$^{\Delta latch}$ mutant, in contrast to the WT protein, is not stimulated by TBP, regardless of the presence of NC2 ([47] and data not shown). Moreover, the latch contains Mot1's nuclear localization signal, which becomes functional only after Mot1 association with TBP [43]. Therefore, the link between Mot1 conformational changes occurring upon association with TBP point toward a possibility that the latch might directly function as an autoinhibitory element or that its interaction with TBP is indirectly modulated by such a mechanism.

5.3 Mot1 initially alters protein substrate–DNA interaction in an ATP-independent way

Mot1, apart from being an essential global transcriptional regulator serves as an attractive model system for structural and mechanistic studies of Swi2/Snf2 enzymes. Currently, different models are considered to explain how Mot1 catalyzes the disruption of TBP–DNA complexes: a) by inducing a conformational change of TATA DNA via the interaction between upstream DNA (i.e. DNA "handle") and Mot1^{CTD}; b) by DNA translocation mechanism, where, according to the general model proposed for all Swi2/Snf2 family enzymes, Mot1 would act as a molecular "snowplow" pushing or pulling off TBP from the promoter; or c) by alteration of TBP–DNA affinity either by a direct influence on TBP molecule or, alternatively, TATA box DNA itself. Several changes reported for the *E. cuniculi* Mot1^{NTD}–TBP–DNA–NC2 complex structure, in comparison to the "product" Mot1^{NTD}–TBP and "substrate" TBP–DNA–NC2 states, provide important insights into the early stage of the Mot-catalyzed reaction. Additional structural information derived from the EM and CX-MS analyses of the complex formed in the presence of the full-length Mot1 additionally extend some of these observations.

First, in comparison to the "product" state, "substrate"-bound Mot1^{NTD} covers almost the whole convex site of TBP. This significantly enhanced contact suggests that Mot1, in order to remove TBP from DNA, might require a tighter grip on TBP. Interestingly, the expanded interface implies a direct interaction between the Mot1^{NTD}'s insertion domain and the TBP's N-terminal tail which, although included in the crystallization construct, was unfortunately not visible in the electron density. Interestingly enough, although this part of TBP's polypeptide chain is evitable [150], it was shown to regulate TBP–DNA binding behavior and promote the formation of so-called "unbent" TBP-DNA species, which are much less stable than normal "bent" complexes [59], [92]. Apart from a possible influence of TBP's N-terminus on Mot1-catalyzed reactions, also the region extending beyond the helix *H5* of NC2β also contributes to the new Mot1^{NTD}–NC2 interface. Interestingly, the QA-rich NC2β C-terminal fragment of human NC2β, although not required for TBP binding, was shown to be required for the repression, but not activation of transcription *in vitro* [99], [113]. Moreover, this part of the NC2β polypeptide representing a repression domain was found to be a target of phosphorylation *in vivo* [151]. Similarly to TBP's N-terminus, however, this part is not well characterized in the electron density. The observation that both TBP's and NC2β's repressive elements are in a direct proximity to the α-helical insertion domain of Mot1 raises intriguing possibility that this element does not only play a structural role. This region inserted between the HEAT repeats is characteristic to Mot1 and is conserved among the orthologs. The functional role of this part of the protein still awaits further characterization.

Second, in the Mot1^{NTD}–TBP–DNA–NC2 complex crystal structure the DNA region flanking the TATA box promoter in the 5' direction according to the "top" strand (i.e. upstream) appears to be altered, if this region is compared to the DNA trajectory in the "substrate" TBP–DNA–NC2 complex as well as other TBP–DNA complexes. Although, as already stressed in the Results section, both ends of the DNA substrate in the crystal structure are partially disordered and involved in the formation of the crystal contacts. Therefore, the arrangement of the DNA trajectory in the upstream part can be partially affected by DNA–DNA interactions within the crystal lattice and, therefore, Mot1^{NTD}-induced changes in DNA conformation might be overrepresented. However, these presence of "straightened" DNA—which is consistent with increased lateral mobility—is in a full agreement with the results of single-molecule FRET experiments, which have shown that *S. cerevisiae* Mot1–TBP–DNA complexes in the absence of any nucleotide or in the presence of AGS and ALF are flexible due to equilibrium between bent and unbent DNA states [88]. Thus, Mot1^{NTD}-induced changes in DNA conformation might be as well over- as underrepresented. Importantly for this discussion, Mot1-induced dynamic DNA behavior in these TBP–DNA complexes was observed on DNA templates which were too short to directly contact Mot1^{CTD}, i.e. having only 3 bp in the upstream region. Several earlier studies also reported that Mot1 might change TBP–DNA interaction and that this process is not linked to any ATP-related conformational change of the ATPase domain; mechanically forced transient alteration of the TBP–promoter affinity would for example explain why Mot1 alters the DNase I digestion protection pattern of TBP even in the absence of ATP [8], [59], [70] and is not able to dissociate TBP from DNA with I–C-substituted TATA region [45]. Intermediate state protein–DNA complexes, in which duplex DNA is distorted prior to ATP hydrolysis have been reported for SF1 helicases, e.g. in case of PcrA–DNA complexes [83]. Strikingly, Mot1-

accociated TBP also loses the ability to discriminate between classical and mutated TATA sequences [49], [87]. Similarly, BTAF1 is able to induce DNA binding for the majority of the DNA-binding surface TBP mutants which are defective both for BTAF1 and DNA binding in solution [49]. Remarkably, ATP analogs were shown to convert Mot1–TBP complexes into a form capable of binding to DNA [48]. Thus, numerous *in vitro* experiments suggest that after Mot1 binding the TBP–DNA interface is altered. Analogously to Mot1, NC2 also induces dynamic behavior in the TBP–DNA interface, thereby enabling TBP to laterally move on core promoter DNA without its dissociation although DNA conformational changes have not been seen in the TBP–DNA–NC2 crystal structure [114]. Therefore, "pre-straightened" Mot1-targeted TBP–DNA–NC2 complexes might facilitate more efficient substrate recognition or dissociation.

Third, as judged from the C_{α} root mean square deviation between the analyzed TBP structures, TBP conformation when bound to the TATA DNA in the presence of Mot1 and NC2 is somewhat distinct to that of TBP bound to TATA DNA alone, and rather similar to TBP bound to Mot1 alone ("product" complex). The observed changes are, however, small and are of borderline significance, but the trend is consistent. On the other hand, even minimal Mot1-dependent alterations might already have a critical impact on TBP–DNA interaction, especially that the severely bent TATA box sequence itself might accelerate this process acting as a "spring" for rapid release of TBP [152]. In this context interesting is that the association of Mot1 with TBP–DNA–NC2 seems to disrupt the NC2β–DNA contact site at *H4*. Remarkably, *H4* is moved towards TBP and "bumps" into TBP's C-terminal stirrup. This is particularly interesting, since two pairs of phenylalanine side chains, which are primarily responsible for introducing the dramatic change of the TATA element conformation, ale localized at or near the TBP's stirrups [91]. Thus, Mot1 might indirectly destabilize TBP-induced kink in DNA via altering NC2 conformation.

Forth, in line with the hypothesis that Mot1 could directly contact the TATA box DNA in the presence of TBP [49], [59], the structural analysis presented here points towards a possibility for a Mot1^{NTD}–DNA interaction. This is additionally strengthen by the observation Mot1^{CTD} is not the only part of the Swi2/Snf2 enzymes that form direct contact to DNA [153]. Since Mot1^{CTD} does not contact TBP [45] and the latch–DNA interaction can be also rather excluded ([48] and data not shown) the Mot1 contribution to this interaction could be mediated via the conserved and negatively charged N-terminus of the HEAT repeat domain (HR 1–2). Although this region does not form direct contacts with DNA, it resides in a close proximity to the DNA in the *E. cuniculi* Mot1^{NTD}–TBP–DNA–NC2 complex structure. Interestingly, the deletions within the fist 100 residues result in inviablitiy or in a dominant-negative phenotype in yeast [48], which would suggest that this region likely forms important contacts in the context of the full-length protein, i.e. with TBP or the ATPase domain.

Fifth, the conclusions drawn from the interpretation of the crystal structure determined in the presence of truncated Mot1 are supported by the CX-MS and negative stain electron microscopy studies of the complex in the presence of Mot1^{CTD}. The results presented in this work show that Mot1^{CTD}, when bound to an ATP analog, directly contacts the NC2^{HF} domain. This interaction site, next to the Mot1^{NTD}–TBP–NC2β contact site could serve as anchor points, which together would be well suited to alter the TBP–NC2 and TBP–DNA interactions, at the same not weakening the Mot1^{NTD}–TBP interaction [43].

Sixth, according to the EM reconstruction, Mot1^{CTD}–DNA association in the presence of ABF does not seem to introduce large changes to the upstream DNA conformation relatively to the TATA box-bound TBP, which would imply that Mot1 does not exploit upstream DNA “handle” in order to introduce e.g. DNA twisting. Instead, as described before, the observed modifications of protein–DNA interactions are explicitly a result of Mot1^{NTD} binding. The limited resolution of the EM reconstruction does not, however, exclude that some additional rearrangements not present in the crystal structure might occur, especially that more extensive compaction of the HEAT repeat array is observed. Therefore, it cannot be ruled out that, due to the binding of Mot1^{CTD} to the upstream DNA, rearrangements at the TATA box are even more pronounced compared to the situation observed in the Mot1^{NTD}–TBP–DNA–NC2 crystal structure. Moreover, many crosslinks between Mot1^{CTD} and TBP detected in all CX-MS experiments, which cannot be explained by the proposed model, were detected. Unfortunately, parallel attempts to obtain negative stain reconstructions of the Mot1–TBP–DNA–NC2 complex in ADP- or AGS-bound state were ineffective. Therefore, the potential differences between to nucleotide and nucleotide-bound states could not have been fully investigated. The complex might be not uniform enough when bound to these nucleotides to allow effective sorting of the negatively stained particles. This might additionally imply that additional large rearrangements occur through

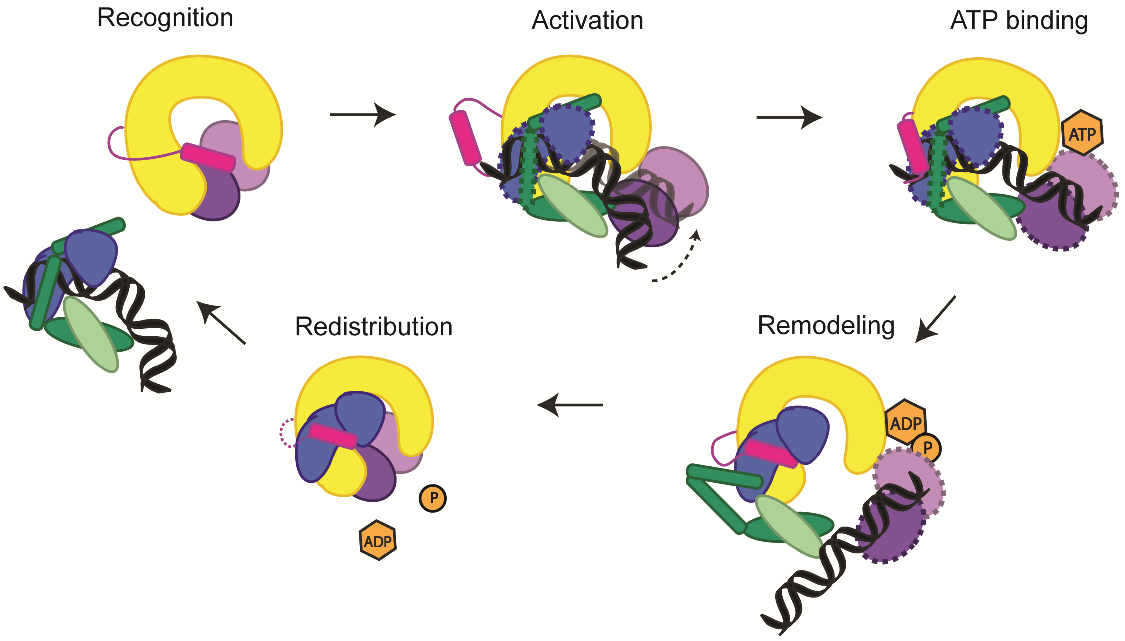

Figure 30. General model for Mot1-catalyzed dissociation.

The binding of Mot1 (Mot1^{NTD} in yellow, RecA1 in pink, RecA2 in purple, latch shown in magenta as cylinder) induces destabilizing conformational changes in the TBP–DNA–NC2 complex (TBP is shown in blue, and the NC2 heterodimer is shown in dark and light green). Subsequently, the ATPase domain stably engages upstream DNA and its ATP hydrolysis-mediated functions directed in the upstream direction cause the final release of TBP and NC2 from DNA.

ATP hydrolysis and phosphate release. However, considering the relative small size of the proteins analyzed in this study as well as the resolution limits of the negative stain EM and CX-MS methods, more detailed information is not available, e.g. from cryo-EM or higher-resolution X-ray analysis.

Taken together, the data presented here suggest the following model for Mot1 action, in the first step, TBP's and NC2's interaction with DNA is destabilized by Mot1 binding. Mot1 first acts on the substrate complexes enforcing a state, in which TBP is incompetent to bind to the TATA box anymore. This process is not directly coupled to ATP hydrolysis and does not necessarily results in TBP removal from DNA (**Figure 30**). Although *E. cuniculi* Mot1^{NTD} binding to TBP–DNA is in principle sufficient to displace TBP from DNA *S. cerevisiae*, full-length Mot1 complexes are fairly stable on longer DNA templates *in vitro* [59], [87]. In the presence of NC2, changes in the TBP–DNA interaction also occur, but the formation of the Mot1^{NTD}–NC2 clamp in Mot1^{NTD}–TBP–DNA–NC2 complexes does not allow premature TBP–DNA dissociation observed for Mot1^{NTD}–TBP–DNA complexes in

EMSA experiments. Subsequent Swi2/Snf2 ATPase-dependent remodeling step triggered by ATP hydrolysis enables dissociation of the “primed” complexes from upstream DNA in an ATP-dependent process.

5.4 Mot1 and other Swi2/Snf2 enzymes

Mechanistic understanding of how ATP hydrolysis is coupled to protein–DNA rearrangements catalyzed by Swi2/Snf2 enzymes is very limited. The interpretation of the structural and biochemical data presented here does not entirely addresses this issue, especially that the Mot1 construct used for the determination of the Mot1^{NTD}–TBP–DNA–NC2 crystal structure lacked Mot1^{CTD} and, therefore, the most valuable high-resolution information is still largely absent. However, low-resolution negative stain imaging, crosslinking and activity experiments performed on the full-length Mot1-containing Mot1–TBP–DNA–NC2 complex presented in this work revealed several interesting findings which show similarities and dissimilarities between Mot1 and other Swi2/Snf2 family members.

Analysis of the CX-MS data analyzed in this work revealed that the nucleotide state of Mot1^{CTD} has a crucial impact on the conformation of the Swi2/Snf2 ATPase domain. This is fully consistent with the conformational changes described for *Sulpholobus solfataricus* Rad54-like Swi2/Snf2 enzyme occurring during the ATP hydrolysis. SsoRad54-like ATPase undergoes drastic conformational alterations involving the changes in the relative reorientation of the two RecA-like subdomains on DNA substrates even in the absence of ATP [138]. Analogously, Mot1 can freely adopt the active conformation in solution even in the absence of ATP and, due to such conformational heterogeneity, is able to dissociate a fraction of TBP–DNA complexes; however, this effect is not observed for the “hinge” mutant of Mot1, which is believed to be impaired in the conversion of the active and inactive ATPase state [59].

The most interesting uncovered parallel to chromatin remodelers is the fact that Mot1^{CTD}, particularly the RecA2-like subdomain, is in a direct proximity to NC2^{HF} and the upstream DNA. A direct involvement of the ATPase domain in nucleosomal substrate recognition as well as in the coupling of ATP hydrolysis to chromatin remodeling function has been shown [154]–[156]. More detailed information about the position to which ATPase engages nucleosome is based on site-specific crosslinking experiments and nucleosome sliding experiments using gapped DNA substrates, which have shown that the Swi2/Snf2 domain of chromatin remodelers directly binds to nucleosome at superhelical location 2 (SHL2)—two turns away from the dyad axis [154], [157]. Notably, the position of Mot1^{CTD} relative to NC2^{HF} in our CX-MS- and EM-derived models is analogous to the association of a Swi2/Snf2 domain bound at SHL2, i.e. in a direct proximity to the H3/H4 histone pair slightly away from the dyad (**Figure 31**). Therefore, is appears that Mot1 and Swi2/Snf2 chromatin remodelers likely act via related mechanism and they share the ability to specifically recognize a histone fold protein–DNA complex as a substrate.

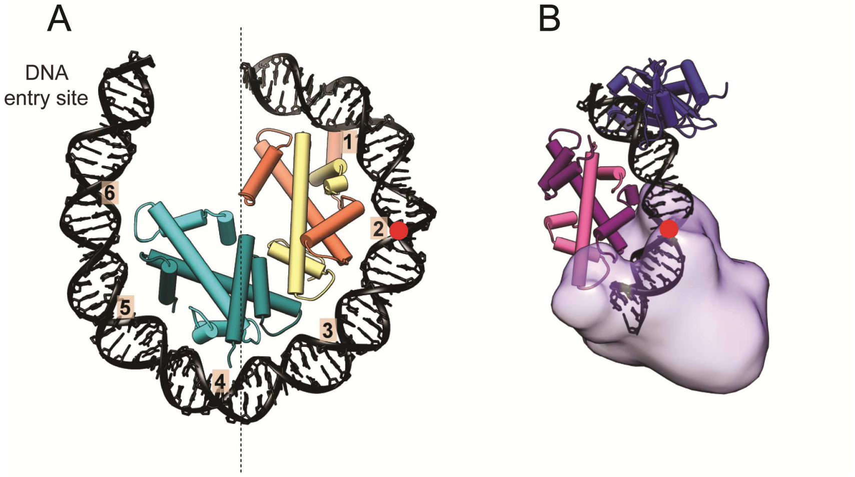

Figure 31. Binding of Swi2/Snf2 ATPase to its histone fold-DNA substrate.

Left: the ATPase domain of a chromatin remodeler specifically recognizes to the nucleosome particle at superhelical location 2 (SHL2), two turns from the dyad (marked with the red dot). This enables ATPase domain to specifically recognize e. g. histone H4 tail modifications. Histones H2A, H2B, H3 and H4 are shown in light cyan, dark cyan, yellow and coral, respectively. The protein and DNA parts symmetric according to the dyad axis were omitted. **Right**: Localization of Mot1^{CTD} segment from the EM reconstruction (purple transparent density) of Mot1–TBP–DNA–NC2 complex relatively to TBP and NC2^{HF}. The DNA particle presented here was superimposed based on the crystal structure of transcription factor NF-Y with DNA, which exhibits nucleosome-like curvature [109]. The position on DNA analogous to SHL2 on the nucleosome is also marked with the red dot.

Notably, the remodeling activity of Swi2/Snf2 chromatin remodelers in some cases requires the presence of histone tails or their modifications or can be modulated in response to the modifications of remodeler subunits themselves [53], [158]–[160]. Thus, the unexpected common feature shared between Swi2/Snf2 family remodeling enzymes and Mot1 to remodel a histone fold–DNA complex point out at a possibility that some modifications of NC2 subunits might affect Mot's affinity to its substrate. Indeed, both NC2 subunits, similarly to histones, have been shown to undergo various posttranslational modifications like phosphorylation, acetylation, methylation and ubiquitination *in vivo* [49], [151], [161]–[172]. The Mot1 region, which could be primarily responsible for "reading the NC2 code", also remains to be defined. For example, Mot1's insertion domain would be well positioned to response to modifications occurring on the C-terminus of NC2β. In analogy to nucleosomal substrates, Mot1^{CTD} itself could recognize modifications occurring on N-terminal tail of NC2α and/or NC2β. In the *E. cuniculi* system, NC2 does not seem to stimulate Mot1's ATPase activity, its TBP–DNA dissociation rate, or affinity to the substrate complexes ([89] and data not shown). Analogously, the ATPase activity of SWI/SNF and RSC remodeling complexes does not require intact nucleosomes for maximal stimulation [53]. In any case, the impact of NC2 modifications on Mot1 activity needs to be further investigated.

The ATPase activity of chromatin remodelers is stimulated both by naked DNA and nucleosomal substrates [53]. In contrast, the ATPase activity of Mot1 has been shown to be activated exclusively by TBP or TBP and DNA synergistically but not by DNA alone [9], [14], [45]–[47]. However, yeast Mot1^{CTD} can bind dsDNA on its own in a nucleotide-dependent manner [88] and the activity of the full-length Mot1 reaches the one of Mot1^{CTD} under very high salt or nonphysiological pH conditions [46]. Thus, the N-terminal part of Mot1 seems to have a regulatory effect on DNA binding, which is unmasked only upon the association with TBP [46]. The influence of DNA on the ATPase activity of Mot1^{CTD} has not been investigated.

The majority of SF2 members include accessory domains formed as N- or C-flanking regions or as inserts within the core ATPase domain [173]. Interestingly, most of the crosslinks between Mot1^{CTD} and NC2^{HF} map to the protrusion region of the RecA2-like subdomain, the major family-specific insertion site of Swi2/Snf2 ATPases [52]. Interestingly, crosslinks between histones H2A/H2B and RecA2 lobe of Ino80, the catalytic subunit of INO80 remodeling complex were detected [174]. A general role of the insertion regions of Swi2/Snf2 ATPases in distorting local DNA structure has already been proposed [175].

Intriguingly, such an extended interaction could suggest a direct role for insertions in inducing DNA distortion. Remarkably, SWI/SNF has been suggested to disturb histone–DNA contacts by wedging the RecA2 lobe between DNA and protein substrates [154]. This has been, however, not observed in the case of ISWI remodeler [154]. Therefore, further structural studies on more Swi2/Snf2 members would be necessary to address this issue in more detail.

Although Mot1 shares some similarities with chromatin remodelers and other Swi2/Snf2 ATPases, the findings presented here disfavor the hypothesis of DNA tracking-related mechanism of action and show that Mot1 rather locally disrupts the DNA interaction. Although the formation of the Mot1–NC2 "clamp" would be appropriate for sliding along DNA track, unobstructed DNA ends were shown not to be required for efficient Mot1-catalyzed dissociation of TBP/TBP–NC2 from DNA substrates [85], [89]. Accounting for slight rearrangements within the HEAT repeats, the CX-MS and EM analyses imply that Mot1^{CTD} would primary contact the non-TATA box-containing strand. According to the 3'–5' tracking direction shown for some Swi2/Snf2 remodelers, this would suggest that Mot1 could track over very short distances, e.g. one or two base pushing the substrates from the promoter

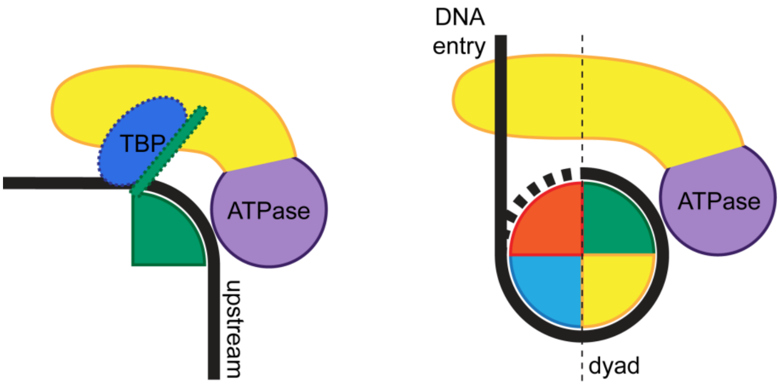

Figure 32. Remodeling of substrate protein–DNA complexes by Mot1 and nucleosome remodelers.

Left side: The binding of Mot1 (Mot1^{NTD} in yellow, Swi2/Snf2 ATPase domain in purple) induces destabilization of TBP–DNA and NC2–DNA interactions (TBP is shown in blue, NC2 is represented by a green shape). **Right side**: a Swi2/Snf2 remodeler bound to nucleosome. The DNA-binding domain engages DNA at the nucleosome entry site. In both cases, the ATPase domains in a similar manner specifically recognize their histone fold–DNA substrates. ATP hydrolysis-mediated conformational changes lead to short-range translocation of Mot1 into upstream direction from the TATA box causing the final release of TBP and NC2 from DNA. Analogously, the ATPase domain of a nucleosome remodeler actively pumps the DNA in 3'–5' direction, according to the tracking strand. The direction of DNA movement is represented by the black arrows.

into the downstream direction. This is, therefore, quite distinct to long-range tracking shown for RSC remodeling complex reaching up to 70 bp [73] or 40 bp for ISWI [71]. Moreover, only fully duplexed upstream DNA supports efficient Mot1–TBP–DNA complex formation and its dissociation [70]. This is again in contrast to other dsDNA translocases which are active on ssDNA substrates and translocate predominantly along one of the strands [71], [73], [75]. Thus, it appears that all Swi2/Snf2 ATPases undergo similar ATP-dependent conformational changes but they exploit them in a different way in response to various stimuli.

5.5 Novel roles for Mot1 and NC2β?

Although the function of NC2α and NC2β in the heterodimeric complex is supported by large body of in vitro and in vivo data, several independent studies postulated that NC2α and NC2β polypeptides might function as separate factors [94], [97], [99], [106], [121]–[123]. Many results are not entirely conclusive in this matter, since very often no direct comparison of the effect of either subunit on transcription process was monitored and the effects observed for NC2α or NC2β were assigned to the function of the whole complex. Thus, in the light of the accumulating data, such discrimination seems to be necessary for the precise data interpretation in future experiments.

The initial analysis of the *E. cuniculi* Mot1^{NTD}–TBP–NC2β complex crystal structure represents a distinct, uncharacterized form of Mot1–NC2β assembly. NC2β subunit is present in an unusually elongated conformation, which has not been reported for any histone fold protein subunit. However, NC2α and NC2β are the only subunits of a histone fold-containing protein complex, which were suggested to function as separate subunits. As described in the results section, the observed novel interaction between TBP, Mot1^{NTD}'s latch and NC2β's *H3* and *H4* would be only possible if Mot1 was a functional dimer. Although multimierization of Mot1^{NTD}–TBP–NC2β complexes was observed in gel filtration experiments, due to Mot1^{NTD}'s preference to crystallize in a particular configuration it is difficult to judge if the observed arrangement is relevant or whether it is a result of nonspecific hydrophobic interactions of the crystal lattice. Clearly, structural analysis of the complex in the presence of full-length Mot1 would be necessary to unambiguously answer some of the questions regarding functional relevance of the presented Mot1^{NTD}–TBP–NC2β crystal structure.

What could be the physiological function of Mot1 and NC2β bound to TBP? This aspect is particularly intriguing, since NC2 is preferentially imported to the nucleus as a preassembled complex [124]. Remarkably, Mot1 was reported to be responsible for ATP-dependent dissociation of the NC2 heterodimer [97]. ATP-independent disassembly of NC2, which is otherwise very resistant to extreme pH and salt conditions, was also observed in the presence of Mot1 for *E. cuniculi* proteins (not shown). Dissociation of NC2 into separate subunits would unmask NES of NC2β polypeptide resulting in different distribution of α and β subunits in the cell [124]. Remarkably, in the Mot1^{NTD}–TBP–NC2β structure the NES stretch of the NC2β subunit is localized at the interface between TBP and Mot1's latch. Therefore, Mot1 apart from catalyzing the dissociation of TBP and NC2 from DNA might be additionally responsible e.g. for blocking the export of NC2β from the nucleus. It is, however, not clear if Mot1^{NTD}–TBP–NC2β represents transcriptionally active ("loading complex") or inactive form ("dead-end" complex) of TBP. Certainly, more experiments including genome-wide ChIP and in vitro activity assays are required to understand the function of Mot1–NC2β assemblies. Additionally, analogous analysis of the NC2α subunit and the impact of posttranslational modifications would be necessary.

6. EXPERIMENTAL PROCEDURES

6.1 Materials

All common chemicals were obtained from Merck, Sigma–Aldrich or Carl–Roth, unless stated otherwise.

6.1.1 Media and antibiotics

2xYT, Lysogeny Broth (LB-Lennox) and Terrific Broth (TB) media used for culturing of the *E.coli* strains were prepared as described in **Table 4**. For the generation of solid media, 1.5% agar (w/v) was added. Sf21 insect cells were grown in Sf-900 III serum-free medium (Life Technologies). High Five insect cells were grown in Express Five serum-free medium (Life Technologies) prepared according to the manufacturer's instructions.

Table 4. Media used for culturing E.coli strains.

Compound	2xYT	LB	TB
Tryptone	16 g	10 g	12 g
Yeast extract	10 g	5 g	24 g
NaCl	5 g	10 g	-
Glycerol	-	-	4 mL
NaOH	pH ~ 7.0	pH ~ 7.0	-
0.17M KH_2PO_4 0.72M K_2HPO_4 (sterile solution)	-	-	100 mL
Distilled water	Up to 1000 mL		

Antibiotics used for the selection of plasmid-carrying *E. coli* clones are listed in **Table 5**. The stocks were used as 1:1000 (v/v) dilutions. Insect cell media were supplemented with 10 µg/mL gentamicin (Roth) and 10 mM L-glutamine (Invitrogen).

Table 5. List of antibiotics used for the maintenance of *E. coli* cultures.

Compound	Stock concentration [mg/mL]	solvent
ampicillin	100	water
chloramphenicol	34	ethanol
kanamycin	50	water
tetracycline	10	ethanol
gentamicin	7	water

6.1.2 Strains

Table 6. *E. coli* strains.

Strain	Supplier	Genotype
XL1 blue	Stratagene	recA1 endA1 gyrA96 thi-1 hsdR17 supE44 relA1 lac [F´proAB lacIqZΔM15 Tn10 (Tetr)]
Rosetta (DE3)	Novagen	F– *ompT hsdS*B (rB– mB-) *gal dcm* (DE3) pRARE2 (CamR)
B834 (DE3)	Novagen	F– ompT hsdSB(rB– mB-) met gal dcm (DE3)
DH10MultiBac	Redbiotech	F– *mcr*A Δ(*mrr*-*hsd*RMS-*mcr*BC) Φ80*lac*ZΔ M15 *lac*X74 *rec*A1 *end*A1 *ara*D139 (*ara*, *leu*)7697 *gal*U *gal*K Δ– *rps*L *nup*G/pMON14272/pMON7124

Table 7. Insect cells.

Strain	Species	Supplier
IPLB-Sf21-AE (Sf21)	*Spodoptera frugiperda*	Life Technologies
BTI-TN-5B1-4 (High Five)	*Trichoplusia ni*	Life Technologies

6.2 Molecular biology methods

All vectors were obtained from Petra Wollmann (Hopfner Group, Gene Center, LMU, Munich). For this study, TEV protease cleave sites were newly introduced between the protein sequences and the expression tags for all plasmids used, with single exception for pET28a-TBPfl vector, for which TEV cleavage site substituted thrombin cleavage site. Oligonucleotides used for cloning (**Table 8**) were purchased from Metabion in a desalted purity grade and in a lyophilized form and before use were diluted in distilled water.

Table 8. Expression plasmids.

Name	Plasmid	Encoded sequence	Restriction site	Tag
pET28TEV-TBPfl	pET28a	E. cuniculi TBP 1–198	NcoI/none	N-H_6 (TEV)
pETDuetTEV-NC2β-NC2α	pET-Duet1	*E. cuniculi* NC2β 1–147 (MCS1) *E. cuniculi* NC2α 1–95 (MCS1)	None/none (MCS1) None/XhoI (MCS2)	N-H_6 (TEV) (MCS1) None (MCS2)
pETDuetTEV-NC2β-NC2α$^{\Delta C}$	pET-Duet1	*E. cuniculi* NC2β 1–147 (MCS1) *E. cuniculi* NC2α 1–79 (MCS1)	None/none (MCS1) None/XhoI (MCS2)	N-H_6 (TEV) (MCS1) None (MCS2)
pFBDM-Mot1(TEV)	pFBDM	*E. cuniculi* Mot1 1–1256	None/NotI (MCS1)	N-H_6 (TEV)
pFBDM-Mot1^{NTD}(TEV)	pFBDM	*E. cuniculi* Mot1 1–778	None/NotI (MCS1)	N-H_6 (TEV)
pFBDM- Mot1$^{NTD\Delta L}$ (TEV)	pFBDM	*E. cuniculi* Mot1 1–778 Δ97–137	None/NotI (MCS1)	N-H_6 (TEV)
pFBDM-Mot1$^{\Delta L}$ (TEV)	pFBDM	*E. cuniculi* Mot1 1–1256 Δ97–137	None/NotI (MCS1)	N-H_6 (TEV)

Table 9. Oligonucleotides used for cloning.

Name	Sequence (5’ – 3’)
TBP_28TEV_F	AAACCTGTATTTTCAGGGACATATGGACGCACCAGATATTTCTTATGAGCATC
TEV_R	TGAAAATACAGGTTTTCGCCGCTGCTGTGATGATGATGATGATG
Mot1_TEV_F	AAACCTGTATTTTCAGGGACATATGAATAGATTAGAGAAGTTCTTCACCACACTGAAC
Duet_NC2b_TEV_F	AAACCTGTATTTTCAGGGACATATGAATATGGAGAAAAACGATGACGAAAACACATTACC
NC2a_P80*_F	TCGTGCTACCGAATCTGATTAAAAATTTGCGTTCCTCAA

6.2.1 Polymerase chain reaction (PCR)

Standard PCR reactions were performed using Phusion Flash High-Fidelity PCR Polymerase Mix (Thermo Scientific). Reaction mixtures were prepared accordingly to the manufacturer's protocol. The temperature of the annealing step was set to a value which was usually 3-5ºC lower than the predicted melting temperature of the used primiers. The melting temperature of the primers was estimated with Oligo Calc online tool (available at http-//www.basic.northwestern.edu/biotools/oligocalc.html). Digestion of the methylated template DNA was performed with DpnI (Thermo Scientific) by adding 1 μL of the enzyme directly to the PCR reaction followed by overnight incubation at 37ºC. Finally, PCR products were purified using Nucleo Spin Extract II Kit (Macherey-Nagel) and eluted in distilled water preheated to 50°C.

6.2.2 Site-directed mutagenesis

The procedure was performed according to QuikChange II Site-Directed Mutagenesis Kit Protocol (Stratagene) using Pfu Ultra DNA Polymerase (Stratagene). The primers introducing single-amino acid changes in the protein sequences were designed using Primer X online tool (http://www.bioinformatics.org/primerx/cgi-bin/protein_1.cg). After whole-plasmid PCR reaction, digestion of the methylated template DNA was performed with DpnI (Thermo Scientific) by adding 1 μL of the enzyme directly to the PCR reaction followed by overnight incubation at 37ºC. The reaction mixture was then directly used for transformation into *E. coli*.

6.2.3 In-Fusion cloning reaction

Molecular cloning was performed using In-Fusion Advantage PCR Cloning Kit (Clonetech). This method allows joining multiple pieces of DNA that have 15 bases of complementarity at their ends without the use of any restriction enzymes. The target insertion sequence was placed on the 5' ends of both cloning primers and the first 15 bp were complementary (see

Table 9, underlined). The In-Fusion cloning mixture was prepared according to the producer's manual using ~50 ng of isolated vector DNA. This protocol was used to introduce TEV cleavage recognition sites between the expression tags and proteins.

6.2.4 Transformation into *E. coli*

Competent cells (50–100 µL in a 1.5 mL microcentrifuge tube) were first thawed on ice. Subsequently, 5 µL of target DNA were added to the competent cells and gently mixed by tapping. The mixture was incubated for 15 minutes on ice. Heat shock was performed for 45 s at 42°C, after which cells were chilled on ice for 1 min. Next, 400 µL of room temperature LB medium was added and the cells were recovered at 37°C for 1 hour (600 rpm). Finally, the cells were spread onto solid LB medium containing appropriate antibiotics enabling positive selection of successfully transformed clones. Plates were incubated overnight at 37°C.

6.2.5 Plasmid DNA isolation and sequencing

Plasmid DNA isolation of single-colony transformants was performed using NucleoSpin Plasmid EasyPure kit (Macherey-Nagel) eluted in preheated distilled water. Plasmid DNA of the selected clones was sequenced by Eurofins.

6.2.6 Transposition into bacmid and bacmid DNA isolation

For the transposition of the donor plasmid into the bacmid, DNA was transformed into *E. coli* DH10MultiBac competent cells. For that, 100 µL of the competent cells were thaw on ice and transferred into a 15 mL polypropylene tube. Approximately 1 µg of the pFBDM plasmid with a gene of interest was added to the cells and incubated on ice for 30 min. After the incubation the cells were heat-shocked by transferring to a water bath heated up to 42°C for 60 s and cooled down on ice for 1 min. Subsequently, 600 µL of 2xYT medium without antibiotics was added and the cells were placed in a shaking incubator for 6–16 h at 37°C (200 rpm). After the recovery, the cells were spread onto agar plates containing kanamycin, gentamicin and tetracycline at 1:1000 dilutions of the stocks listed in **Table 5**, as well as X-Gal (100 µg/mL) and IPTG (0.5 mM). The plates were incubated for 2–3 days at 37°C. Afterwards, white colonies containing recombinant bacmid were streaked to confirm the phenotype. Positive colonies were inoculated into 5 mL of 2xYT medium containing kanamycin, gentamicin and tetracycline (**Table 5**) and grown overnight in a shaking incubator at 37°C (200 rpm). Bacmid DNA was isolated using isopropanol precipitation protocol according to the instructions included in Bac-to-Bac Baculovirus Expression Systems user manual from Invitrogen.

6.3 Protein expression and purification

6.3.1 Insect cell expression system

Insect cell expression system was used to express N-terminally His_6-tagged full-length *E. cuniculi* Mot1 (1–1256) and Mot1^{NTD} (1–778), *E. cuniculi* Mot1$^{\Delta latch}$ (1–1256, Δ97–137) and Mot1$^{NTD\Delta latch}$ (1–778, Δ97–137).

Propagation of the virus in the Sf21 insect cells

200 µl of Sf-900 III SFM medium (Life Technologies) was mixed with 3 µl of FuGene transfection reagent (Promega) and with 1–3 µg of isolated bacmid DNA. Prepared mixtures were incubated for 45 min at room temperature. In the meantime, 2 mL of Sf21 cells per one transfection reaction at $4 \cdot 10^5$/mL suspended in Sf-900 III SFM medium were prepared and left at 27.5°C for 30 min. After the incubation times finished, transfection mixtures were added to the cells and incubated at 27.5°C. After 3 to 4 days the media containing P0 virus were collected and centrifuged at 3000 rpm for 15 min. The supernatants (2 mL) were added to 10 mL of Sf21 cells at $1 \cdot 10^6$/mL suspended in Sf-900 III SFM medium per each construct and incubated in a shaker at 27.5°C for 3 days. Next, the cells were counted and the cultures were centrifuged. Only the best-transfecting viruses were selected for further amplification.

The selection was based on the viability of the transfected cells after the incubation time as well as on the number of the cells and average cell diameter in comparison to the not transfected control culture. Therefore usually two independent transfection reactions were prepared for each construct and more potent virus was chosen on this stage for the final experiments. Chosen P1-containing media (0.02–2 mL) were added to 20 mL of Sf21 cells diluted at $4 \cdot 10^5$/mL in Sf-900 III SFM medium per each construct. The volume of the P1 virus supernatant depended on the strength of the virus. The cultures were incubated in a shaker at 27.5°C for another 3 days. Afterwards the cells were counted and centrifuged at 3000 rpm for 15 min. The supernatants containing strong P2 viruses were stored at 4°C.

Protein expression

0.5–1L of High Five cells at $1 \cdot 10^6$/mL cultured in Express Five medium (Life Technologies) was infected with P2 virus in 1:1000 ratio and harvested 60–72 h afterwards. Pellets were frozen in liquid nitrogen and stored at -80°C or the purification was performed directly after harvesting.

Protein purification

Harvested cells were disrupted by brief sonication (30 s, 50% power, 30% duration) in the lysis buffer A1 or A2 for full-length Mot1 and Mot1^{NTD}, respectively. All the buffers used for the purification of the recombinantly expressed proteins are listed in **Table 10**. Soluble fraction was separated from the cell debris by centrifugation at 4° for 40 min at 15000 rpm. Supernatant was filtrated through a 45 µm filter (Merck Millipore) and loaded onto a gravity flow column with pre-equilibrated Ni-NTA beads (QIAGEN) at 4°. The flow-through fraction was reloaded onto the beads at least two more times. Unspecifically bound proteins were washed out extensively with buffer A and remaining fraction was eluted with elution buffer B. Elution fractions together with TEV protease (30:1 w/w) were dialyzed overnight against low salt ion exchange buffer C1 or C2 for full-length Mot1 and Mot1^{NTD}, respectively. After the dialysis the sample was centrifuged for 15 min at 4 at 1x000g and applied onto a 5 mL HiTrapQ column (GE Healthcare). Bound proteins were eluted from the column using linear gradient of high salt buffer D1 or D2 for full-length Mot1 and Mot1^{NTD}, respectively. Fractions containing protein of interest were concentrated to final volume of 3 mL (Merck Millipore) and loaded onto S200 16/60 gel filtration column pre-equilibrated in gel filtration buffer D. Protein fractions were concentrated to 10–20 mg/mL, pipetted as 15–50 µl aliquots, frozen in liquid nitrogen and stored at -80°C.

Selenomethionine labeling

Selenomethionine labeling in insect cells was performed for N-terminally His_6-tagged $Mot1^{NTD}$ construct. First, 100 mL of High 5 insect cell culture was adapted to Sf-900 II SFM medium (Life Technologies) by growing the cells from a starting concentration of $4\cdot10^5$/mL in a shaker for 4 days at 27.5°C. Subsequently, the cells were diluted to $1\cdot10^6$/mL in 0.5 L of Sf-900 II SFM medium and infected 1-750 v/v with P2 virus. The culture was grown for 12 h and centrifuged at 800rpm for 10 min. The cell pellet was resuspended in 0.5 L of Sf-900 II SFM medium supplied with 75 mg of L-cysteine (Sigma). After 4 h of methionine depletion the cells were centrifuged again and resuspended in 0.5 L of Sf-900 III SFM medium supplied with 75 mg of L-cysteine and 35 mg of L-selenomethionine (Acros Organics). The expression was carried out for another 48 h in a shaker at 27.5°C. The media were supplied with 1.4 µg/mL gentamicin.

6.3.2 *Escherichia coli* expression system

E. coli expression system was used to produce recombinant *E. coli* expression system was used to produce N-terminally His_6-tagged full-length *E. cuniculi* TBP (residues 1–198), His_6-tagged full-length NC2β (residues 1–147) and to co-express His_6-tagged full-length NC2β with an untagged version of full-length NC2α (1–95). His_6-tagged full-length NC2β was co-expressed from a plasmid carrying truncated NC2α construct (NC2α 1–79), which did not co-purify.

Protein expression

The constructs were expressed in *E.coli* Rosetta (DE3) strain by inducing the expression from the lactose promoter by adding 0.5 mM IPTG (final concentration) to the medium. The induction was performed after the optical cell density measured at 600 nm reached 0.6–1.0.

The expression was carried out at 18°C for around 20 h (overnight).

Protein purification

Initial protein purification step for TBP was performed using buffer A3 and A2 for NC2α/β heterodimer. The resuspended cells were sonicated two times for 5 min (50% power, 30% duration) using a sonicator and centrifuged at 4° for 40 min at 15000 rpm. The supernatant was mixed with pre-equilibrated Ni-NTA beads (QIAGEN) and incubated for 2h at 4° in a batch mode. After the incubation the resin was loaded onto a gravity flow column and washed extensively with buffer A. Remaining proteins were eluted with elution buffer B. TEV protease was added to the elution fractions (30:1 w/w) to cut off the His_6 tag. The sample was dialyzed overnight against low salt ion exchange buffer C2 and centrifuged for 15 min at 4 at 1000g. Further purification was performed by ion exchange chromatography applying the sample on a 5 mL HiTrapS. Bound proteins were eluted from the column using a linear gradient of high salt buffer D2. Elution fractions were concentrated to a final volume of 3 mL by ultrafiltration (Millipore) and loaded onto S75 16/60 gel filtration column (GE Healthcare) pre-equilibrated in gel filtration buffer D. Protein fractions were concentrated to 4-20 mg/mL, pipetted as 50 µl aliquots, frozen in liquid nitrogen and stored at -80°C.

Table 10. Buffers used for the purification of the recombinantly expresses proteins.

Name		Content
Lysis	A1	50 mM Hepes, 300 mM NaCl, 5 mM Imidazole, 5% glycerol (v/v), 10 mM B-ME, pH 7.5, Protease Inhibitor Cocktail Tablets, EDTA-Free (Sigma)
	A2	50 mM Hepes, 400 mM NaCl, 10 mM Imidazole, 10 mM B-ME, pH 7.5
	A3	50 mM Hepes, 1.5M NaCl, 10 mM Imidazole, 10 mM B-ME, pH 7.5
Elution	B	50 mM Hepes, 200 mM NaCl, 300 mM Imidazole, 10 mM B-ME, pH 7.5
IEX low salt	C1	20 mM Hepes, 100 mM NaCl, 2 mM DTT, 0.5 mM EDTA, 5% glycerol (w/w), pH 8.0
	C2	20 mM Hepes, 100 mM NaCl, 2 mM DTT, pH 8.0
IEX high salt	D1	20 mM Hepes, 1 M NaCl, 2 mM DTT, 0.5 mM EDTA, 5% glycerol (w/w), pH 8.0
	D2	20 mM Hepes, 1 M NaCl, 2 mM DTT, pH 8.0
Gel filtration	E	20 mM Hepes 7.5, 200mM NaCl and 2mM DTT

Selenomethionine labeling

The plasmids were transformed according to the standard protocol into *E. coli* Rosetta B834 cells and plated on LB–agar plates. The 200 mL precultures were inoculated into LB media and grown overnight at 37° with continuous agitation. The main cultures were grown in Selenomethionine Medium Base supplemented with Nutrient Mix (Molecular Dimensions). Additionally, selenomethionine solution was added at a final concentration of 42 mg/L to the sterile medium prior to inoculation. The media and selenomethionine solution were prepared according to the manual supplied by the producers. The cultures were grown in a shaker (160 rpm) at 37° until OD_{600} reached 0.4. Next, the temperature was set to 18° and the cultures were further grown until $OD_{600} \approx 0.7$. The expression was initiated by adding IPTG at final concentration of 0.5 mM and carried out further at 18°C overnight. All of the media were supplemented with chloramphenicol and additional antibiotics dependent on the resistance-coding expression plasmids. The applied protein purification protocols did not differ from the ones used for the purification of unlabeled proteins.

6.4 Protein biochemistry

6.4.1 Protein quantification

Protein concentration was calculated based on UV absorbance at 280 nm using NanoDrop 1000 spectrophotometer (Thermo Scientific). Due to high absorption of DNA at 280 nm, protein concentration of the protein–DNA complex samples was performed using Bio-Rad Protein Assay Dye Reagent Concentrate (BioRad) according to the manufacturer's instruction, which is based on the Bradford method [176]. Bovine serum albumin (Roth) was used to generate the calibration curve.

6.4.2 SDS-PAGE

Protein sample analysis was performed using NuPAGE Bis-Tris Precast Gel system (Life Technologies) according to the manufacturer's instructions. Prior to loading, the samples were boiled for 5 min at 95°C in the presence of 4x concentrated Sample Buffer (see **Table 11**).

Table 11. Solutions used performing SDS-PAGE analysis.

4x Sample buffer	**Coomassie staining solution**
110 mM Tris pH 6.8	7% (w/v) acetic acid
16% glycerol	50% (w/v) EtOH
4% (w/v) SDS	0.2% (w/v) Coomassie Brilliant Blue R-250
5% 2-ME	
0.6% bromphenol blue	

Coomassie staining

The gels were placed in a plastic container and briefly rinsed with water. Next, Coomassie staining solution (see **Table 11**) was added to fully cover the gel and was incubated for at least 30 min on an agitating shaker. The gels were destained in water.

Silver staining

Silver staining protocol was based on the Bloom method ([177] and **Table 12**).

Table 12. Silver staining solutions.

Solution	**Ingredients**
A	10% acetic acid, 45% methanol
B	0.8 mM $Na_2S_2CO_3$
C	2 mg/mL $AgNO_3$, 0.026% formaldehyde
D	6% Na_2CO_3, 0.0185% formaldehyde, 16 µM $Na_2S_2CO_3$

The gel was rinsed with distilled water and fixed in solution A for 2 min and again for 20 min using fresh buffer (50 rpm). Subsequentially, the gel was washed two times for 10 min with 50% ethanol and once for 10 min with 30% ethanol. Next, the gel was sensitized in buffer B by 60 s incubation (50 rpm) and washed three times for 20 s in distilled water. The staining was performed using solution C for 20 min (50 rpm) followed by the washing step (3x, 20 s in distilled water). Reduction was performed using solution D until the band intensity reached satisfying intensity. The reaction was stopped by the addition of 10% acetic acid. Finally, the solution was exchanged to 1% acetic acid and incubated for further 20 min. The gels were then stored in distilled water.

6.4.3 Electrophoretic mobility shift assays (EMSA)

The assays performed on *E. cuniculi* proteins shown in **Figure 28** were by Prof. David Auble (Department of Biochemistry and Molecular Genetics, University of Virginia Health System, Charlottesville, USA) as described [47], [89] using 47 bp oligonucleotide labeled with fluorescein at the 5’ end of one strand (5’–GGGTACGGCCGGGCGCCCCGGATGGGGGGCTATAAAAGGGGGTGGGC–3’ top).

The assays shown in **Figure 9** were performed as follows. DNA oligos (ds 5’–CAGTACGGCCGGGCGCCCGGCATGGCGGCCTATAAAAGGGTC–3’, top strand) were mixed with TBP at 20 and 200 nM final concentration, respectively, in a final volume of 15 µL. The DNA–TBP complexes were incubated for 5 min at 4°C. Subsequently, 15 µL of serial dilutions of NC2 or NC2β were added (covering the range from 1 to 10 molar excess over TBP). The samples were further incubated for 5 min at 4°C. Next, 20 µL of each sample were loaded onto 0.5% agarose gel prepared in 1xTAE (40 mM Tris pH 8.0, 20 mM acetic acid, 1 mM EDTA) and run at 4°C at 60V for approximately 1h in 1x TAE buffer. All DNA and protein dilutions were prepared in 20 mM Tris 7.5, 100 mM NaCl, 5 mM $MgCl_2$ and 10% (v/v) glycerol. To enable visualization of the DNA-bound complexes, the 5’ end of the bottom strand was labeled with 5-FAM. The visualization was performed using Typhoon 9400 fluorescence scanner (GE Healthcare).

6.4.4 Sample preparation for crystallization and analytical purposes

For the preparation of the complex thawed aliquots of single components were mixed in a stepwise manner and purified by gel filtration. For the DNA-containing complexes first DNA and TBP were mixed in 1.2:1 to 1.5:1 molar ratio and incubated at 4° for 5 minutes. At higher concentrations of the stocks protein precipitation was common at this step. After addition of

5 M NaCl stock so that the final concentration increased from ~200 to 300 or 400 mM of NaCl the precipitate resolubilized. In the second step NC2/NC2β was added so that the molar ratio is equal and the sample was incubated for another 5 min followed by the final addition of Mot1^{NTD}/Mot1$^{NTD\Delta latch}$/Mot1/Mot1$^{\Delta latch}$, 5 min incubation and centrifugation. The amount of Mot1 was always substoichometric to DNA, TBP and NC2 in order to avoid any presence of free Mot1 constructs. Any remaining DNA single proteins or lower-order complexes were easy to separate from the main complex fraction in contrast to free Mot1 and homodimeric Mot1^{NTD} and Mot1$^{NTD\Delta latch}$. In the case of complexes formed without DNA, Mot1 was always substoichometrically mixed with NC2/NC2β and TBP (usually 1:1.5). In this case the order of adding the components did not affect the complex formation. To separate the complex of interest from the excess of single components the sample was applied onto Superdex 200 10/300GL or Superdex 200 Increase 10/300GL columns. For analytical purposes, Superdex 200 5/150 GL or Superdex 200 Increase 5/150 columns were used (all from GE Healthcare). Gel filtration experiments shown in section **4.1.1** were performed in 20 mM MES (KOH) pH 6, 60 mM KCl, 5 mM $MgCl_2$ and 2 mM DTT buffer.

6.5 X-ray crystallography

6.5.1 Crystallization

For the crystallization experiments fractions containing homogeneous complex were concentrated to ~2–5 mg/mL and centrifuged before the setups. The complexes were screened for crystallization in a 96 well sitting-drop format (MRC Crystallization Plate, Molecular Dimensions) using commercial screens using Phoenix Crystallization robot (Art Robbins). After obtaining initial hits the crystals were optimized by growing in hanging drop vapor diffusion format at 22°C by mixing 1 µL of the sample with 1 µL of the reservoir (500 µL). Seeding experiments were performed using Seeding Tool from Hampton Research after one hour to one day of equilibration.

Mot1$^{NTD\Delta latch}$/Mot1^{NTD}–TBP–DNA–NC2 complex crystals

Sample preparation in gel filtration was performed in 20 mM MES, 60 mM KCl, 5 mM $MgCl_2$ and 2 mM DTT as described in section **6.4.4**. The crystals of the Mot1$^{NTD\Delta latch}$/Mot1^{NTD}–TBP–DNA–NC2 complex grew for 1–14 days only in conditions containing PEG polymers as precipitants with no obvious preferences for salts, additives or pH. In all of the refined conditions crystals were characterized by very similar morphology and growing behavior. **Table 13** and **Table 14** list all DNA nucleotides tested. Oligonucleotides used for crystallization experiments were HPLC- or PAGE-purified and obtained from Biomers in a lyophilized form. These oligomers were resuspended in 40 mM TRIS pH 8.0, 100 mM NaCl, 10 mM $MgCl_2$ at 1mM final concentration, mixed with the complementary strand in 1:1 molar ratio and annealed. The annealing process was performed by heating up the sample to 95ºC, followed by 5 min incubation at this temperature and gradual cooling down to reach the final room temperature (0.1°C/s).

Despite extensive crystal optimization, Mot1$^{NTD\Delta latch}$–TBP–DNA–NC2 complex crystals did not show diffraction better than ~7 Å. Different post-crystallization crystal handling methods like crystal annealing, dehydration or crosslinking with glutaraldehyde were applied in order to improve the diffraction quality. None of them showed any positive effect. Crystals of Mot1^{NTD}–TBP–DNA–NC2 complex showed very similar morphology and the preference for crystallization conditions although the length of the DNA was slightly different. Best crystals of Mot1^{NTD}–TBP–DNA–NC2 complex were grown containing 0.2 M imidazole malate pH 5.0–6.0 and 9–16% PEG4000. Diffraction quality crystals were obtained from the streak-seeded selenomethionine-derivatized Mot1^{NTD}–TBP–DNA–NC2 complex grown in 0.2 M imidazole malate pH 5.1 and 11% PEG4000. Native crystals of the complex from the same condition were used for the seeding.

Table 13. DNA oligos used in the crystallization experiments including Mot1$^{NTD\Delta latch}$ construct.
The sequence of only one strand in presented

Name	Construct	Sequence
12/8/6	26ds	GTGAAGTAGGGCTATAAAAGGGGGTG
12/8/6-2(5)tb	24ds + 5'overhangs	GTGAAGTAGGGCTATAAAAGGGGG top
8/8/8	24ds	AGTAGGGCTATAAAAGGGGGAGTA

10/8/6	24ds	GAAGGGGGGCTATAAAAGGGGGTG
8/8/8-2(3)t	22ds + 3’ overhang top	AGTAGGGCTATAAAAGGGGGAGTA top
8/8/8-2(3)b	22ds + 3’ overhang	TACTCCCCCTTTTATAGCCCTACT bot
10/8/6-2(5)t	22ds + 5’ overhang top	GAAGTAGGGCTATAAAAGGGGGAG top
10/8/6-2(3)b	22ds + 3’ overhang bot	CTCCCCCTTTTATAGCCCTACTTC bot
9/8/6	23ds	AAGTAGGGCTATAAAAGGGGGTG
8/8/6	22ds	AGTAGGGCTATAAAAGGGGGTG
8/8/6-2(5)t	20ds + 5’ overhang top	AGTAGGGCTATAAAAGGGGGAG
8/8/6-2(3)t	20ds + 3’ overhang top	AGTAGGGCTATAAAAGGGGGAG top
8/8/6-2(3)b	20ds + 3’ overhang bot	CTCCCCCTTTTATAGCCCTACT bot
8/8/6-2(3)b	20ds + 3’ overhang bot	CTCCCCCTTTTATAGCCCTACT bot
7/8/6	21ds	ATAGGGCTATAAAAGGGGGTG
8/8/4	20ds	AGTAGGGCTATAAAAGGGGG
5/8/6	19ds	GGGGCTATAAAAGGGGGTG
8/8/3	19ds	AGTAGGGCTATAAAAGGGG
8/8/1	17ds	AGTAGGGCTATAAAAGG
3/8/3	14ds	GGCTATAAAAGGGG

Table 14. DNA oligos used in the crystallization experiments including Mot1^{NTD} construct.
The sequence of only one strand in presented

Name	**Construct**	**Sequence**
10/8/6	24ds	GAAGGGGGGCTATAAAAGGGGGTG
10/8/8	26ds	GAAGTAGGGCTATAAAAGGGGGAGTA
9/8/9	26ds	AAGTAGGGCTATAAAAGGGGGTGGCA
8/8/9	25ds	AGTAGGGCTATAAAAGGGGGTGGAA
9/8/8	25ds	AAGTAGGGCTATAAAAGGGGGGTGGC
8/8/9	25ds	AGTAGGGCTATAAAAGGGGGTGGCA
8/8/8	24ds	AGTAGGGCTATAAAAGGGGGTGGC
8/8/8-2(3)t	22ds + 3’ overhang top	AGTAGGGCTATAAAAGGGGGAGTA top
8/8/8-2(3)b	22ds + 3’ overhang bot	TACTCCCCCTTTTATAGCCCTACT bottom
8/8/7	23ds	AGTAGGGCTATAAAAGGGGGTGG
7/8/8	23ds	GTAGGGCTATAAAAGGGGGAGTA
8/8/4	20ds	AGTAGGGCTATAAAAGGGGG
8/8/1	17ds	AGTAGGGCTATAAAAGG
3/8/3	14ds	GGCTATAAAAGGGG

Mot1^{NTD}–TBP–NC2β complex crystals

Sample preparation in gel filtration was performed in 20 mM HEPES (HCl), 100 mM NaCl, 1 mM $MgCl_2$ and 2 mM DTT as described in section **6.4.4**. The initial crystals appeared in few PEG-containing conditions and were growing in form of needle bundles or clusters of thin plates, which were useless for diffraction experiments or diffracted very poorly (maximally 5 Å). Improved crystal morphology and diffraction quality was obtained by streak seeding of the self-nucleated crystals grown in conditions containing 0.1 M sodium citrate pH 5–6 and PEG4000, supplemented with 0.1 M sodium malonate, 0.2 M ammonium sulphate, or 0.1 M magnesium acetate. Best diffraction quality crystals (3.3 Å) were obtained from the condition containing sodium malonate and appeared 3–14 days after seeding. The seeded crystals were not extensively optimized (tested on the synchrotron only once) and it is thus likely that further refinement would lead to even better diffracting crystals. Crystals grown in magnesium acetate conditions were quite reluctant to seeding and turned out to be Mot1^{NTD}–TBP crystals of the same space group, unit cell dimensions and organization of the asymmetric unit as in already published structure [47].

6.5.2 Data collection and processing

Before the data collection crystals were flash-frozen in liquid nitrogen using 25% glycerol or 25% ethylene glycol (final v/v) as a croprotectant.

Mot1^{NTD}–TBP–DNA–NC2 structure

Diffraction data was collected at the European Synchrotron Radiation Facility (ID-29) at 100K and λ=0.9796 Å. The reflections were indexed, integrated and scaled with *XDS* [178] in the space group C *1 2 1* (a= 150.6 Å, b= 140.3 Å, c= 90.8 Å, α= 90.0°, β= 113.7°, γ= 90.0°). The calculation of Matthew's coefficient (*MATTHEWS_COEF*, CCP4 package [131], [179], [180]) suggested one complex per asymmetric unit and 60% of the solvent content. The calculation is based on the analysis of the solvent content distribution among PDB entries giving the most probable number of molecules in the asymmetric unit of a known molecular mass.

Unfortunately, the verification of the presence and location of the selenium K absorption edge was not performed due to technical problems at the beamline and the data set was collected at the theoretical wavelength of the selenium K absorption edge. Owing to poor crystal diffraction and lack of experimentally determined optimal wavelength, the anomalous signal was insufficient to allow experimental phasing. Nevertheless the structure was successfully solved by molecular replacement method with *Phaser*, part of the *CCP4* software suite [131], [181] using first *E. cuniculi* Mot1^{NTD} and TBP (PDB-ID 3OC3 [47]) as search models. The initial model of DNA was based on the human TBP–DNA–NC2 structure (PDB-ID 1JFI [107]) Homology model of the NC2 heterodimer was prepared using *CHAINSAW* (*CCP4* [131], [182]) based on the human TBP–NC2–DNA complex structure and the C subunit of NF-Y complex (PDB-ID 4AWL [109]). The NC2 subunits were manually fitted into the density. The structure was refined in *BUSTER* (v. 2.10.1) at 3.8 Å using TLS refinement strategy [183] and manually rebuilt in *Coot* [184]. Applying density modification methods, i.e. solvent flattening with *PARROT* (*CCP4*) [131], [132] as well as *B*-factor sharpening and calculation of feature-enhanced $2F_o - F_c$ map with *PHENIX* [133] enabled unambiguous density interpretation. The histone fold region was characterized by relatively high *B*-factors and poor density and therefore the side chains of the residues NC2α 15–89 and NC2β 12–101 were omitted in the final model. The sequence register was confirmed by computing anomalous difference density map, which showed signal of the selenium atoms (**Figure 12**).

Mot1^{NTD}–TBP–NC2β structure

Diffraction data was collected at the X06SA beamline of the Swiss Light Source (Villigen, Switzerland). A 180 ° dataset was collected at λ= 0.9797 Å and 100 K. The data set was indexed, integrated and scaled in space group $P\ 1\ 2_1\ 1$ (a=116.8 Å, b=150.1 Å, c=172.8 Å, α=90.0°, β=107.1°, γ=90.0°) to 3.3 Å using *XDS* [178]. The calculation of Matthew's coefficient [131], [179], [180] suggested four complexes per asymmetric unit with 55% solvent content. The structure was solved by molecular replacement with *Phaser*, part of the *CCP4* software suite [131], [181] using the *E. cuniculi* Mot1^{NTD} and TBP from the Mot1^{NTD}–TBP complex crystal structure [47] as separate search models. The NC2β subunit was modeled into the $2\ F_o - F_c$ and $F_o - F_c$ density maps using *Coot* [184] and iteratively rebuilt and refined with *PHENIX* [133] at 3.3 Å using non-crystallographic symmetry restraints (NCS) and group *B*-factor refinement strategy. The sequence register of four short α-helices most probably belonging to NC2β chains could not be unambiguously defined due to the discontinuities in the polypeptide chains and relatively low resolution. Thus, these helices were included in the models as poly-alanine stretches. Higher resolution data would be required to confirm the identity of these helices and assure the sequence register.

6.6 Electron microscopy

6.6.1 Sample preparation

The complex formation protocol was same as described in section **6.4.4** with some modifications; the complex was formed on a 38 bp DNA substrate (5'–CAGGCCGGGCGCCCGGCATGGCGGCCTATAAAAGGGTC–3', top strand and 20 mM HEPES pH 8.2, 60 mM KCl, 5 mM $MgCl_2$ and 2 mM DTT was used in the gel filtration step. After the separation, the main peak fractions were supplied with 1 mM ABF (formed by mixing ADP:$BeCl_2$:NaF in 1:1:4 molar ratio), 1 mM AGS or 1 mM ADP added right after the gel filtration. The ADP stock at 60 mM was prepared in 0.5 M HEPES pH 8.0 and AGS at 50 mM in 0.1 M HEPES 8.0. According to the Bradford assay, the final concentration of the sample used for the experiment was 25 µg/mL. Negatively stained grids were prepared immediately after the complex sample was available.

Further handling of the sample, data collection, processing and validation was done by Jan Schuller (Förster Group, Max Planck Institute of Biochemistry, Martinsried, Germany) and is described in detail elsewhere [89].

6.6.2 Modeling into EM density

The rigid-body docking of Mot1^{NTD}–TBP–DNA–NC2 crystal structure was performed using *colores* applying a 10° sampling step size to the down-filtered (22 Å) search probe [144]. The

DNA was omitted from the model. Additionally, Laplacian filter maximizing the fitting contrast was applied. The fitting was preformed for the correct and mirrored reconstruction and resulted in several possible fits for the Mot1^{NTD}–TBP–NC2 module. After manual inspection, one of the solutions (for the rightful hand) was qualified as the correct solution. The other fits were nonsense fits resulted from template drifting, which often occurs at low resolution when the structure represents only a part of the density it is docked into [144].

6.7 Chemical protein–protein crosslinking and mass spectrometry analysis

6.7.1 Sample preparation

The complex formation protocol used is described in section **6.5.1**. The complex was first formed in the presence of 42 bp promoter DNA in 20 mM HEPES pH 8.2, 60 mM KCl, 5 mM $MgCl_2$ (ds 5'–CAGTACGGCCGGGCGCCCGGCATGGCGGCCTATAAAAGGGTC–3' top strand). After the separation, the main peak fraction samples were supplied with the nucleotides as described in section **6.4.4**. The final concentration of the sample used for the experiment was 0.66 mg/mL, as calculated by the Bradford assay.

6.7.2 Titration of the crosslinker

Di-sulfo-succinimidyl-glutarate (DSSG, Creative Molecules) was initially dissolved in dimethylformamide (DMF) to a final concentration of 25 mM (heavy/light). The stock was diluted with water and added to the protein sample (~50 µg) placed in a 1.5 mL polypropylene tube to yield final desirable molar concentration (0.05–2 lysines:DSSG). The crosslinking reaction was carried out at 30°C with continuous shaking and quenched after 35 min by the addition of 0.1 (v/v) 1 M TRIS pH 8.5 followed by 15 min incubation at 30°C. Titration of DSSG was analyzed by running 1 µg of each the crosslinked sample on an SDS-PAGE gel followed by silver staining. The titration of the crosslinker was done in order to find optimal concentrations of the compound under given conditions leading to maximal crosslinking efficiency which does not cause formation of aggregates between the complexes in the solution. Molar ratio of 1:1 lysines:DSSG was selected for the main experiments. Trypsine digestion, extraction of the peptides, and mass spectrometric analysis of the crosslinked peptides was performed by Gabriele Stoehr (Hopfner Group, Gene Center, LMU, Munich). Experimental procedures explaining this part of the experiments can be found elsewhere [89].

6.7.3 Analysis of the theoretical crosslinks within the Mot1^{NTD}–TBP–NC2 module

In order to analyze the distribution of distances between all lysines within the complex, script K_sites_xlinks.sh was created (K_sites.xlinks.sh, **Script 1**). The script reads input files provided as continuous one-letter amino acid sequences of unlimited number of protein sequences (but one file per each protein) and creates an output list (in CSV format) containing all possible pairs of lysines within this complex. Additionally, the number of lysines found in each sequence, total number of lysines nad the number of “nonredundant” crosslinks are written to a .txt file. The final output CSV file additionally includes redundant “crosslinks” with reversed order of sites, e.g. K125 ProteinA–K33 ProteinB as well as K33 ProteinB–K125 ProteinA and, similarly, lists “crosslinks” to the same residue, i.e. K125 ProteinA–K125 ProteinA. These are, however, ignored by Chimera Xlink analyzer plug-in which reads the CSV output file, maps the crosslinks on the structural models and writes out the distances [185].

6.7.4 Analysis of the crosslinks between the Mot1^{NTD}–TBP–NC2 module and Mot1^{CTD}

The set of Mot1^{CTD} orientations (n=20,000) was generated using *RANCH*, part of the EOM package [141]. The eight amino acid linker between Mot1^{NTD} and Mot1^{CTD} (not present in any of the atomic models) was assumed to flexibly join these two domains. Models were generated in the “compact” mode, i.e. using C_α angles distribution consistent with disordered proteins but forcing the reconstructed linkers to be rather compact [141]. Next, all models were displayed and the distances were measured using a set of scripts enabling easy handling

Script 1. K_sites.xlinks.sh

```
#!/bin/bash
# K_sites_xlinks.sh
# Generate a file with a list of all lysines present in the *.seq input files
for f in *.seq;do cat $f | sed 's/\(.\{1\}\)/\1 /g' > $f.seq2;done
for f in *.seq.seq2;do cat $f | tr ' ' '\n' | cat -n | sed 's/ //g' | sed 's/\t/ /g'> $f.seq3;done
for f in *.seq.seq2.seq3;do sed '/K/!d' $f > $f.seq4;done
for f in *.seq.seq2.seq3.seq4;do awk '{print $0,FILENAME}' $f > $f.seq5;done
for f in *.seq.seq2.seq3.seq4.seq5;do awk -F. '{print $1}' $f > $f.seq6;done
for f in *.seq.seq2.seq3.seq4.seq5.seq6;do cat $f >> list.txt;done

# Generate a file with a list of all possible linkages between lysines
while IFS= read -r i
        do while IFS= read -r k
                do printf "%s %s\n" "$i" "$k"
                done < list.txt
        done < list.txt > total_xlinks.txt

awk '{print $0,"40"}' total_xlinks.txt > total_xlinks_40.txt       #Adds column with ld-Score value (40)
cut -d" "  -f-1,3-4,6- total_xlinks_40.txt > total_xlinks_40_cut.txt         # Deletes columns with residue name
awk '{if($2==$4) print $0,"intra-protein xl";else print $0,"inter-protein xl"}'total_xlinks_40_cut.txt /
> total_xlinks_40_cut_anal.txt        # Adds inter/intra link tag to each crosslink
sed -i 1i"AbsPos1 Protein1 AbsPos2 Protein2 ld-Score XLType" / total_xlinks_40_cut_anal.txt # Adds headers

# Write as .CSV file and define inter- and intraprotein crosslinks
sed 's/ /,/g' total_xlinks_40_cut_anal.txt > K_sites_xlinks1.csv
sed 's/intra-protein,xl/intra-protein xl/g' K_sites_xlinks1.csv > K_sites_xlinks2.csv
sed 's/inter-protein,xl/inter-protein xl/g' K_sites_xlinks2.csv > K_sites_xlinks.csv

# Write out additional file with number of found sites and generated crosslinks
for f in *.seq.seq2.seq3.seq4;do wc -l $f >> 1.txt;done
awk '{s+=$0} END {print s " total_lysines_found"}' 1.txt >> 1.txt
echo $(wc -l < total_xlinks.txt) "total_created_xlinks" >> 1.txt
awk -F. '{print $1}' < 1.txt > 2.txt
tac 2.txt > sites.txt
a=$(awk 'FNR==1 {print $1}' sites.txt)
b=$(awk 'FNR==2 {print $1}' sites.txt)
c=$(((a - b) / 2))
echo "$c total_non-redundant_xlinks" >> sites.txt

# Removes all files except for the script, input and output files
shopt -s extglob
rm !(*.seq|K_sites_xlinks.csv|sites.txt|K_sites_xlinks.sh)
```

of the generated data. First of them (pymol_template.py, **Script 2**) was a modified version of PyMOL script “Measure Distance” (source code available at http://www.pymolwiki.org/). Running it would open a file defined as name, create file name.txt and write out distances between C_α atom of residue 1 belonging to chain A and residue 2 belonging to chain B. Separate template scripts were created for each of the crosslinking data sets, where all nonredundant linkages detected in particular experiment were listed. Since the total number of the models would not allow to manually run this script for each of the computer models, another script was used to save a separate *.py file for each of the models by changing the **name** field in pymol_template.py (distances_batch.sh, **Script 3**). Third script created a text file (batch.txt), which would be then finally launched in PyMOL. As a result, *.pdb.py.txt files were created, each containing number of the distances between the atoms defined in the template pymol_template.py file.

Script 2. Modified “Measure Distance” script executed in PyMOL (pymol_template.py).

```
from pymol import cmd
cmd.load('/path/name')
f=open('/path/name.txt','w')
dst=cmd.distance('i. 1 and chain A and n. CA','i. 2 and chain B and n. CA')
f.write("%8.3f\n"%dst)
f.close()
cmd.reinitialize()
```

Script 3. distances_batch.sh.

```
#!/bin/bash
# distances_batch.sh

# Substitutes the name field in the template script for the name of the model
for f in *.pdb;do sed -e "s/name/$f/" path/pymol_template.py > path/$f.py;done

# Generates a batch file to run the modified template scripts for each of the models
for f in *.pdb.py;do echo "run path/$f" >> batch.txt;done

# Removes all files except for the script, input and output files
shopt -s extglob
rm !(*.pdb|distances_batch.txt|distances_batch.sh)
```

Finally, the models were scored according to the number of crosslinks violating the 30 Å cutoff distance [142]. To perform this, script scores.sh (**Script 4**) was used to count the number of distances, which are greater or equal to a given value (here: 30) and write the number of counts to *.pdb.py.txt.violations files. Finally, same script enabled to count the number of the crosslinks which were not fulfilled according to the used threshold value defined in violations.sh and write out the final score to a *.pdb.py.txt.violations.score file for each of the models. To enable easy data handling, all scores were combined into a single text file score_list.txt, where name of the model and the final score was listed.

Script 4. scores.sh.

```
#!/bin/bash
# scores.sh

for f in *.txt;do awk '$1>=30' $f > path/$f. violations;done        # Lists only crosslinks >= 30 Å

for f in *.violations;do wc -l $f > path/$f.score;done   # Counts the violated crosslinks

for f in *.score;do cat *.score > score_list.txt;done      # Lists violation score for each model

# Removes all files except for the script, input and output files
shopt -s extglob
rm !(*.txt|score_list.txt|scores.sh)
```

For the residues NC2α K61, K62, K92 and NC2β K27, which were not visible in the crystal structure (i. e. comprising short loop regions) but important for the analysis, the distances refer to the position which could be unambiguously modeled based on the crystal structure of NF-Y complex (PDB-ID 4AWL [109]).

6.8 Figure preparation

Molecular graphics and analyses were performed with the UCSF Chimera package [146], PyMOL Molecular Graphics System (v. 1.5.0.4 Schrödinger, LLC), OriginPro 8G (OriginLab) and Adobre Illustrator CS4 v14.0.0 (Adobe Systems).

7. REFERENCES

[1] B. P. Cormack and K. Struhl, “The TATA-binding protein is required for transcription by all three nuclear RNA polymerases in yeast cells.” *Cell*, vol. 69, pp. 685–696, 1992.

[2] N. Klages and M. Strubin, “Stimulation of RNA polymerase II transcription initiation by recruitment of TBP in vivo.” *Nature*, vol. 374, pp. 822–823, 1995.

[3] S. Hahn, S. Buratowski, P. A. Sharp, and L. Guarente, “Yeast TATA-binding protein TFIID binds to TATA elements with both consensus and nonconsensus DNA sequences.” *Proc. Natl. Acad. Sci. U. S. A.*, vol. 86, pp. 5718–5722, 1989.

[4] T. Juven-Gershon and J. T. Kadonaga, “Regulation of gene expression via the core promoter and the basal transcriptional machinery.” *Developmental Biology*, vol. 339. pp. 225–229, 2010.

[5] T. Matsui, J. Segall, P. A. Weil, and R. G. Roeder, “Multiple factors required for accurate initiation of transcription by purified RNA polymerase II.” *J. Biol. Chem.*, vol. 255, pp. 11992–11996, 1980.

[6] H. T. M. Timmers and P. A. Sharp, “The mammalian TFIID protein is present in two functionally distinct complexes.” *Genes Dev.*, vol. 5, pp. 1946–1956, 1991.

[7] H. T. M. Timmers, R. E. Meyers, and P. A. Sharp, “Composition of transcription factor B-TFIID.” *Proc. Natl. Acad. Sci. U. S. A.*, vol. 89, pp. 8140–8144, 1992.

[8] D. T. Auble and S. Hahn, “An ATP-dependent inhibitor of TBP binding to DNA.” *Genes Dev.*, vol. 7, no. 5, pp. 844–856, 1993.

[9] D. T. Auble, K. E. Hansen, C. G. F. Mueller, W. S. Lane, J. Thorner, and S. Hahn, “Mot1, a global repressor of RNA polymerase II transcription, inhibits TBP binding to DNA by an ATP-dependent mechanism.” *Genes Dev.*, vol. 8, pp. 1920–1934, 1994.

[10] J. L. Davis, R. Kunisawa, and J. Thorner, “A Presumptive Helicase (MOT1 Gene Product) Affects Gene Expression and Is Required for Viability in the Yeast Saccharomyces cerevisiae.” *Microbiology*, vol. 12, pp. 1879–1892, 1992.

[11] G. Prelich and F. Winston, “Mutations That Suppress the Deletion of an Upstream Activating Sequence in Yeast: Involvement of a Protein Kinase and Histone H3 in Repressing Transcription in Vivo.” *Genetics*, vol. 135, pp. 665-676, 1993.

[12] G. Prelich, “Saccharomyces cerevisiae BUR6 encodes a DRAP1/NC2alpha homolog that has both positive and negative roles in transcription in vivo.” *Mol. Cell. Biol.*, vol. 17, pp. 2057–2065, 1997.

[13] D. Poon, A. M. Campbell, Y. Bai, and P. A. Weil, “Yeast Taf170 is encoded by MOT1 and exists in a TATA box-binding protein (TBP)-TBP-associated factor complex distinct from transcription factor IID.” *J. Biol. Chem.*, vol. 269, no. 37, pp. 23135–23140, 1994.

[14] J. J. Chicca, D. T. Auble, and B. F. Pugh, "Cloning and biochemical characterization of TAF-172, a human homolog of yeast Mot1." *Mol. Cell. Biol.*, vol. 18, no. 3, pp. 1701–1710, 1998.

[15] J. A. van der Knaap, J. W. Borst, P. C. van der Vliet, R. Gentz, and H. T. Timmers, "Cloning of the cDNA for the TATA-binding protein-associated factorII170 subunit of transcription factor B-TFIID reveals homology to global transcription regulators in yeast and Drosophila." *Proc. Natl. Acad. Sci. U. S. A.*, vol. 94, pp. 11827–11832, 1997.

[16] R. Goldman-Levi, C. Miller, J. Bogoch, and N. B. Zak, "Expanding the Mot1 subfamily: 89B helicase encodes a new Drosophila melanogaster SNF2-related protein which binds to multiple sites on polytene chromosomes." *Nucleic Acids Res.*, vol. 24, no. 16, pp. 3121–3128, 1996.

[17] P. A. Wade and J. A. Jaehning, "Transcriptional corepression in vitro: a Mot1p-associated form of TATA-binding protein is required for repression by Leu3p." *Mol. Cell. Biol.*, vol. 16, no. 4, pp. 1641–1648, 1996.

[18] J. C. Andrau, C. J. C. Van Oevelen, H. A. A. M. Van Teeffelen, P. A. Weil, F. C. P. Holstege, and H. T. M. Timmers, "Mot1p is essential for TBP recruitment to selected promoters during in vivo gene activation." *EMBO J.*, vol. 21, no. 18, pp. 5173–5183, 2002.

[19] J. V Geisberg, Z. Moqtaderi, L. Kuras, and K. Struhl, "Mot1 associates with transcriptionally active promoters and inhibits association of NC2 in Saccharomyces cerevisiae." *Mol. Cell. Biol.*, vol. 22, no. 23, pp. 8122–8134, 2002.

[20] A. Dasgupta, R. P. Darst, K. J. Martin, C. A. Afshari, and D. T. Auble, "Mot1 activates and represses transcription by direct, ATPase-dependent mechanisms." *Proc. Natl. Acad. Sci. U. S. A.*, vol. 99, no. 5, pp. 2666–2671, 2002.

[21] M. A. Choukrallah, D. Kobi, I. Martianov, W. W. M. P. Pijnappel, N. Mischerikow, T. Ye, A. J. R. Heck, H. T. M. Timmers, and I. Davidson, "Interconversion between active and inactive TATA-binding protein transcription complexes in the mouse genome." *Nucleic Acids Res.*, vol. 40, no. 4, pp. 1446–1459, 2012.

[22] Y. Cang, D. T. Auble, and G. Prelich, "A new regulatory domain on the TATA-binding protein." *EMBO J.*, vol. 18, no. 23, pp. 6662–6671, 1999.

[23] T. A. Muldrow, A. M. Campbell, P. A. Weil, and D. T. Auble, "MOT1 can activate basal transcription in vitro by regulating the distribution of TATA binding protein between promoter and nonpromoter sites." *Mol. Cell. Biol.*, vol. 19, no. 4, pp. 2835–2845, 1999.

[24] M. A. Collart, "The NOT, SPT3, and MOT1 genes functionally interact to regulate transcription at core promoters." *Mol. Cell. Biol.*, vol. 16, no. 12, pp. 6668–6676, 1996.

[25] J. M. Madison and F. Winston, "Evidence that Spt3 functionally interacts with Mot1, TFIIA, and TATA-binding protein to confer promoter-specific transcriptional control in Saccharomyces cerevisiae." *Mol. Cell. Biol.*, vol. 17, pp. 287–295, 1997.

[26] G. Spedale, C. A. Meddens, M. J. E. Koster, C. W. Ko, S. R. Van Hooff, F. C. P. Holstege, H. T. M. Timmers, and W. W. M. P. Pijnappel, "Tight cooperation between Mot1p and NC2beta in regulating genome-wide transcription, repression of transcription following heat shock induction and genetic interaction with SAGA." *Nucleic Acids Res.*, vol. 40, no. 3, pp. 996–1008, 2012.

[27] R. O. Sprouse, M. N. Wells, and D. T. Auble, "TATA-binding protein variants that bypass the requirement for Mot1 in vivo." *J. Biol. Chem.*, vol. 284, pp. 4525–4535, 2009.

[28] G. E. Zentner and S. Henikoff, "Mot1 redistributes TBP from TATA-containing to TATA-less promoters." *Mol. Cell. Biol.*, vol. 33, no. 24, pp. 4996–5004, 2013.

[29] R. O. Sprouse, I. Shcherbakova, H. Cheng, E. Jamison, M. Brenowitz, and D. T. Auble, "Function and structural organization of Mot1 bound to a natural target promoter." *J. Biol. Chem.*, vol. 283, pp. 24935–24948, 2008.

[30] M. J. E. Koster, A. D. Yildirim, P. A. Weil, F. C. P. Holstege, and H. T. M. Timmers, "Suppression of intragenic transcription requires the MOT1 and NC2 regulators of TATA-binding protein." *Nucleic Acids Res.*, vol. 42, pp. 4220–4229, 2014.

[31] K. Poorey, R. O. Sprouse, M. N. Wells, R. Viswanathan, S. Bekiranov, and D. T. Auble, "RNA synthesis precision is regulated by preinitiation complex turnover." *Genome Res.*, vol. 20, no. 12, pp. 1679–1688, 2010.

[32] M. J. E. Koster and H. T. M. Timmers, "Regulation of anti-sense transcription by Mot1p and NC2 via removal of TATA-binding protein (TBP) from the 3′-end of genes." *Nucleic Acids Res.* , pp. 1–10, 2015.

[33] J. V. Geisberg and K. Struhl, "Cellular stress alters the transcriptional properties of promoter-bound Mot1–TBP complexes." *Mol. Cell*, vol. 14, pp. 479–489, 2004.

[34] A. Dasgupta, S. A. Juedes, R. O. Sprouse, and D. T. Auble, "Mot1-mediated control of transcription complex assembly and activity." *EMBO J.*, vol. 24, no. 9, pp. 1717–1729, 2005.

[35] M. Lemaire, J. Xie, M. Meisterernst, and M. A. Collart, "The NC2 repressor is dispensable in yeast mutated for the Sin4p component of the holoenzyme and plays roles similar to Mot1p in vivo." *Mol. Microbiol.*, vol. 36, no. 1, pp. 163–173, 2000.

[36] J. Y. Hsu, T. Juven-Gershon, M. T. Marr, K. J. Wright, R. Tjian, and J. T. Kadonaga, "TBP, Mot1, and NC2 establish a regulatory circuit that controls DPE-dependent versus TATA-dependent transcription." *Genes Dev.*, vol. 22, pp. 2353–2358, 2008.

[37] B. J. Venters, J. D. Irvin, P. Gramlich, and B. F. Pugh, "Genome-wide transcriptional dependence on conserved regions of Mot1.", *Mol. Cell. Biol.*, vol. 31, no. 11, pp. 2253–2261, 2011.

[38] S. J. Zanton and B. F. Pugh, "Changes in genomewide occupancy of core transcriptional regulators during heat stress." *Proc. Natl. Acad. Sci. U. S. A.*, vol. 101, pp. 16843–16848, 2004.

[39] C. J. C. van Oevelen, H. A. A. M. van Teeffelen, and H. T. M. Timmers, “Differential requirement of SAGA subunits for Mot1p and Taf1p recruitment in gene activation.” *Mol. Cell. Biol.*, vol. 25, pp. 4863–4872, 2005.

[40] Y. Wang and W. E. Stumph, “RNA polymerase II/III transcription specificity determined by TATA box orientation.” *Proc. Natl. Acad. Sci. U. S. A.*, vol. 92, pp. 8606–8610, 1995.

[41] S. K. Whitehall, G. A. Kassavetis, and E. P. Geiduschek, “The symmetry of the yeast U6 RNA gene’s TATA box and the orientation of the TATA-binding protein in yeast TFIIIB.” *Genes Dev.*, vol. 9, pp. 2974–2985, 1995.

[42] A. Dasgupta, R. O. Sprouse, S. French, P. Aprikian, R. Hontz, S. A. Juedes, J. S. Smith, A. L. Beyer, and D. T. Auble, “Regulation of rRNA synthesis by TATA-binding protein-associated factor Mot1.” *Mol. Cell. Biol.*, vol. 27, pp. 2886–2896, 2007.

[43] J. I. Adamkewicz, K. E. Hansen, W. A. Prud’homme, J. L. Davis, and J. Thorner, “High Affinity Interaction of Yeast Transcriptional Regulator, Mot1, with TATA Box-binding Protein (TBP).” *J. Biol. Chem.*, vol. 276, no. 15, pp. 11883–11894, 2001.

[44] L. A. Pereira, J. A. Van Der Knaap, V. Van Den, F. a J. Van Den Heuvel, and H. T. M. Timmers, “TAF II 170 Interacts with the Concave Surface of TATA-Binding Protein To Inhibit Its DNA Binding Activity TAF II 170 Interacts with the Concave Surface of TATA-Binding Protein To Inhibit Its DNA Binding Activity.” *Mol. Cell. Biol.*, vol. 21, pp 7523-7534, 2001.

[45] D. T. Auble, D. Wang, K. W. Post, and S. Hahn, “Molecular analysis of the SNF2/SWI2 protein family member MOT1, an ATP-driven enzyme that dissociates TATA-binding protein from DNA.” *Mol. Cell. Biol.*, vol. 17, no. 8, pp. 4842–4851, Aug. 1997.

[46] J. I. Adamkewicz, C. G. F. Mueller, K. E. Hansen, W. A. Prud’homme, and J. Thorner, “Purification and Enzymic Properties of Mot1 ATPase, a Regulator of Basal Transcription in the Yeast Saccharomyces cerevisiae.” *J. Biol. Chem.* , vol. 275 , no. 28 , pp. 21158–21168, Jul. 2000.

[47] P. Wollmann, S. Cui, R. Viswanathan, O. Berninghausen, M. N. Wells, M. Moldt, G. Witte, A. Butryn, P. Wendler, R. Beckmann, D. T. Auble, and K.-P. Hopfner, “Structure and mechanism of the Swi2/Snf2 remodeller Mot1 in complex with its substrate TBP.” *Nature*, vol. 475, no. 9, pp. 403–407, 2011.

[48] R. P. Darst, A. Dasgupta, C. Zhu, J. Y. Hsu, A. Vroom, T. Muldrow, and D. T. Auble, “Mot1 regulates the DNA binding activity of free TATA-binding protein in an ATP-dependent manner.” *J. Biol. Chem.*, vol. 278, no. 15, pp. 13216–13226, 2003.

[49] M. P. Klejman, X. Zhao, F. M. A. van Schaik, W. Herr, and H. T. M. Timmers, “Mutational analysis of BTAF1–TBP interaction: BTAF1 can rescue DNA-binding defective TBP mutants.” *Nucleic Acids Res.*, vol. 33, no. 17, pp. 5426–5436, 2005.

[50] L. A. Pereira, M. P. Klejman, C. Ruhlmann, F. Kavelaars, M. Oulad-Abdelghani, H. T. M. Timmers, and P. Schultz, “Molecular architecture of the basal transcription factor B-TFIID.” *J. Biol. Chem.*, vol. 279, no. 21, pp. 21802–21807, May 2004.

[51] A. E. Gorbalenya and E. V. Koonin, “Helicases: amino acid sequence comparisons and structure-function relationships.” *Curr. Opin. Struct. Biol.*, vol. 3. pp. 419–429, 1993.

[52] A. Flaus, D. M. A Martin, G. J. Barton, and T. Owen-Hughes, “Identification of multiple distinct Snf2 subfamilies with conserved structural motifs.” *Nucleic Acids Res.*, vol. 34, no. 10, pp. 2887–2905, 2006.

[53] L. A. Boyer, C. Logie, E. Bonte, P. B. Becker, P. A. Wade, A. P. Wolffe, C. Wu, A. N. Imbalzano, and C. L. Peterson, “Functional delineation of three groups of the ATP-dependent family of chromatin remodeling enzymes.” *J. Biol. Chem.*, vol. 275, pp. 18864–18870, 2000.

[54] G. Hauk, J. N. McKnight, I. M. Nodelman, and G. D. Bowman, “The Chromodomains of the Chd1 Chromatin Remodeler Regulate DNA Access to the ATPase Motor.” *Mol. Cell*, vol. 39, no. 5, pp. 711–723, 2010.

[55] A. Alexeev, A. Mazin, and S. C. Kowalczykowski, “Rad54 protein possesses chromatin-remodeling activity stimulated by the Rad51-ssDNA nucleoprotein filament.” *Nat. Struct. Biol.*, vol. 10, no. 3, pp. 182–186, 2003.

[56] P. Bork and E. V Koonin, “An expanding family of helicases within the ‘DEAD/H’ superfamily.” *Nucleic Acids Res.*, vol. 21, no. 3, pp. 751–752, 1993.

[57] E. M. Seitz, C. A. Haseltine, and S. C. Kowalczykowski, “DNA recombination and repair in the Archaea.” *Adv Appl Microbiol*, vol. 50, pp. 101–169, 2001.

[58] R. M. Story, I. T. Weber, and T. A. Steitz, “The structure of the E. coli recA protein monomer and polymer.” *Nature*, vol. 355, pp. 318–325, 1992.

[59] R. O. Sprouse, M. Brenowitz, and D. T. Auble, “Snf2/Swi2-related ATPase Mot1 drives displacement of TATA-binding protein by gripping DNA.” *EMBO J.*, vol. 25, no. 7, pp. 1492–1504, 2006.

[60] H. Y. Fan, K. W. Trotter, T. K. Archer, and R. E. Kingston, “Swapping function of two chromatin remodeling complexes.” *Mol. Cell*, vol. 17, pp. 805–815, 2005.

[61] L. Mohrmann and C. P. Verrijzer, “Composition and functional specificity of SWI2/SNF2 class chromatin remodeling complexes.” *Biochim. Biophys. Acta - Gene Struct. Expr.*, vol. 1681, pp. 59–73, 2005.

[62] K.-P. Hopfner, C.-B. Gerhold, K. Lakomek, and P. Wollmann, “Swi2/Snf2 remodelers: hybrid views on hybrid molecular machines.” *Curr. Opin. Struct. Biol.*, vol. 22, no. 2, pp. 225–233, 2012.

[63] A. Flaus and T. Owen-Hughes, “Mechanisms for ATP-dependent chromatin remodelling: the means to the end.” *FEBS J.*, vol. 278, no. 19, pp. 3579–95, 2011.

[64] D. P. Ryan and T. Owen-Hughes, “Snf2-family proteins: chromatin remodellers for any occasion.” *Curr. Opin. Chem. Biol.*, vol. 15, no. 5, pp. 649–656, 2011.

[65] A. H. Sarker, S. E. Tsutakawa, S. Kostek, C. Ng, D. S. Shin, M. Peris, E. Campeau, J. A. Tainer, E. Nogales, and P. K. Cooper, “Recognition of RNA polymerase II and

transcription bubbles by XPG, CSB, and TFIIH: Insights for transcription-coupled repair and Cockayne syndrome." *Mol. Cell*, vol. 20, pp. 187–198, 2005.

[66] S. Van Komen, G. Petukhova, S. Sigurdsson, and P. Sung, "Functional cross-talk among Rad51, Rad54, and replication protein A in heteroduplex DNA joint formation." *J. Biol. Chem.*, vol. 277, pp. 43578–43587, 2002.

[67] S. Yu, T. Owen-Hughes, E. C. Friedberg, R. Waters, and S. H. Reed, "The yeast Rad7/Rad16/Abf1 complex generates superhelical torsion in DNA that is required for nucleotide excision repair." *DNA Repair (Amst).*, vol. 3, pp. 277–287, 2004.

[68] M. V. Sukhodolets, J. E. Cabrera, H. Zhi, and Ding Jun Jin, "RapA, a bacterial homolog of SWI2/SNF2, stimulates RNA polymerase recycling in transcription." *Genes Dev.*, vol. 15, pp. 3330–3341, 2001.

[69] I. Topalidou, M. Papamichos-Chronakis, G. Thireos, and D. Tzamarias, "Spt3 and Mot1 cooperate in nucleosome remodeling independently of TBP recruitment." *EMBO J.*, vol. 23, no. 9, pp. 1943–1948, 2004.

[70] R. P. Darst, D. Wang, and D. T. Auble, "MOT1-catalyzed TBP-DNA disruption: uncoupling DNA conformational change and role of upstream DNA." *EMBO J.*, vol. 20, no. 8, pp. 2028–2040, 2001.

[71] I. Whitehouse, C. Stockdale, A. Flaus, M. D. Szczelkun, and T. Owen-Hughes, "Evidence for DNA translocation by the ISWI chromatin-remodeling enzyme." *Mol. Cell. Biol.*, vol. 23, no. 6, pp. 1935–1945, 2003.

[72] M. Zofall, J. Persinger, S. R. Kassabov, and B. Bartholomew, "Chromatin remodeling by ISW2 and SWI/SNF requires DNA translocation inside the nucleosome." *Nat. Struct. Mol. Biol.*, vol. 13, no. 4, pp. 339–346, 2006.

[73] A. Saha, J. Wittmeyer, and B. R. Cairns, "Chromatin remodeling by RSC involves ATP-dependent DNA translocation." *Genes Dev.*, vol. 16, pp. 2120–2134, 2002.

[74] P. Soultanas, M. S. Dillingham, P. Wiley, M. R. Webb, and D. B. Wigley, "Uncoupling DNA translocation and helicase activity in PcrA: direct evidence for an active mechanism." *EMBO J.*, vol. 19, no. 14, pp. 3799–3810, 2000.

[75] L. K. Stanley, R. Seidel, C. van der Scheer, N. H. Dekker, M. D. Szczelkun, and C. Dekker, "When a helicase is not a helicase: dsDNA tracking by the motor protein EcoR124I." *EMBO J.*, vol. 25, no. 10, pp. 2230–2239, 2006.

[76] H. Dürr, C. Körner, M. Müller, V. Hickmann, and K. P. Hopfner, "X-Ray structures of the sulfolobus solfataricus SWI2/SNF2 ATPase core and its complex with DNA." *Cell*, vol. 121, pp. 363–373, 2005.

[77] N. H. Thomä, B. K. Czyzewski, A. a Alexeev, A. V Mazin, S. C. Kowalczykowski, and N. P. Pavletich, "Structure of the SWI2/SNF2 chromatin-remodeling domain of eukaryotic Rad54." *Nat. Struct. Mol. Biol.*, vol. 12, no. 4, pp. 350–356, 2005.

[78] G. Shaw, J. Gan, Y. N. Zhou, H. Zhi, P. Subburaman, R. Zhang, A. Joachimiak, D. J. Jin, and X. Ji, "Structure of RapA, a Swi2/Snf2 Protein that Recycles RNA Polymerase During Transcription." *Structure*, vol. 16, pp. 1417–1427, 2008.

[79] T. Sengoku, O. Nureki, A. Nakamura, S. Kobayashi, and S. Yokoyama, “Structural Basis for RNA Unwinding by the DEAD-Box Protein Drosophila Vasa.” *Cell*, vol. 125, pp. 287–300, 2006.

[80] F. Jiang, A. Ramanathan, M. T. Miller, G.-Q. Tang, M. Gale, S. S. Patel, and J. Marcotrigiano, “Structural basis of RNA recognition and activation by innate immune receptor RIG-I.” *Nature*, vol. 479, no. 7373, pp. 423–427, 2011.

[81] B. Wu, A. Peisley, C. Richards, H. Yao, X. Zeng, C. Lin, F. Chu, T. Walz, and S. Hur, “Structural basis for dsRNA recognition, filament formation, and antiviral signal activation by MDA5.” *Cell*, vol. 152, no. 1–2, pp. 276–289, 2013.

[82] S. Myong, S. Cui, P. V Cornish, A. Kirchhofer, M. U. Gack, J. U. Jung, K.-P. Hopfner, and T. Ha, “Cytosolic viral sensor RIG-I is a 5’-triphosphate-dependent translocase on double-stranded RNA.” *Science*, vol. 323, pp. 1070–1074, 2009.

[83] S. S. Velankar, P. Soultanas, M. S. Dillingham, H. S. Subramanya, and D. B. Wigley, “Crystal structures of complexes of PcrA DNA helicase with a DNA substrate indicate an inchworm mechanism.” *Cell*, vol. 97, pp. 75–84, 1999.

[84] H. Dürr, A. Flaus, T. Owen-Hughes, and K. P. Hopfner, “Snf2 family ATPases and DExx box helicases: Differences and unifying concepts from high-resolution crystal structures.” *Nucleic Acids Res.*, vol. 34, no. 15, pp. 4160–4167, 2006.

[85] D. T. Auble and S. M. Steggerda, “Testing for DNA tracking by MOT1, a SNF2/SWI2 protein family member.” *Mol. Cell. Biol.*, vol. 19, no. 1, pp. 412–423, 1999.

[86] R. Viswanathan and D. T. Auble, “One small step for Mot1; one giant leap for other Swi2/Snf2 enzymes?” *Biochim. Biophys. Acta - Gene Regul. Mech.*, vol. 1809, pp. 488–496, 2011.

[87] O. H. Gumbs, A. M. Campbell, and P. A. Weil, “High-affinity DNA binding by a Mot1p-TBP complex: implications for TAF-independent transcription.” *EMBO J.*, vol. 22, no. 12, pp. 3131-3141, 2003.

[88] G. Moyle-Heyrman, R. Viswanathan, J. Widom, and D. T. Auble, “Two-step mechanism for modifier of transcription 1 (Mot1) enzyme-catalyzed displacement of TATA-binding protein (TBP) from DNA.” *J. Biol. Chem.*, vol. 287, no. 12, pp. 9002–9012, 2012.

[89] A. Butryn, J.M. Schuller, G. Stoehr, P. Runge-Wollmann, F. Förster, D.T. Auble, K.-P. Hopfer, “Structural basis for recognition and remodeling of the TBP:DNA:NC2 complex by Mot1.”, *eLife*, vol. 4, e07432, 2015.

[90] D. T. Auble, “The dynamic personality of TATA-binding protein.” *Trends Biochem. Sci.*, vol. 34, no. 2, pp. 49–52, 2009.

[91] J. L. Kim, D. B. Nikolov, and S. K. Burley, “Co-crystal structure of TBP recognizing the minor groove of a TATA element.” *Nature*, vol. 365, pp. 520–527, 1993.

[92] X. Zhao and W. Herr, “A regulated two-step mechanism of TBP binding to DNA: A solvent-exposed surface of TBP inhibits TATA box recognition.” *Cell*, vol. 108, pp. 615–627, 2002.

[93] R. Blair, J. Goodrich, and J. Kugel, “Single molecule FRET shows uniformity in TBP-induced DNA bending and heterogeneity in bending kinetics.” *Biochemistry*, vol. 51, no. 38, pp. 7444–7455, 2012.

[94] M. Meisterernst and R. G. Roeder, “Family of proteins that interact with TFIID and regulate promoter activity.” *Cell*, vol. 67, pp. 557–567, 1991.

[95] J. A. Inostroza, F. H. Mermelstein, W. S. Lane, and D. Reinberg, “Dr1 , a TATA-binding phosphoprotein and inhibitor of class II gene transcription.” *Cell*, vol. 70, pp. 477–489, 1992.

[96] A. Goppelt, G. Stelzer, F. Lottspeich, and M. Meisterernst, “A mechanism for repression of class II gene transcription through specific binding of NC2 to TBP-promoter complexes via heterodimeric histone fold domains.” *EMBO J.*, vol. 15, pp. 3105–3116, 1996.

[97] F. J. Van Werven, H. Van Bakel, H. A. A. M. Van Teeffelen, A. F. M. Altelaar, M. G. Koerkamp, A. J. R. Heck, F. C. P. Holstege, and H. T. M. Timmers, “Cooperative action of NC2 and Mot1p to regulate TATA-binding protein function across the genome.” *Genes Dev.*, vol. 22, pp. 2359–2369, 2008.

[98] E. L. Gadbois, D. M. Chao, J. C. Reese, M. R. Green, and R. A Young, “Functional antagonism between RNA polymerase II holoenzyme and global negative regulator NC2 in vivo.” *Proc. Natl. Acad. Sci. U. S. A.*, vol. 94, pp. 3145–3150, 1997.

[99] S. Kim, J. G. Na, M. Hampsey, and D. Reinberg, “The Dr1/DRAP1 heterodimer is a global repressor of transcription in vivo.” *Proc. Natl. Acad. Sci. U. S. A.*, vol. 94, pp. 820–825, 1997.

[100] J. Xie, M. Collart, M. Lemaire, G. Stelzer, and M. Meisterernst, “A single point mutation in TFIIA suppresses NC2 requirement in vivo.” *EMBO J.*, vol. 19, no. 4, pp. 672–682, 2000.

[101] J. V Geisberg, F. C. Holstege, R. A Young, and K. Struhl, “Yeast NC2 associates with the RNA polymerase II preinitiation complex and selectively affects transcription in vivo.” *Mol. Cell. Biol.*, vol. 21, pp. 2736–2742, 2001.

[102] Y. Cang and G. Prelich, “Direct stimulation of transcription by negative cofactor 2 (NC2) through TATA-binding protein (TBP).” *Proc. Natl. Acad. Sci. U. S. A.*, vol. 99, no. 20, pp. 12727–12732, 2002.

[103] T. K. Albert, K. Grote, S. Boeing, G. Stelzer, A. Schepers, and M. Meisterernst, “Global distribution of negative cofactor 2 subunit-alpha on human promoters.” *Proc. Natl. Acad. Sci. U. S. A.*, vol. 104, no. 24, pp. 10000–10005, 2007.

[104] L. Peiró-Chova and F. Estruch, “Specific defects in different transcription complexes compensate for the requirement of the negative cofactor 2 repressor in Saccharomyces cerevisiae.” *Genetics*, vol. 176, no. 1, pp. 125–138, 2007.

[105] P. Masson, E. Leimgruber, S. Creton, and M. a. Collart, “The dual control of TFIIB recruitment by NC2 is gene specific.” *Nucleic Acids Res.*, vol. 36, no. 2, pp. 539–549, 2008.

[106] K. C. Yeung, J. A. Inostroza, F. H. Mermelstein, C. Kannabiran, and D. Reinberg, “Structure-function analysis of the TBP-binding protein Dr1 reveals a mechanism for repression of class II gene transcription.” *Genes Dev.*, vol. 8, pp. 2097–2109, 1994.

[107] K. Kamada, F. Shu, H. Chen, S. Malik, G. Stelzer, R. G. Roeder, M. Meisterernst, and S. K. Burley, “Crystal structure of negative cofactor 2 recognizing the TBP-DNA transcription complex.” *Cell*, vol. 106, no. 1, pp. 71–81, 2001.

[108] K. Luger, A. W. Mäder, R. K. Richmond, D. F. Sargent, and T. J. Richmond, “Crystal structure of the nucleosome core particle at 2.8 A resolution.” *Nature*, vol. 389, pp. 251–260, 1997.

[109] M. Nardini, N. Gnesutta, G. Donati, R. Gatta, C. Forni, A. Fossati, C. Vonrhein, D. Moras, C. Romier, M. Bolognesi, and R. Mantovani, “Sequence-specific transcription factor NF-Y displays histone-like DNA binding and H2B-like ubiquitination.” *Cell*, vol. 152, no. 1–2, pp. 132–43, 2013.

[110] E. M. Huber, D. H. Scharf, P. Hortschansky, M. Groll, and A. A. Brakhage, “DNA Minor Groove Sensing and Widening by the CCAAT-Binding Complex.” *Structure*, vol. 20, no. 10, pp. 1757–1768, 2012.

[111] J. H. Geiger, S. Hahn, S. Lee, and P. B. Sigler, “Crystal structure of the yeast TFIIA/TBP/DNA complex.” *Science*, vol. 272, pp. 830–836, 1996.

[112] M. Bleichenbacher, S. Tan, and T. J. Richmond, “Novel interactions between the components of human and yeast TFIIA/TBP/DNA complexes.” *J. Mol. Biol.*, vol. 332, pp. 783–793, 2003.

[113] Y. Kim, Y. W. Ebright, A. R. Goodman, D. Reinberg, and R. H. Ebright, “Nonradioactive, ultrasensitive site-specific protein-protein photocrosslinking: Interactions of α-helix 2 of TATA-binding protein with general transcription factor TFIIA and transcriptional repressor NC2,” *Nucleic Acids Res.*, vol. 36, no. 19, pp. 6143–6154, 2008.

[114] P. Schluesche, G. Stelzer, E. Piaia, D. C. Lamb, and M. Meisterernst, “NC2 mobilizes TBP on core promoter TATA boxes.” *Nat. Struct. Mol. Biol.*, vol. 14, no. 12, pp. 1196–1201, 2007.

[115] P. J. Willy, R. Kobayashi, and J. T. Kadonaga, “A basal transcription factor that activates or represses transcription.” *Science*, vol. 290, pp. 982–985, 2000.

[116] T. K. Albert, K. Grote, S. Boeing, and M. Meisterernst, “Basal core promoters control the equilibrium between negative cofactor 2 and preinitiation complexes in human cells.” *Genome Biol.*, vol. 11, p. R33, 2010.

[117] W. Deng, B. Malecová, T. Oelgeschläger, and S. G. E. Roberts, “TFIIB recognition elements control the TFIIA-NC2 axis in transcriptional regulation.,” *Mol. Cell. Biol.*, vol. 29, no. 6, pp. 1389–1400, 2009.

[118] P. de Graaf, F. Mousson, B. Geverts, E. Scheer, L. Tora, A. B. Houtsmuller, and H. T. M. Timmers, “Chromatin interaction of TATA-binding protein is dynamically regulated in human cells.” *J. Cell Sci.*, vol. 123, pp. 2663–2671, 2010.

[119] R. O. Sprouse, T. S. Karpova, F. Mueller, A. Dasgupta, J. G. McNally, and D. T. Auble, "Regulation of TATA-binding protein dynamics in living yeast cells." *Proc. Natl. Acad. Sci. U. S. A.*, vol. 105, no. 36, pp. 13304–13308, 2008.

[120] D. R. Arnett, J. L. Jennings, D. L. Tabb, A. J. Link, and P. A. Weil, "A proteomics analysis of yeast Mot1p protein-protein associations: insights into mechanism." *Mol. Cell. Proteomics*, vol. 7, pp. 2090–2106, 2008.

[121] M. P. Klejman, L. A Pereira, H. J. T. van Zeeburg, S. Gilfillan, M. Meisterernst, and H. T. M. Timmers, "NC2alpha interacts with BTAF1 and stimulates its ATP-dependent association with TATA-binding protein." *Mol. Cell. Biol.*, vol. 24, no. 22, pp. 10072–10082, 2004.

[122] K. Yeung, S. Kim, and D. Reinberg, "Functional dissection of a human Dr1-DRAP1 repressor complex." *Mol. Cell. Biol.*, vol. 17, no. 1, pp. 36–45, 1997.

[123] S. Creton, J. Q. Svejstrup, and M. A. Collart, "The NC2 alpha and beta subunits play different roles in vivo." *Genes Dev.*, vol. 16, no. 24, pp. 3265–3276, 2002.

[124] J. Kahle, E. Piaia, S. Neimanis, M. Meisteremst, and D. Doenecke, "Regulation of nuclear import and export of negative cofactor 2," *J. Biol. Chem.*, vol. 284, no. 14, pp. 9382–9393, 2009.

[125] R. J. White, B. C. Khoo, J. A. Inostroza, D. Reinberg, and S. P. Jackson, "Differential regulation of RNA polymerases I, II, and III by the TBP-binding repressor Dr1." *Science*, vol. 266, no. 16, pp. 448–450, 1994.

[126] T. Kantidakis and R. J. White, "Dr1 (NC2) is present at tRNA genes and represses their transcription in human cells." *Nucleic Acids Res.*, vol. 38, no. 4, pp. 1228–1239, 2009.

[127] S. Gilfillan, G. Stelzer, E. Piaia, M. G. Hofmann, and M. Meisterernst, "Efficient binding of NC2·TATA-binding protein to DNA in the absence of TATA," *J. Biol. Chem.*, vol. 280, pp. 6222–6230, 2005.

[128] B. Heras and J. L. Martin, "Post-crystallization treatments for improving diffraction quality of protein crystals." *Acta Crystallographica Section D: Biological Crystallography*, vol. 61. pp. 1173–1180, 2005.

[129] T. S. Walter, C. Meier, R. Assenberg, K. F. Au, J. Ren, A. Verma, J. E. Nettleship, R. J. Owens, D. I. Stuart, and J. M. Grimes, "Lysine Methylation as a Routine Rescue Strategy for Protein Crystallization." *Structure*, vol. 14, pp. 1617–1622, 2006.

[130] S. Doublié, "Preparation of selenomethionyl proteins for phase determination." *Methods Enzymol.*, vol. 276. pp. 523–530, 1997.

[131] M. D. Winn, C. C. Ballard, K. D. Cowtan, E. J. Dodson, P. Emsley, P. R. Evans, R. M. Keegan, E. B. Krissinel, A. G. W. Leslie, A. McCoy, S. J. McNicholas, G. N. Murshudov, N. S. Pannu, E. A. Potterton, H. R. Powell, R. J. Read, A. Vagin, and K. S. Wilson, "Overview of the CCP4 suite and current developments." *Acta Crystallogr. Sect. D Biol. Crystallogr.,* vol. 67, pp. 235–242, 2011.

[132] K. Cowtan, "Recent developments in classical density modification." *Acta Crystallogr. Sect. D Biol. Crystallogr.*, vol. 66, pp. 470–478, 2010.

[133] P. D. Adams, P. V. Afonine, G. Bunkóczi, V. B. Chen, I. W. Davis, N. Echols, J. J. Headd, L. W. Hung, G. J. Kapral, R. W. Grosse-Kunstleve, A. J. McCoy, N. W. Moriarty, R. Oeffner, R. J. Read, D. C. Richardson, J. S. Richardson, T. C. Terwilliger, and P. H. Zwart, “PHENIX: A comprehensive Python-based system for macromolecular structure solution.” *Acta Crystallogr. Sect. D Biol. Crystallogr.*, vol. 66, pp. 213–221, 2010.

[134] B. Rupp, *Biomolecular crystallography: principles, practice, and application to structural biology*. Garland Science, 2009.

[135] B. DeLaBarre and A. T. Brunger, “Considerations for the refinement of low-resolution crystal structures.” *Acta Crystallogr. Sect. D Biol. Crystallogr.*, vol. 62, pp. 923–932, 2006.

[136] E. Krissinel and K. Henrick, “Inference of Macromolecular Assemblies from Crystalline State.” *J. Mol. Biol.*, vol. 372, pp. 774–797, 2007.

[137] M. Grünwald, D. Lazzaretti, and F. Bono, “Structural basis for the nuclear export activity of Importin13.” *EMBO J.*, vol. 32, no. 6, pp. 899–913, 2013.

[138] R. Lewis, H. Dürr, K. P. Hopfner, and J. Michaelis, “Conformational changes of a Swi2/Snf2 ATPase during its mechano-chemical cycle.” *Nucleic Acids Res.*, vol. 36, no. 6, pp. 1881–1890, 2008.

[139] M. A. Ponomarev, V. P. Timofeev, and D. I. Levitsky, “The difference between ADP-beryllium fluoride and ADP-aluminium fluoride complexes of the spin-labeled myosin subfragment 1.” *FEBS Lett.*, vol. 371, no. 3, pp. 261–263, 1995.

[140] C. Lambert, N. Léonard, X. De Bolle, and E. Depiereux, “ESyPred3D: Prediction of proteins 3D structures.” *Bioinformatics*, vol. 18, pp. 1250–1256, 2002.

[141] M. V. Petoukhov, D. Franke, A. V. Shkumatov, G. Tria, A. G. Kikhney, M. Gajda, C. Gorba, H. D. T. Mertens, P. V. Konarev, and D. I. Svergun, “New developments in the ATSAS program package for small-angle scattering data analysis.” *J. Appl. Crystallogr.*, vol. 45, pp. 342–350, 2012.

[142] A. Politis, F. Stengel, Z. Hall, H. Hernández, A. Leitner, T. Walzthoeni, C. V Robinson, and R. Aebersold, “A mass spectrometry-based hybrid method for structural modeling of protein complexes.” *Nat. Methods*, vol. 11, pp. 403–6, 2014.

[143] M. Ohi, Y. Li, Y. Cheng, and T. Walz, “Negative Staining and Image Classification – Powerful Tools in Modern Electron Microscopy.” *Biol. Proced. Online*, vol. 6, pp. 23–34, 2004.

[144] P. Chacón and W. Wriggers, “Multi-resolution contour-based fitting of macromolecular structures.” *J. Mol. Biol.*, vol. 317, pp. 375–384, 2002.

[145] W. Wriggers, “Using Situs for the integration of multi-resolution structures.” *Biophys. Rev.*, vol. 2, pp. 21–27, 2010.

[146] E. F. Pettersen, T. D. Goddard, C. C. Huang, G. S. Couch, D. M. Greenblatt, E. C. Meng, and T. E. Ferrin, “UCSF Chimera--a visualization system for exploratory research and analysis.” *J. Comput. Chem.*, vol. 25, pp. 1605–1612, 2004.

[147] R. Aramayo, M. B. Sherman, K. Brownless, R. Lurz, A. L. Okorokov, and E. V. Orlova, “Quaternary structure of the specific p53-DNA complex reveals the mechanism of p53 mutant dominance.” *Nucleic Acids Res.*, vol. 39, pp. 8960–8971, 2011.

[148] M. Anandapadamanaban, C. Andresen, S. Helander, Y. Ohyama, M. I. Siponen, P. Lundström, T. Kokubo, M. Ikura, M. Moche, and M. Sunnerhagen, “High-resolution structure of TBP with TAF1 reveals anchoring patterns in transcriptional regulation.” *Nat. Struct. Mol. Biol.*, vol. 20, no. 8, pp. 1008–14, 2013.

[149] L. Wang, O. Limbo, J. Fei, L. Chen, B. Kim, J. Luo, J. Chong, and R. C. Conaway, “By a Novel Conserved Leucine Latch Motif.” pp. 2–7, 2014.

[150] B. P. Cormack, M. Strubin, A. S. Ponticelli, and K. Struhl, “Functional differences between yeast and human TFIID are localized to the highly conserved region.” *Cell*, vol. 65, no. 2, pp. 341–348, 1991.

[151] N. Dephoure, C. Zhou, J. Villén, S. A. Beausoleil, C. E. Bakalarski, S. J. Elledge, and S. P. Gygi, “A quantitative atlas of mitotic phosphorylation.” *Proc. Natl. Acad. Sci. U. S. A.*, vol. 105, pp. 10762–10767, 2008.

[152] L. Tora and H. T. M. Timmers, “The TATA box regulates TATA-binding protein (TBP) dynamics in vivo.” *Trends Biochem. Sci.*, vol. 35, no. 6, pp. 309–314, 2010.

[153] K. Yamada, T. D. Frouws, B. Angst, D. J. Fitzgerald, C. DeLuca, K. Schimmele, D. F. Sargent, and T. J. Richmond, “Structure and mechanism of the chromatin remodelling factor ISW1a.” *Nature*, vol. 472, no. 7344, pp. 448–453, 2011.

[154] M. L. Dechassa, S. K. Hota, P. Sen, N. Chatterjee, P. Prasad, and B. Bartholomew, “Disparity in the DNA translocase domains of SWI/SNF and ISW2.” *Nucleic Acids Res.*, vol. 40, no. 10, pp. 4412–4421, 2012.

[155] F. Mueller-Planitz, H. Klinker, J. Ludwigsen, and P. B. Becker, “The ATPase domain of ISWI is an autonomous nucleosome remodeling machine.” *Nat. Struct. Mol. Biol.*, vol. 20, no. 1, pp. 82–9, 2013.

[156] C. L. Smith and C. L. Peterson, “A Conserved Swi2/Snf2 ATPase Motif Couples ATP Hydrolysis to Chromatin Remodeling.” vol. 25, no. 14, pp. 5880–5892, 2005.

[157] W. Dang and B. Bartholomew, “Domain architecture of the catalytic subunit in the ISW2-nucleosome complex.” *Mol. Cell. Biol.*, vol. 27, no. 23, pp. 8306–8317, 2007.

[158] H. Ferreira, A. Flaus, and T. Owen-Hughes, “Histone Modifications Influence the Action of Snf2 Family Remodelling Enzymes by Different Mechanisms.” *J. Mol. Biol.*, vol. 374, pp. 563–579, 2007.

[159] A. Dutta, M. Gogol, J.-H. Kim, M. Smolle, S. Venkatesh, J. Gilmore, L. Florens, M. P. Washburn, and J. L. Workman, “Swi/Snf dynamics on stress-responsive genes is governed by competitive bromodomain interactions.” *Genes Dev.* , vol. 28 , no. 20 , pp. 2314–2330, 2014.

[160] C. R. Clapier, K. P. Nightingale, and P. B. Becker, “A critical epitope for substrate recognition by the nucleosome remodeling ATPase ISWI.” *Nucleic Acids Res.*, vol. 30, pp. 649–655, 2002.

[161] A. Lundby, K. Lage, B. T. Weinert, D. B. Bekker-Jensen, A. Secher, T. Skovgaard, C. D. Kelstrup, A. Dmytriyev, C. Choudhary, C. Lundby, and J. V. Olsen, “Proteomic Analysis of Lysine Acetylation Sites in Rat Tissues Reveals Organ Specificity and Subcellular Patterns.” *Cell Rep.*, vol. 2, pp. 419–431, 2012.

[162] H. Zhou, S. Di Palma, C. Preisinger, M. Peng, A. N. Polat, A. J. R. Heck, and S. Mohammed, “Toward a comprehensive characterization of a human cancer cell phosphoproteome.” *J. Proteome Res.*, vol. 12, pp. 260–271, 2013.

[163] E. L. Huttlin, M. P. Jedrychowski, J. E. Elias, T. Goswami, R. Rad, S. A. Beausoleil, J. Villén, W. Haas, M. E. Sowa, and S. P. Gygi, “A tissue-specific atlas of mouse protein phosphorylation and expression.” *Cell*, vol. 143, pp. 1174–1189, 2010.

[164] K. Sharma, R. C. J. D’Souza, S. Tyanova, C. Schaab, J. R. Wiśniewski, J. Cox, and M. Mann, “Ultradeep Human Phosphoproteome Reveals a Distinct Regulatory Nature of Tyr and Ser/Thr-Based Signaling.” *Cell Reports*, 2014.

[165] Z. Wang, M. Gucek, and G. W. Hart, “Cross-talk between GlcNAcylation and phosphorylation: site-specific phosphorylation dynamics in response to globally elevated O-GlcNAc.” *Proc. Natl. Acad. Sci. U. S. A.*, vol. 105, pp. 13793–13798, 2008.

[166] D. Van Hoof, J. Muñoz, S. R. Braam, M. W. H. Pinkse, R. Linding, A. J. R. Heck, C. L. Mummery, and J. Krijgsveld, “Phosphorylation Dynamics during Early Differentiation of Human Embryonic Stem Cells.” *Cell Stem Cell*, vol. 5, pp. 214–226, 2009.

[167] S. Zhao, W. Xu, W. Jiang, W. Yu, Y. Lin, T. Zhang, J. Yao, L. Zhou, Y. Zeng, H. Li, Y. Li, J. Shi, W. An, S. M. Hancock, F. He, L. Qin, J. Chin, P. Yang, X. Chen, Q. Lei, Y. Xiong, and K.-L. Guan, “Regulation of cellular metabolism by protein lysine acetylation.” *Science*, vol. 327, pp. 1000–1004, 2010.

[168] A. Guo, H. Gu, J. Zhou, D. Mulhern, Y. Wang, K. a Lee, V. Yang, M. Aguiar, J. Kornhauser, X. Jia, J. Ren, S. a Beausoleil, J. C. Silva, V. Vemulapalli, M. T. Bedford, and M. J. Comb, “Immunoaffinity enrichment and mass spectrometry analysis of protein methylation.” *Mol. Cell. Proteomics*, vol. 13, pp. 372–87, 2014.

[169] S. A. Wagner, P. Beli, B. T. Weinert, C. Scholz, C. D. Kelstrup, C. Young, M. L. Nielsen, J. V. Olsen, C. Brakebusch, and C. Choudhary, “Proteomic analyses reveal divergent ubiquitylation site patterns in murinetissues.” *Mol. Cell. Proteomics,* 2012.

[170] B. T. Weinert, C. Schölz, S. A. Wagner, V. Iesmantavicius, D. Su, J. A. Daniel, and C. Choudhary, “Lysine succinylation is a frequently occurring modification in prokaryotes and eukaryotes and extensively overlaps with acetylation.” *Cell Rep.*, vol. 4, pp. 842–851, 2013.

[171] W. Kim, E. J. Bennett, E. L. Huttlin, A. Guo, J. Li, A. Possemato, M. E. Sowa, R. Rad, J. Rush, M. J. Comb, J. W. Harper, and S. P. Gygi, “Systematic and quantitative assessment of the ubiquitin-modified proteome.” *Mol. Cell*, vol. 44, pp. 325–340, 2011.

[172] M. P. Alcolea, P. Casado, J.-C. Rodriguez-Prados, B. Vanhaesebroeck, and P. R. Cutillas, “Phosphoproteomic Analysis of Leukemia Cells under Basal and Drug-

treated Conditions Identifies Markers of Kinase Pathway Activation and Mechanisms of Resistance." *Mol. Cell. Proteomics*, vol. 11. pp. 453–466, 2012.

[173] M. R. Singleton, M. S. Dillingham, and D. B. Wigley, "Structure and mechanism of helicases and nucleic acid translocases." *Annu. Rev. Biochem.*, vol. 76, pp. 23–50, 2007.

[174] A. Tosi, C. Haas, F. Herzog, A. Gilmozzi, O. Berninghausen, C. Ungewickell, C. B. Gerhold, K. Lakomek, R. Aebersold, R. Beckmann, and K. P. Hopfner, "Structure and subunit topology of the INO80 chromatin remodeler and its nucleosome complex." *Cell*, vol. 154, no. 6, pp. 1207–1219, 2013.

[175] G. Hauk and G. D. Bowman, "Structural insights into regulation and action of SWI2/SNF2 ATPases." *Curr. Opin. Struct. Biol.*, vol. 21, no. 6, pp. 719–727, 2011.

[176] M. M. Bradford, "A rapid and sensitive method for the quantitation of microgram quantities of protein utilizing the principle of protein-dye binding." *Anal. Biochem.*, vol. 72, pp. 248–254, 1976.

[177] H. Blum, H. Beier, and H. J. Gross, "Improved silver staining of plant proteins, RNA and DNA in polyacrylamide gels." *Electrophoresis*, vol. 8, pp. 93–99, 1987.

[178] W. Kabsch, "XDS." *Acta Crystallogr. Sect. D Biol. Crystallogr.*, vol. 66, pp. 125–132, 2010.

[179] K. A. Kantardjieff and B. Rupp, "Matthews coefficient probabilities: Improved estimates for unit cell contents of proteins, DNA, and protein-nucleic acid complex crystals." *Protein Sci.*, vol. 12, pp. 1865–1871, 2003.

[180] B. W. Matthews, "Solvent content of protein crystals.," *J. Mol. Biol.*, vol. 33, pp. 491–497, 1968.

[181] A. J. McCoy, R. W. Grosse-Kunstleve, P. D. Adams, M. D. Winn, L. C. Storoni, and R. J. Read, "Phaser crystallographic software." *J. Appl. Crystallogr.*, vol. 40, pp. 658–674, 2007.

[182] N. Stein, "CHAINSAW: A program for mutating pdb files used as templates in molecular replacement." *J. Appl. Crystallogr.*, vol. 41, pp. 641–643, 2008.

[183] G. Bricogne, E. Blanc, M. Brandl, C. Flensbueg, P. Keller, W. Paciorek, P. Roversi, A. Sharff, O. S. Smart, C. Vonrhein, and T. O. Womack, "BUSTER version 2.10.1.," *Cambridge, United Kingdom Glob. Phasing Ltd.*, 2011.

[184] P. Emsley, B. Lohkamp, W. G. Scott, and K. Cowtan, "Features and development of Coot." *Acta Crystallogr. Sect. D Biol. Crystallogr.*, vol. 66, pp. 486–501, 2010.

[185] J. Kosinski, A. von Appen, A. Ori, K. Karius, C. W. Müller, and M. Beck, "Xlink Analyzer: Software for analysis and visualization of cross-linking data in the context of three-dimensional structures." *J. Struct. Biol.*, 2015.

8. ABBREVIATIONS

ABF	ADP-beryllium fluride
ADP	adenosine diphosphate
AGS	adenosine 5'-O-(3-thio)triphosphate, ATPγS
ATP	adenosine triphosphate
β-ME	β-mercaptoethanol
bp	base pairs
ChIP	chromatin immunoprecipitation
CRIP	crosslinking restriction digest-coupled immunoprecipitation
CSB	Cockayne syndrome protein B
CX-MS	protein–protein crosslinking coupled to mass spectrometry
dsDNA	double-stranded DNA
DSSG	di-sulfo-succinimidyl-glutarate
DTT	dithiothreitol
EM	electron microscopy
EMSA	electrophoretic mobility shift assay
FEM	feature-enhanced map
FRAP	fluorescence recovery after photobleaching
FRET	Förster resonance energy transfer
GTF	general transcription factor
HEAT	Huntingtin, elongation factor 3, protein phosphatase 2A, lipid kinase TOR
HEPES	4-(2-hydroxyethyl)-1-piperazineethanesulfonic acid
IDB	inhibitory DNA binding surface
Mot1	Modifier of transcription 1
NC2	Negative Cofactor 2
NES	nuclear export signal
NLS	nuclear localization sequence
NTP	nucleoside triphosphate
ORGANIC	sequencing of occupied regions of genomes from affinity-purified naturally isolated chromatin
PEG	polyethylene glycol
PIC	preinitiation compelx
RCE	restriction digest-coupled electrophoretic mobility shift
r.m.s.d.	root mean square deviation
RNA pol	RNA polymerase
SDS-PAGE	sodium dodecyl sulfate polyacrylamide gel electrophoresis

ssDNA	single-stranded DNA
Swi2/Snf2	Switching defective/Sucrose nonfermenting 2
TRIS	tris-hydroxymethyl-aminomethane
WCE	whole cell extract
WT	wild type

9. ACKNOWLEDGEMENTS

First of all I would like to thank my supervisor Prof. Dr. Karl-Peter Hopfner for the opportunity to continue on the Mot1 project. In particular I am grateful for giving me the privilege to learn on my own mistakes.

I would like to express my sincere gratitude to Prof. Dr. Roland Beckmann and Prof. Dr. Dietmar Martin for support and dedicating their precious time to review this work.

I am most grateful to Prof. Dr. David Auble for shearing his contagious enthusiasm and critical opinion, especially in Mot1 and NC2 biology field. Without him and our collaboration this work would not have been possible.

Special thanks to Gabi Stoehr, Sebastian Eustermann, and Petra Runge-Wollmann, who also directly contributed to this work.

I would like to thank Matthew Bennett for introducing me to the reciprocal space and for his support during the harsh no-data-whatsoever and no-useful-data times.

I want to thank all other members of the Hopfner group who supported me over the past years. Thank all of you for your advice, encouragement, great atmosphere in the lab and shearing your supplies of chocolate. I am sorry to all of you who have ever felt offended by my bluntness and notorious cursing.

W szczególności chciałabym bardzo podziękować mojej najbliższej Rodzinie: Mamie i Tacie, Waldkowi i Ani, Julii, Zosi i Franiowi. Dziękuję za wasze wsparcie oraz za głęboką wyrozumiałość do mojego niedzwonienia i niebycia poprzez mój cały pobyt w Monachium.

10. CURRICULUM VITAE

Name	**Agata Anna BUTRYN**
Nationality	Polish
Birth date	February 10th 1986
Birth place	Stalowa Wola, Poland
Gender	female

Education

Since 09.2010	Doctoral Thesis in Biochemistry, Ludwig-Maximilians University, Faculty of Chemistry and Pharmacy, Department of Biochemistry Munich, Germany As part of Max Planck Research School for Molecular and Cellular Life Sciences (IMPRS-LS) PhD program
10.2005–06.2010	Master of Science, Biotechnology Jagiellonian University, Faculty of Biochemistry, Biophysics and Biotechnology, Department of Microbiology, Kraków, Poland

Work experience

Since 09.2010	Doctoral thesis in the group of Prof. Dr. Karl-Peter Hopfner Ludwig-Maximilians University, Faculty of Chemistry and Pharmacy, Department of Biochemistry Munich, Germany
07.2009–12.2009	Master thesis in the group of Prof. Dr. Karl-Peter Hopfner Ludwig-Maximilians University, Faculty of Chemistry and Pharmacy, Department of Biochemistry Munich, Germany
09.2008–02.2009	Erasmus exchange program student in the group of Prof. Dr. Hans Brandstetter, Salzburg University, Department of Molecular Biology, Salzburg, Austria
10.2007–06.2010	Undergraduate student in the group of Dr. Grzegorz Dubin Jagiellonian University, Faculty of Biochemistry, Biophysics and Biotechnology, Department of Microbiology, Krakow, Poland

Presentations

Poster presentation at the Congress and General Assembly of the International Union of Crystallography, August 5th–12th 2014, Montreal, Canada

Language skills

Polish	native
English	fluent
German	fluent